

Rochester Institute of Technology

## RIT Digital Institutional Repository

---

### Theses

---

12-6-2017

# Modeling and Implementation of HfO<sub>2</sub>-based Ferroelectric Tunnel Junctions

Spencer Allen Pringle  
sap1951@rit.edu

Follow this and additional works at: <https://repository.rit.edu/theses>

---

#### Recommended Citation

Pringle, Spencer Allen, "Modeling and Implementation of HfO<sub>2</sub>-based Ferroelectric Tunnel Junctions" (2017). Thesis. Rochester Institute of Technology. Accessed from

---

# **Modeling and Implementation of HfO<sub>2</sub>-based Ferroelectric Tunnel Junctions**

SPENCER ALLEN PRINGLE

---

---

# **Modeling and Implementation of HfO<sub>2</sub>-based Ferroelectric Tunnel Junctions**

SPENCER ALLEN PRINGLE

December 6, 2017

A Thesis Submitted  
in Partial Fulfillment  
of the Requirements for the Degree of  
Master of Science  
in  
Microelectronic Engineering

**R·I·T** | KATE GLEASON  
*College of* ENGINEERING

# **Modeling and Implementation of HfO<sub>2</sub>-based Ferroelectric Tunnel Junctions**

SPENCER ALLEN PRINGLE

## **Committee Approval:**

We, the undersigned committee members, certify that Spencer Pringle has completed the requirements for the Master of Science degree in Microelectronic Engineering.

---

Dr. Santosh Kurinec *Advisor*  
Professor, Microelectronic Engineering

Date

---

Dr. Dhireesha Kudithipudi  
Professor, Computer Engineering

Date

---

Mr. Mark Indovina  
Lecturer, Electrical Engineering

Date

---

Dr. Robert Pearson  
Programs Director, Microelectronic Engineering

Date

---

Dr. Sohail Dianat  
Dept. Head, Kate Gleason College of Engineering

Date

## Acknowledgments

The author would like to thank Dr. Santosh Kurinec for being consistently helpful, encouraging, and supportive throughout the completion of this work. Her helpful advice and fruitful discussions of quantum mechanics were always productive. Huge thanks to Mr. Mark Indovina for assistance implementing address systems and other system design. Many thanks to Dr. Dhireesha Kudithipudi for help learning and understanding the implementation of FTJ devices in neuromorphic systems and the many applications of such architectures. Also, many thanks to NamLAB and the University of California, Berkeley, for agreeing to deposit their own ferroelectric films for further implementation and testing of ferroelectric tunnel junctions.

This work was supported in part by the National Science Foundation, Grant # ECCS-1541090. Any opinions, findings, and conclusions or recommendations expressed in this material are those of the author and do not necessarily reflect the views of the National Science Foundation.

Thanks to Dr. Pearson for consistent departmental help and process knowledge. Lastly, the staff of engineers and technicians working at the Semiconductor & Microsystems Fabrication Laboratory (SMFL) at RIT are some of the most helpful, hardworking, caring, and exceptional people I've ever had the privilege to work with. Thank you all so much for being incredible.

*I would like to dedicate this work to my mother, Sharon Allen Pringle. Without your encouragement and help, none of this would have been possible. You're my inspiration to keep striving to be a better person.*

*Love, Spencer*

## Abstract

HfO<sub>2</sub>-based ferroelectric tunnel junctions (FTJs) represent a unique opportunity as both a next-generation digital non-volatile memory and as synapse devices in brain-inspired logic systems, owing to their higher reliability compared to filamentary resistive random-access memory (ReRAM) and higher speed and lower power consumption compared to competing devices, including phase-change memory (PCM) and state-of-the-art FTJ. Ferroelectrics are often easier to deposit and have simpler material structure than films for magnetic tunnel junctions (MTJs). Ferroelectric HfO<sub>2</sub> also enables complementary metal-oxide-semiconductor (CMOS) compatibility, since lead zirconate titanate (PZT) and BaTiO<sub>3</sub>-based FTJs often are not.

No other groups have yet demonstrated a HfO<sub>2</sub>-based FTJ (to best of the author's knowledge) or applied it to a suitable system. For such devices to be useful, system designers require models based on both theoretical physical analysis and experimental results of fabricated devices in order to confidently design control systems. Both the CMOS circuitry and FTJs must then be designed in layout and fabricated on the same die.

This work includes modeling of proposed device structures using a custom python script, which calculates theoretical potential barrier heights as a function of material properties and corresponding current densities (ranging from  $8 \times 10^3$  to  $3 \times 10^{-2}$  A/cm<sup>2</sup> with  $R_{\text{HRS}}/R_{\text{LRS}}$  ranging from  $5 \times 10^5$  to 6, depending on ferroelectric thickness). These equations were then combined with polynomial fits of experimental timing data and implemented in a *Verilog-A* behavioral analog model in *Cadence Virtuoso*. The author proposes tristate CMOS control systems, and circuits, for implementation of FTJ devices as digital memory and presents simulated performance. Finally, a process flow for fabrication of FTJ devices with CMOS is presented. This work has therefore enabled the fabrication of FTJ devices at RIT and the continued investigation of them as applied to any appropriate systems.

# Contents

---

<b>Signature Sheet</b>	i
<b>Abstract</b>	iv
<b>Table of Contents</b>	v
<b>List of Figures</b>	viii
<b>List of Tables</b>	xi
<b>List of Symbols</b>	xii
<b>1 Introduction</b>	1
1.1 Research objectives . . . . .	2
1.2 Thesis organization . . . . .	2
1.3 Neuromorphic Computing with Memristors, ReRAM . . . . .	4
1.4 Using Ferroelectric Tunnel Junctions . . . . .	5
<b>2 Physics of Ferroelectric Materials</b>	6
2.1 Crystal structure . . . . .	6
2.2 Polarization in ferroelectrics and dielectrics . . . . .	7
2.3 Non-intrinsic ferroelectrics . . . . .	8
2.4 Ferroelectric domains . . . . .	9
2.5 Area-dependent effects . . . . .	9
<b>3 Brief History and Applications of FTJ Implementations</b>	11
3.1 Early memory using large-dimension PZT . . . . .	11
3.2 More recent implementations with BaTiO <sub>3</sub> . . . . .	11
3.3 Applications of FTJs . . . . .	13
3.4 Alternative technologies . . . . .	14
3.4.1 Filamentary ReRAM . . . . .	14
3.4.2 Magnetic tunnel junctions . . . . .	15
3.4.3 Phase-change memory . . . . .	15

---

## CONTENTS

<b>4 Analysis of M1-Fe-M2 Structure</b>	<b>17</b>
4.1 Band structure in the absence of polarization field . . . . .	17
4.2 Band structure under polarization . . . . .	18
4.3 Extraction of tunnel Current and (by extension) resistance states . . . . .	21
<b>5 Design of Ferroelectric HfO<sub>2</sub>-based FTJs and Integration with CMOS Process</b>	<b>23</b>
5.1 FTJ design . . . . .	23
5.2 State of the art FTJs . . . . .	26
5.3 Designed CMOS-process with FTJ-fabrication steps . . . . .	28
5.4 Process simulation . . . . .	36
<b>6 System Design and Simulations for Digital Memory Applications</b>	<b>38</b>
6.1 Read/Write scheme . . . . .	38
6.2 Linear resistance change simulation . . . . .	40
6.3 Timing-based simulation . . . . .	41
6.4 Address systems . . . . .	43
6.5 Simulation results - 4×4 Array . . . . .	45
<b>7 Conclusions</b>	<b>50</b>
7.1 Future Work . . . . .	51
<b>A Python Program Code</b>	<b>59</b>
A.1 Core Code . . . . .	59
A.2 GUI Code . . . . .	78
<b>B Partial Process - FTJ-devices only</b>	<b>90</b>
<b>C Athena code</b>	<b>93</b>
<b>D sap1951_FTJ_THESES_45</b>	<b>97</b>
D.1 Linear Resistance FTJ Model . . . . .	97
D.1.1 Verilog Model . . . . .	98
D.2 Polarization-Timing FTJ Model . . . . .	101
D.2.1 Verilog Model . . . . .	102
D.3 SAP_ADDRESS_COLUMN_R . . . . .	115
D.4 SAP_ADDRESS_COLUMN_W . . . . .	118
D.5 SAP_ADDRESS_ROW_R . . . . .	121

## **CONTENTS**

---

D.6	SAP_ADDRESS_ROW_W . . . . .	124
D.7	SAP_ADDRESS_GND_vcc . . . . .	127
D.8	SAP_FTJ_DIGITAL_LOW_4_x_4 . . . . .	130
D.9	SAP_TRISTATE_MEM_4x_vcc . . . . .	132
D.10	SAP_TRISTATE_MEM_4x_TESTBENCH . . . . .	134
D.10.1	Verilog Model . . . . .	135

# List of Figures

---

1.1	Diagram representation of the dependencies of various implementation stages of the technology presented in this thesis. . . . .	3
2.1	Ferroelectric polarization (a) and weak magnetic moment (b) of multi-ferroic $\text{Bi}_2\text{NiMnO}_6$ at 7K, from Shimakawa et. al [1]. The red line on (a) is what this plot would look like for a perfect dielectric. . . . .	7
2.2	Simple representation of the atomic structures of a ferroelectric as its prototype phase (left) relaxes into one of two polar phases (middle and right) after the application of an external field. A ferroelectric would remain in the corresponding state even after the removal of $\mathcal{E}_{app}$ , while a dielectric would deflect (as shown) during stimulus application but relax to the non-polar phase (left) once that field was removed. . . . .	7
2.3	Simple diagram of domains in a model ferroelectric film. . . . .	9
3.1	”Bender memory” schematic from [2]. This 8-bit device stores data as remanent polarization in the top-most ferroelectric material. Write pulse is $\approx 1$ ms of 20-30 V/mil. . . . .	12
3.2	Performance of FTJs for (a) fresh device with PZT ferroelectric and (b) device with $\text{BaTiO}_3$ ferroelectric after -1.2V priming pulse, taken from Contreras et. al [3]. . . . .	13
3.3	Simple diagram of (left) a physical model of neurons and synapses, the brain’s computation devices, and (right) their electronic implementation in a typical brain-inspired computing system. . . . .	15
4.1	The energy band diagram of an metal-insulator-metal (MIM) with a 2 nm thick insulator with $E_a = 2$ eV and metals having $\chi_1 = 4.08$ eV, $\chi_2 = 4.85$ eV, normalized to the fermi energy. . . . .	18
4.2	The Fowler-Nordheim tunneling current of an MIM with material properties listed in Section 4.1. . . . .	19
4.3	(a) Diagram of charge densities created for left polarized ferroelectric and (b) corresponding generated potentials across an FTJ, having electrodes with dissimilar screening lengths, from Zhuravlev et. al [4]. . . . .	20

---

**LIST OF FIGURES**

---

4.4	The energy band diagrams, at $V = 0$ , of an FTJ with material properties given in Section 4.2, for positive (towards electrode 1 (M1)) and negative (towards electrode 2 (M2)) polarization. . . . .	21
4.5	The Fowler-Nordheim tunneling current of an FTJ with material properties consistent with those used in Figure 4.4, showing a memory window $HRS/LRS \approx 2.3$ . . . . .	22
5.1	Simulated HRS/LRS increases with larger screening length ratio before plateauing around $\frac{\delta_2}{\delta_1} \approx 60$ . For an Al/Al:HfO <sub>2</sub> /p+ Si FTJ with 2 nm ferroelectric. . . . .	24
5.2	Simulated HRS/LRS for increasing $\delta_1$ , showing a maximum. For an Al/Al:HfO <sub>2</sub> /p+ Si FTJ with 2 nm ferroelectric. . . . .	25
5.3	Simulated HRS/LRS and HRS resistivity for an Al/Al:HfO <sub>2</sub> /p+ Si FTJ with varying ferroelectric thickness. . . . .	25
5.4	Athena simulation of CMOS devices tuned for low threshold voltages (left) and FTJ device (right). . . . .	36
5.5	Athena simulation of FTJ device (SiO <sub>2</sub> substituted for ferroelectric). .	37
5.6	Zoom of FTJ device showing $\approx 250$ nm device width. . . . .	37
6.1	An address scheme which, though appropriate for a stand-alone device, would be inappropriate for devices in an array. . . . .	39
6.2	A simple schematic showing the typical connectivity of FTJ devices in an array, for both memory or neuromorphic logic applications. Lines and columns only connect through FTJ devices and do not connect at intersections. Dotted lines indicate an arbitrary number of repeated lines and columns. . . . .	39
6.3	An address scheme appropriate for FTJs in an array. . . . .	40
6.4	Non-addressed devices in the same row, for various write/read states. Non-addressed devices in the same column would experience the opposite bias. In this way, these devices will not be disturbed. . . . .	40
6.5	Changing polarization as a function of time for varying applied voltages for a sample with $V_c \approx 0.9$ V. . . . .	42
6.6	Changing polarization as a function of time binned for domains existing in 0.2V intervals for a sample with $V_c \approx 0.9$ V. Only a subset of curves are plotted. The models work best when binned from 0.2V to 3V in 0.2V intervals. . . . .	43

## LIST OF FIGURES

---

6.7	Maximum polarization for domains binned to 0.2V intervals, resembling a noisy normal distribution with a long right-sided tail. . . . .	44
6.8	Time until polarization saturation for domains binned to 0.2V intervals. Higher energy domains (oriented less parallel to the applied field) switch faster due to excess energy. . . . .	45
6.9	Schematic of address systems connected to a single FTJ. Note the inverted output taken above the reference resistor and the pass transistor to bypass that resistor while writing and applying vcc. The FTJ simulates with a low resistance state (LRS) of 300 K $\Omega$ and high resistance state (HRS) of 10 M $\Omega$ . The reference resistor is 2 M $\Omega$ . . . . .	47
6.10	Simulation results from a single FTJ device connected to address circuitry designed with 45 nm CMOS. Wen $\langle 1 \rangle$ follows the same curve as Wen $\langle 2 \rangle$ in this simulation. Notice that the output, Y, transitions low when reading (Ren high) an FTJ in LRS and transitions high when reading an HRS FTJ. Write and read times are 10 ns. . . . .	48
6.11	Simulation results from a single FTJ device connected to address circuitry designed with 45 nm CMOS. Wen $\langle 1 \rangle$ is constantly off in this simulation; testing for write disturb when programming a different device in the same row, once in an array. The FTJ state remains unchanged even after write enable toggles for high and low writes, verifying that this system is robust against write disturbs of non-addressed devices.	48
6.12	Small portion of waveform while writing binary 0 to 15 in one row while all other FTJ in the 4 $\times$ 4 array are in HRS. . . . .	49
6.13	Waveform and simulation log for random binary numbers being written to random rows of the 4 $\times$ 4 array. . . . .	49

## List of Tables

---

3.1	Performance of alternative technologies compiled from various sources. MTJ values from Aziz et. al and Lee et. al. [5,6], all other from Ebong et. al. and Kim [7,8] unless otherwise referenced in table. . . . .	14
5.1	Tables comparing relevant performance data for this research work to state of the art FTJs. LSMO stands for $\text{La}_x\text{Sr}_{1-x}\text{MnO}_3$ and CCMO is $\text{Ca}_{0.96}\text{Ce}_{0.04}\text{MnO}_3$ . Area units are $\mu\text{m}^2$ . Pd is surface power density and $P_r$ is remanent polarization in ( $\mu\text{C}/\text{cm}^2$ ). . . . .	27

## List of Symbols

---

Term	Description	Units/Value
$P$	Polarization	$\mu\text{C}/\text{cm}^2$
$P_r$	Remanent polarization	$\mu\text{C}/\text{cm}^2$
$t_{\text{sat}}$	Saturation time	s
$t_{\text{pdf}}$	Propagation delay falling	s
$t_{\text{pdr}}$	Propagation delay rising	s
$t_f$	Fall time	s
$t_r$	Rise time	s
$\sigma_p$	Polarization surface charge density (in ferroelectric)	$\mu\text{C}/\text{cm}^2$
$\sigma_s$	Screening charge density (in electrode)	$\mu\text{C}/\text{cm}^2$
$\mathcal{E}$	Electric field	V/cm
$\mathcal{E}_c$	Coercive electric field of ferroelectric	V/cm
$V_c$	Coercive voltage of ferroelectric film	V
$V$	Applied voltage	V
$d$	Thickness of ferroelectric	nm
$\delta_x$	Screening length in electrode "x"	nm
$E_c$	Energy at the conduction band edge	eV
$E_v$	Energy at the valence band edge	eV
$E_F$	Fermi level	eV
$E_g$	Band gap energy	eV
$\chi_x$	Work function of metal "x"	eV
$E_a$	Electron affinity of dielectric	eV
$\psi$	Potential	eV
$k_B$	Boltzmann's constant	$8.617 \times 10^{-5}$ eV/K
$J_{\text{tun}}$	Fowler-nordheim tunneling current density	A/cm <sup>2</sup>
$J_{\text{th}}$	Thermionic emission current density	A/cm <sup>2</sup>
$\bar{\psi}$	Average potential barrier	eV
$\psi'$	Maximum potential barrier	eV
$m^*$	Electron effective mass	kg
$m_e$	Electron rest mass	$9.11 \times 10^{-31}$ kg
$N_A$	Acceptor concentration	cm <sup>-3</sup>
$N_D$	Donor concentration	cm <sup>-3</sup>

Term	Description	Units/Value
$N_x$	Carrier concentration (of appropriate type)	$\text{cm}^{-3}$
$c_0$	Atomic density	$\text{cm}^{-3}$
$V_{DD}$	Write voltage high rail	V
$V_{SS}$	Write voltage low rail	V
$v_{dda}$	Read voltage high rail	V
$v_{ssa}$	Read voltage low rail	V
$gnd$	0V, ground	V
$q$	Elementary charge	$1.602 \times 10^{-19}$ C
$T$	Temperature	K
$\epsilon_0$	Vacuum permittivity	$8.854 \times 10^{-14}$ F/cm
$\epsilon_f$	Ferroelectric permittivity	F/cm
$\epsilon_{Si}$	Silicon permittivity	11.7 F/cm

# Chapter 1

---

## Introduction

Traditional CMOS devices are reaching fundamental physical limits of scaling and nonvolatile memory devices based on charge-storage are no longer meeting requirements for future high-speed systems [9–12]. In addition, the trend towards portable computers, smart phones, health telemetry, and smart building integration has renewed desire for ultra-low-power devices [13]. Neuromorphic computing (NMC) systems show huge potential to enable such power performance; taking inspiration from information processing in electro-chemical biological systems (specifically the brain) and emulating or reproducing that operation using electronic devices [11].

Any system for neuromorphic computing (NMC) endeavors to mimic the stimuli response of the human brain. Often such a system is composed of an array of elements which emulate the response of synapses (two-terminal connections) between two neurons, interconnected appropriately as the system requires, which exhibit increasing output in response to more frequent potentiation, called spike-timing dependent plasticity (STDP) [14]. In simpler terms; an element which has not seen stimulus for a long time will provide less response when presented with stimulus than an element which has recently seen many stimulus events. Though less accurate than traditional Von-Neumann computation schemes, neuromorphic systems have been shown to have incredible speed and power consumption advantages when working with images, pattern recognition, etc. Specifically, the "CAVIAR" system reports speed increase of

more than 3 orders of magnitude compared to conventional image processing [15], and the SpiNNaker chip proves power consumption improvement by consuming merely a few nanojoules per neuron event [16]. Further, one can look to the IBM TrueNorth and SyNAPSE chips for more proof of high speed and low power computation. However, optimal synapse devices must be two-terminal devices which exhibit low power operation, high speed, high reliability, high endurance, and good memory window with continuous states. Three potential candidates are ReRAM, covered more completely in Section 3.4.1, MTJs, and FTJs.

## 1.1 Research objectives

This thesis work evaluates incorporation of HfO<sub>2</sub>-based FTJ in NMC and nonvolatile digital memory applications, specifically focusing on device performance/optimization and system enablement. It explores material properties, basic device performance, process development for CMOS integration, and related system design including simulated performance. By optimizing material properties of its various parts, the device can exhibit a range of performance from ultra low power with large memory window to low power with better speed performance when implemented with address systems (lower  $\tau = RC$ ). This research work thereby endeavors to provide a full foundation, see Figure 1.1, for further exploration and fabrication of HfO<sub>2</sub>-based FTJ, both specifically at RIT and (with process modifications for varying CMOS device types and sizes) at any facility.

## 1.2 Thesis organization

This introductory Chapter 1 highlights applications for which FTJ devices can enhance performance and simplify implementation and documents the research objectives and organization of this thesis. Chapter 2 presents an overview of the physical

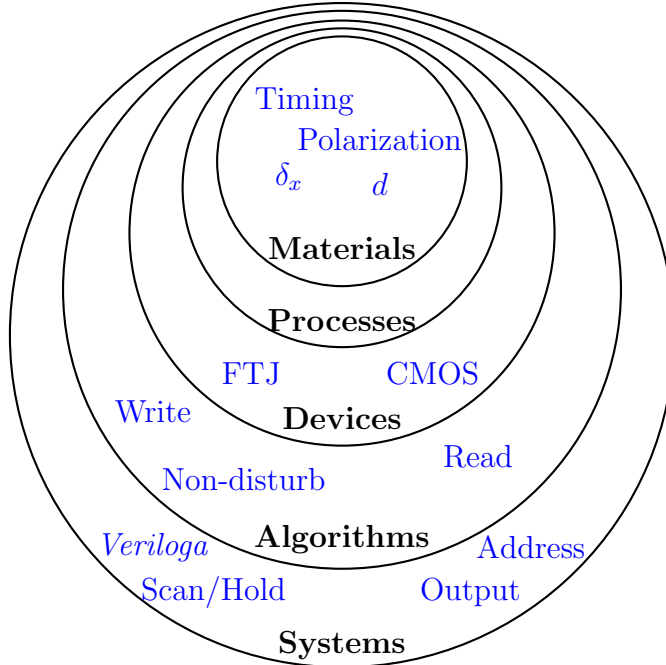


**Figure 1.1:** Diagram representation of the dependencies of various implementation stages of the technology presented in this thesis.

properties of ferroelectric materials and highlights some specific aspects which are of concern to their implementation in FTJs. Chapter 3 reviews the history of ferroelectric memories, the discovery and subsequent explanation of FTJs, and the ideal applications of these devices while also presenting alternative technologies and comparing their performance. After demonstrating the advantages of FTJs, Chapter 4 presents simulation (from quantum-mechanical basis) of device operation, with corresponding band structures and current densities in each memory state (using a custom python script). Finally, an FTJ using ferroelectric HfO<sub>2</sub> is designed and simulated in Chapter 5 and its performance is compared to other state of the art FTJs. In this same chapter, a CMOS-integrated fabrication process for HfO<sub>2</sub>-based FTJ devices is designed and discussed. Chapter 6 presents related address schemes and systems; with schematics, simulations, *Verilog* descriptions, and layouts, designed for digital memory applications using *Cadence Virtuoso* and a 45-nm process design kit (PDK). Finally, the results of this work are summarized in Chapter 7 and future work is pre-

sented. This work therefore provides a nearly comprehensive overview of FTJ devices from materials to systems, including ferroelectric HfO<sub>2</sub> device simulation, the design of a full CMOS-integrated fabrication process, and *Cadence Virtuoso* system design and simulation with custom *Verilog-A* behavioral analog models of designed FTJs.

### 1.3 Neuromorphic Computing with Memristors, ReRAM

Neuromorphic systems with ReRAM as synapse elements have been reported which take advantage of the intrinsic similarity between such devices and synapses (both are two-terminal and behave memristively). ReRAM devices inherently pass more current as they are programmed further (provided they can be so-designed) and therefore provide both space-reduction (compared to larger CMOS elements or register implementation) and simplification of STDP response generation. In their papers, Ambrogio et. al report low-power ( $\approx 10^5$  power reduction) generation of STDP signals with ReRAM 1 transistor - 1 resistor (1T1R) synapse elements constituting a neuromorphic system capable of unsupervised learning of MNIST handwritten digits achieving 86% accuracy [17]. Further, the power consumption of the system was reduced to  $1 \times 10^{-12}$  Joules per neuron event, using a series of short pulses for write/read, and enable ultra-low power computation [18]. Park et. al used TiO<sub>x</sub>-based ReRAM in a neuromorphic system having a 250 node hidden layer followed by a 125 node secondary hidden layer and 10 bit output layer for recognition of 528-bit hand-drawn digits (0 through 9) from the MNIST database. The system uses a different scheme for pulse generation, consisting of discretizing element conductivity to 64 "conductance states" and achieves up to 84% accuracy [19]. Resistive devices as synaptic elements therefore provide a unique opportunity in ultra low-power high speed systems for applications requiring highly-parallel computation.

## 1.4 Using Ferroelectric Tunnel Junctions

An FTJ is very similar to a ReRAM device in function (both two terminal memristors), but differs in mechanism. Where ReRAM elements are either filamentary (create/break a mechanical filament on program/erase) or non-filamentary (often involving changing concentration of oxygen vacancies at the barrier interface) [20], a change in resistance for an FTJ is based on the changing internal polarization field magnitude and direction of a ferroelectric material separated by two electrodes of different materials (specifically having differing Debye lengths) [4]. Since, optimally, a synaptic element will have a smooth (analog) transition from having seen no potentiation (and little response) to many recent potentiations (and large response), an FTJ for such application should include a ferroelectric material with as many domains as possible and a low coercive electric field such that the ferroelectric depolarizes under the absence of repeated stimuli. Such a film will be slightly thicker than typical for FTJ used in non-volatile memory (NVM) and of a larger area. These properties are in contrast to those required for NVM (high coercive field and low # of polarization domains). Ferroelectric HfO<sub>2</sub> is a good candidate due to the large difference in resistive states possible, the ability to get a large number of domains in even small areas, and high speed performance with write/read times of 10 ns [21]. Interestingly, HfO<sub>2</sub>-based FTJ can be designed to provide optimal NVM performance or NMC performance, explored more in Sections 5.1 and 5.2.

# Chapter 2

---

## Physics of Ferroelectric Materials

Ferromagnetism (permanent magnetic moment) was the first ferroic property discovered and was so-named because it occurs often in iron-containing alloys. Ferroelectricity is a property of materials which exhibit spontaneous electric polarization (dipole moment density) and although most ferroelectrics do not contain iron, was so-named because of its relation to the other ferroics (materials which can polarize in some way) and was classified as such. In a basic sense, a ferroelectric is a dielectric that (once stimulated) exhibits a non-zero reversible polarization at 0 applied electric field, as shown in Figure 2.1. This remanent polarization,  $P_r$ , is due to an internal potential, covered in more detail in the next few sections. Most ferroelectrics are either transition metal oxides or chalcogenides. Additionally, materials can exhibit any ferroic property independent of the others, and will also always be piezoelectric, and a material which exhibits any two or more (excluding piezoelectricity) is considered "multiferroic" [22].

### 2.1 Crystal structure

The internal electric field which ferroelectric materials exhibit, below their curie temperature, is a result of their crystal structures. Though the material can maintain a so-called "prototype" phase above the curie temperature, due to available phonon energy, at lower temperatures the crystal precipitates into a phase which is polar,

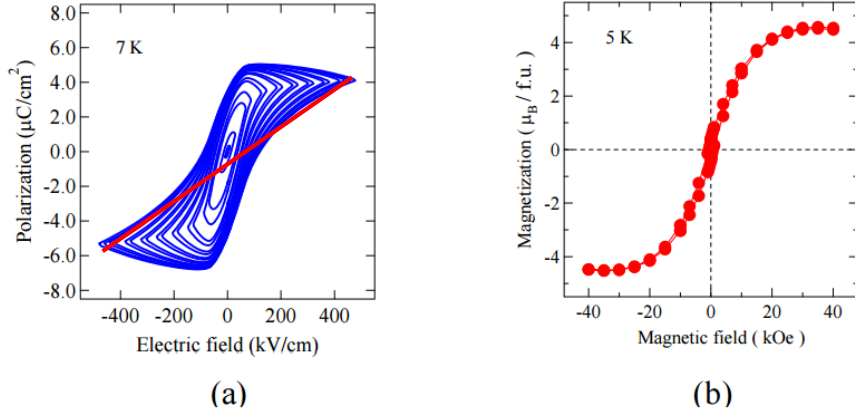


**Figure 2.1:** Ferroelectric polarization (a) and weak magnetic moment (b) of multiferroic  $\text{Bi}_2\text{NiMnO}_6$  at 7K, from Shimakawa et. al [1]. The red line on (a) is what this plot would look like for a perfect dielectric.

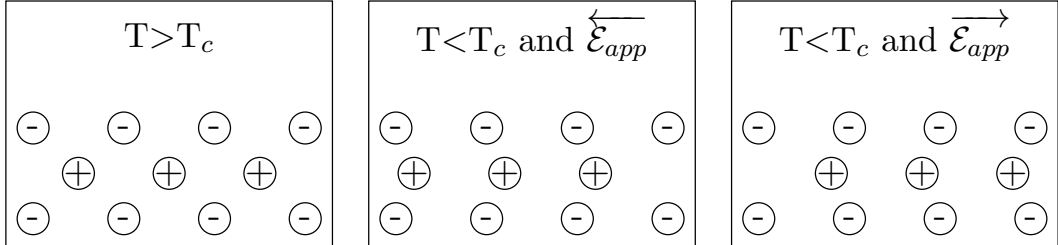


**Figure 2.2:** Simple representation of the atomic structures of a ferroelectric as its prototype phase (left) relaxes into one of two polar phases (middle and right) after the application of an external field. A ferroelectric would remain in the corresponding state even after the removal of  $\mathcal{E}_{app}$ , while a dielectric would deflect (as shown) during stimulus application but relax to the non-polar phase (left) once that field was removed.

represented in Figure 2.2, and exhibits an aggregate total polarization field based on the orientation of domains (as a function of defects and grain boundaries). This topic (and more complicated derivations of the physical phenomena of ferroelectrics) is explored more completely in the famous book by Lines and Glass [22].

## 2.2 Polarization in ferroelectrics and dielectrics

The atoms in dielectric materials respond to external bias, as shown in Figure 2.2, by deflecting from their zero-field position due to the applied electrostatic attraction/repulsion of the field. Considering a single unit cell, the energy required for an

atom to remain in that position (along an arbitrary plane) follows a quadratic curve with only one minimum at the zero-field position. This is because a simple dielectric has a centrosymmetric crystal structure. A similar plot of atomic energy versus position in a ferroelectric unit cell would instead behave as  $(x^2 + a)(x^2 + b) + c$  and exhibit two separate minimas. This is because the crystal structure of a ferroelectric is non-centrosymmetric, and is the physical origin of the macroscopic polarizability of a ferroelectric film [22]. Furthermore, the polarization at zero applied field is called remanent polarization,  $P_r$ . It can be either expressed in each polarization state (positive  $P_{r,+}$  or negative  $P_{r,-}$ ) or as the total of both states  $2P_r = P_{r,+} + P_{r,-}$  (often in the case of symmetric states, where  $P_{r,+} = -P_{r,-}$ ). The electric field required to transition from one polarization state to the other (where  $P$  passes through 0) is called the coercive electric field,  $\mathcal{E}_c = V_c/d$  [22]. Figure 2.1 shows a ferroelectric film with  $2P_r = 8\mu\text{C}/\text{cm}^2$  and  $\mathcal{E}_c = 0.1 \text{ MV}/\text{cm}$ .

### 2.3 Non-intrinsic ferroelectrics

Though most ferroelectrics were classically demonstrated as bulk materials and later implemented as thin films, recent improvements in film deposition technologies have enabled the engineering of materials which could be called "non-intrinsic" ferroelectrics. Typically, the crystallization of a material proceeds in an effort to minimize total energy and occurs unconstrained (meaning the atoms are free to move within the lattice). Recently, a group from NamLAB deposited films of  $\text{HfO}_2$  by atomic layer deposition (ALD) and incorporated varying atomic % of Si atoms. After annealing, unconstrained, the material crystallizes to a mixture of typical monoclinic/tetragonal phases (which are centrosymmetric). However, by capping the  $\text{HfO}_2$  with a thin film of TiN and annealing at a temperature such that the TiN atoms were likely still in a stable form, the  $\text{HfO}_2$  crystallizes to orthorhombic phase and is non-centrosymmetric [23]. This change in state is likely due to a combined interaction

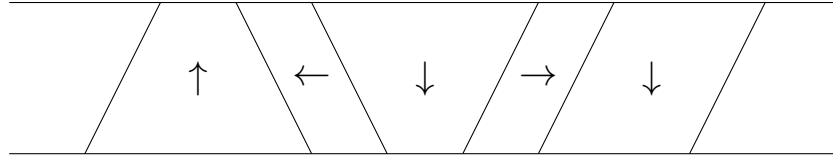


**Figure 2.3:** Simple diagram of domains in a model ferroelectric film.

of the atomic stress from Si doping, the extra strain energy introduced by the capping material, and the inhibition of relaxation modes available when un-capped. The Ferroelectric Device Research at RIT (FeDR RIT) group, working with NaMLAB, have successfully demonstrated similar material results at RIT by doping HfO<sub>2</sub> with Al, using similar capping and anneal strategies.

## 2.4 Ferroelectric domains

A realistic ferroelectric film will not be perfectly oriented all the same direction, as considered in Figure 2.2, but instead have many differently oriented crystal clusters, due to defects. A very basic visualization of this effect is shown in Figure 2.3, and is explored more thoroughly in the book by Lines and Glass [22]. In general, the maximum size of a domain can be extracted based on crystal parameters but for most materials is roughly 20 to 100 nm.

## 2.5 Area-dependent effects

The response of an FTJ can be affected by the domains which exist in the ferroelectric, with reference to the area of the device. Consider, if the maximum domain size is close to the area of FTJ devices, some devices will encompass only one domain which is oriented parallel to the applied field. These devices would have maximum performance, since the entire film contributes to polarization ( $P_{\max}$ ). However, this also means that some devices will happen to lie over a domain which is entirely perpendicular to applied field and therefore cannot be polarized by the electrodes!

These devices would simply not work at all. Therefore, for highest reliability, a film should have maximum domain sizes much smaller than the desired area of FTJ devices. This way, every device will have some domains directed parallel and some perpendicular. Every device in an array would therefore work, but will have reduced performance ( $P \approx 0.5P_{\max}$ ).

# Chapter 3

---

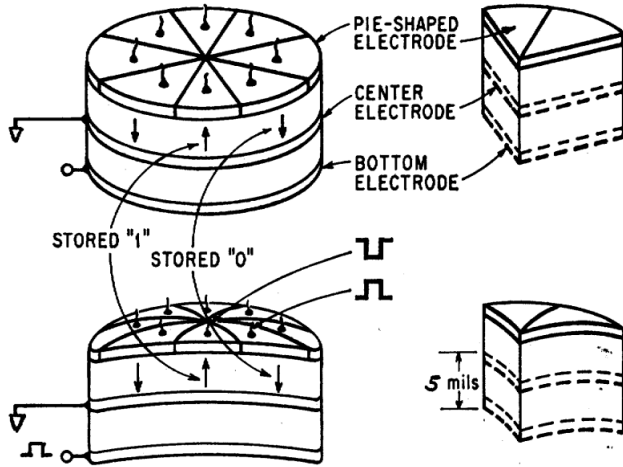
## Brief History and Applications of FTJ Implementations

### 3.1 Early memory using large-dimension PZT

Though not FTJs, ferroelectric memories were first reported in an MIT masters thesis by Dudley Allen Buck in 1952 [24]. Larger ferroelectric memory arrays by Bell Labs were also discussed in a Scientific American article in 1955 by Ridenour [25] though a good explanation of such devices was not given until a 1973 IEEE article by Kaufman [2]. These "bender memory" devices used 5 mil (127  $\mu\text{m}$ ) thick PZT ferroelectric films sandwiched between conducting electrodes, shown in Figure 3.1, to store data in polarization which creates a positive or negative pulse (while clamped, due to the electrostrictive and piezoelectric response) in response to application of a read voltage. These devices were very high power (30 V/mil write, 45V read) and very slow ( $\approx 1 \text{ ms}$ ) [2].

### 3.2 More recent implementations with BaTiO<sub>3</sub>

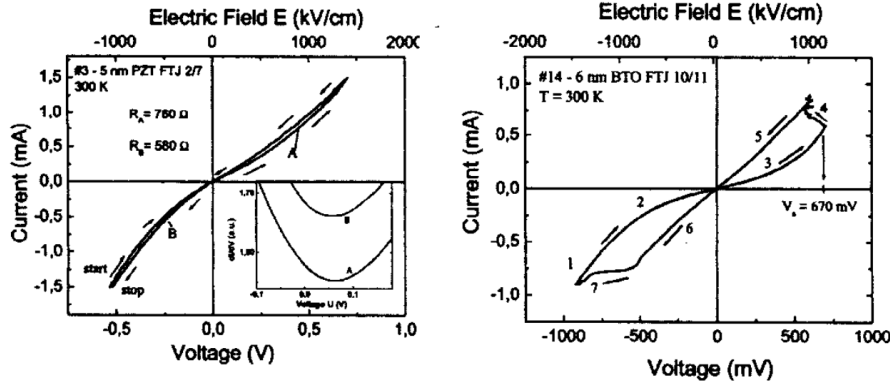
As covered briefly in Section 4.2, Contreras et. al discovered the first FTJ using BaTiO<sub>3</sub>, a ferroelectric well known since its initial synthesis as a bulk material. In that paper, the group had investigated both Pt/PZT/SrRuO<sub>3</sub> and SrRuO<sub>3</sub>/BaTiO<sub>3</sub>/SrRuO<sub>3</sub> FTJs. The PZT FTJ displayed poor performance (likely due to vanishing polarization density at small dimensions) while, although having similar electrodes, the BaTiO<sub>3</sub>-



**Figure 3.1:** "Bender memory" schematic from [2]. This 8-bit device stores data as remanent polarization in the top-most ferroelectric material. Write pulse is  $\approx 1$  ms of 20-30 V/mil.

based FTJ had a memory window of  $HRS/LRS \approx 3$ , shown in Figure 3.2 [3]. As already discussed in Section 4.2, the memory window is heavily dependent on the dissimilarity of screening lengths between electrodes and, considering this FTJ has the same material for both electrodes, it's surprising that the performance is so good. The group (Contreras, Kohlstedt, et. al) clears up this incongruity in their 2005 paper where, in addition to using the findings of Zhuravlev et. al [4] to explain FTJ performance, they report that the interface between bottom electrode and ferroelectric exhibits a Ruddelsen-Popper interfacial layer which modifies the effective screening length for that electrode, increasing asymmetry and therefore memory window [26].

Groups have continued to research  $\text{BaTiO}_3$ -based FTJs, including a recent 2013 paper by Wang et. al which presents a device with  $\text{Co}$  and  $\text{La}_{0.67}\text{Sr}_{0.33}\text{MnO}_3$  as electrodes. The group achieves a memory window  $HRS/LRS \approx 100$  with a 2 nm ferroelectric and demonstrates switching times as fast as 13 ns (for relatively high write voltages,  $\approx 3V_c$ ). They also use extracted values to design a *Verilog-A* model of their devices [10].

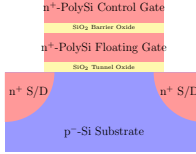


**Figure 3.2:** Performance of FTJs for (a) fresh device with PZT ferroelectric and (b) device with BaTiO<sub>3</sub> ferroelectric after -1.2V priming pulse, taken from Contreras et. al [3].

### 3.3 Applications of FTJs

FTJ devices are ideal for two main applications; non-volatile digital memory and brain-inspired computing. Portable electronics demand fast, low-power storage devices and, as shown in Table 3.1, FTJ provide the highest speed and lowest power.

Brain-inspired computing is the implementation of CMOS devices, which mimic the integrate-and-fire responses of neurons, interconnected by devices with modifiable signal strength, the function of a synapse, as shown in Figure 3.3. These types of systems are most applicable to spatio-temporal data sets which are tolerant to noise. For instance, facial recognition in video monitoring was demonstrated by Chevitarese et. al using the IBM neuromorphic chip (which uses filamentary ReRAM devices) and achieves 99% accuracy with total power consumption of 222mW [30]. Digitization of pen-stroke inputs and word-detection in audio signals could also benefit from neuromorphic implementation. The easiest type of synapse to implement is a two-terminal memristor which can be programmed to either have a high resistance (low connective strength) or low resistance (high connective strength). Of available memristor devices, shown in Table 3.1, FTJs are at a clear advantage. Though occupying more area than PCM and FTJ devices, FTJs are faster and operate at lower power compared to all other devices. For this reason they are optimal for both neuromorphic

Device	NAND/NOR	ReRAM	PCM	MTJ	FTJ
Visual (Red and blue boxes are two different states in time)					
Mechanism	Vt Shift	O <sub>2</sub> Vac./Filamentary	Phase change	e <sup>-</sup> Spin (Mag)	Polarization
Speed (s)	400u [27]	500n	50n	30n [27]	10n
Power (J)	15u [28]	250n	6p	1.4u	30f
Cell Area	4F <sup>2</sup> or 10F <sup>2</sup> [29]	25F <sup>2</sup>	16F <sup>2</sup>	1.3F <sup>2</sup>	22F <sup>2</sup>
Material	Si	Ag, a-Si, W	Ge <sub>2</sub> Sb <sub>2</sub> Te <sub>5</sub>	MgO(mag)	BaTiO <sub>2</sub> (now HfO <sub>2</sub> )

**Table 3.1:** Performance of alternative technologies compiled from various sources. MTJ values from Aziz et. al and Lee et. al [5, 6], all other from Ebong et. al. and Kim [7, 8] unless otherwise referenced in table.

and non-volatile memory applications.

## 3.4 Alternative technologies

Memristors can be implemented by a few different technologies, each with their own characteristic strengths and shortcomings, which are discussed in this section.

### 3.4.1 Filamentary ReRAM

These devices operate by forming and destroying a nanofilament of conducting material in an insulating or high-resistance "switching" medium. Many types of these devices exist, but generally the most used CMOS-compatible versions are Ag/SiO<sub>2</sub>/Pt or W/SiGe/a-Si/Ag. The first type forms/destroys Ag nanofilaments through the SiO<sub>2</sub> layer while the latter forms/destroys Ag nanofilaments through the a-Si layer [31, 32]. Both switching mediums are  $\approx 20$  nm thick. Though these types of devices

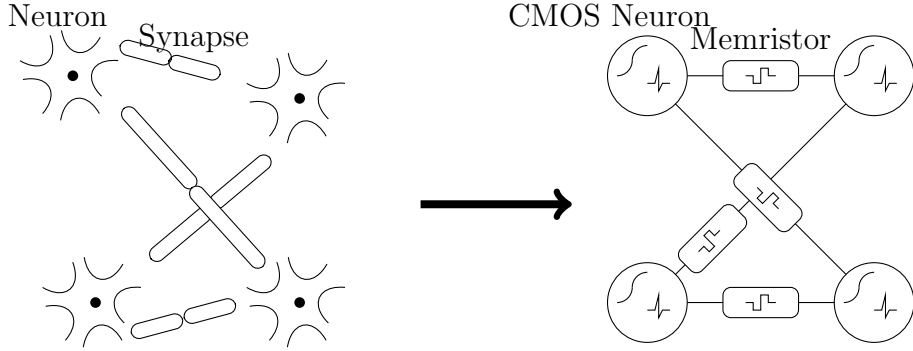


**Figure 3.3:** Simple diagram of (left) a physical model of neurons and synapses, the brain's computation devices, and (right) their electronic implementation in a typical brain-inspired computing system.

are well-understood and widely used, they are not very low power ( $3.5V$  program pulses applied to devices with  $R_{avg} \approx 1M\Omega$ ) and are rather slow ( $\approx 100 \mu s$  program times,  $\approx 500 \mu s$  read) [32].

### 3.4.2 Magnetic tunnel junctions

The MTJ is designed as a tunnel oxide sandwiched between two ferromagnetic materials. One of the ferromagnets is pinned to be magnetized in a direction, while the other is free to magnetize parallel or anti-parallel to it (controlled by inducing a magnetic field in it by passing a large current through a nearby conducting material). When both magnetic films are oriented parallel the tunnel resistance through the device is lower than when anti-parallel (due to the effect of spin-transfer torque). These devices can achieve memory windows as high as  $HRS/LRS \approx 1000$ , but usually have higher current density in both states than FTJs and also require rather large current pulses to write the magnetic state [5, 6].

### 3.4.3 Phase-change memory

Lastly, PCM stores data by changing the crystal phase of a material in a junction. When fresh, the material is in a crystalline (low resistance) state. By passing sufficient current through a heater, the phase change material is melted and quickly quenched

### **CHAPTER 3. BRIEF HISTORY AND APPLICATIONS OF FTJ IMPLEMENTATIONS**

---

by passing a large current through it. This forces the material to remain amorphous and have a higher resistance, usually  $HRS/LRS \approx 1000$ . To return to low resistance state, a moderate current pulse is passed through the material, melting it, and held there long enough melt and facilitate crystallization of the material. Though typical current density in both states are lower than MTJ, they are still not as low as FTJ and, like MTJ, the PCM requires rather large currents to write [33]. Therefore, it is not ideal for low-power computing.

# Chapter 4

---

## Analysis of M1-Fe-M2 Structure

At its core, an FTJ is a modified MIM so it's logical to start by examining an MIM and modifying our analysis to reflect the different material properties. All band structure and current density figures in this section, except Figure 4.3, are simulated results performed in this work using a custom python program included in Appendix A.

### 4.1 Band structure in the absence of polarization field

An MIM with non-ferroelectric insulator has no internal polarization field and therefore returns to the same zero-field band structure, shown in Figure 4.1, after any external field application (for  $d = 2$  nm thick insulator with  $E_a = 2$  eV and metals having  $\chi_1 = 4.08$  eV,  $\chi_2 = 4.85$  eV). The thermionic emission current, from electrons which gain sufficient energy from phonon interaction to surmount the barrier, of such a device is calculated using Equation 4.1, and for our example is roughly  $1e-41$  A/cm<sup>2</sup> (practically "0" current) at 0.5V. Since this MIM has an insulator with thickness less than the penetration distance of the electron wave, an appreciable current occurs due to Fowler-Nordheim tunneling,  $J_{\text{tun}}$ , when electrons are able to quantum-mechanically tunnel through the triangular or trapezoidal energy barrier. This current, calculated using Equation 4.2, is shown in Figure 4.2 and is the main current contributing mechanism for this type of device ( $7e4$  A/cm<sup>2</sup> at 0.5V for this example). Like most MIMs, this device's tunnel current density has a separation around zero applied voltage

where the current becomes "zero" and also has a slight asymmetry between curves under negative and positive applied voltage.

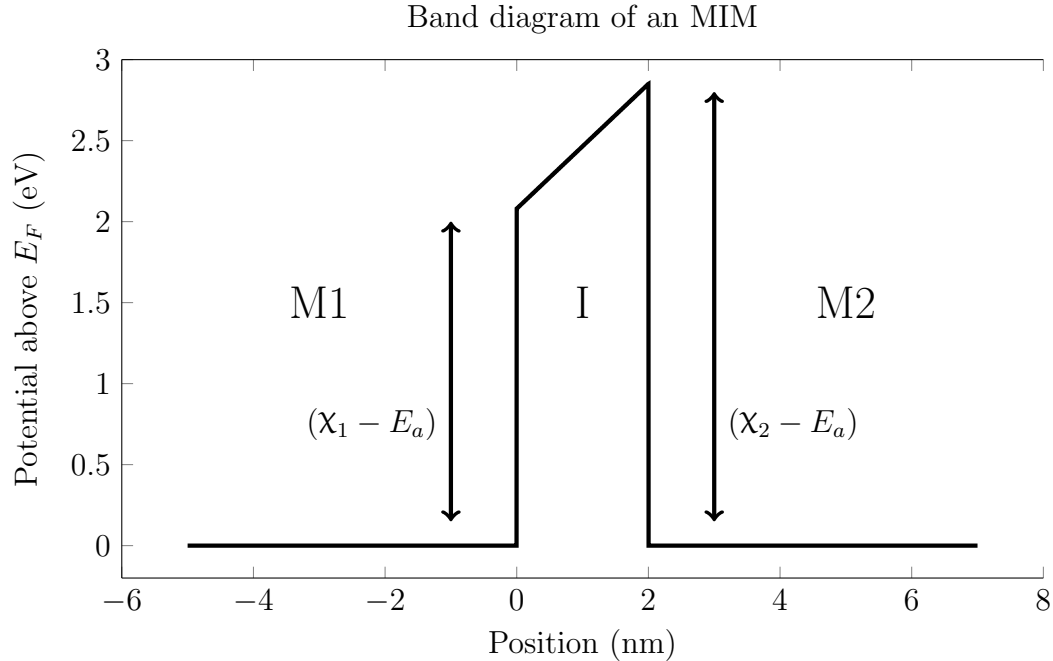


**Figure 4.1:** The energy band diagram of an MIM with a 2 nm thick insulator with  $E_a = 2$  eV and metals having  $\chi_1 = 4.08$  eV,  $\chi_2 = 4.85$  eV, normalized to the fermi energy.

$$J_{th} = A_{th} T^2 \exp(-\psi'/k_B T) (1 - \exp(-qV/k_B T)) \quad (4.1)$$

where,  $A_{th} = \frac{4\pi m^* q k_B^2}{h^3}$

$$J_{tun} = J_0 \left\{ \bar{\psi} \exp \left( -A_{tun} \sqrt{\bar{\psi}} \right) - (\bar{\psi} + qV) \exp \left( -A_{tun} \sqrt{\bar{\psi} + qV} \right) \right\} \quad (4.2)$$

$$J_0 = \frac{q}{2\pi h(\beta d)^2} \quad \bar{\psi} = \frac{1}{d} \int_0^d \psi(x) dx, \text{ is mean barrier height}$$

$$A_{tun} = \frac{4\pi\beta d \sqrt{2m^*}}{h} \quad \beta \text{ is a correction factor, usually 1}$$

## 4.2 Band structure under polarization

When the first FTJ was discovered by Contreras et. al in 2002, BaTiO<sub>3</sub> ferroelectric with SrRuO<sub>3</sub> and PZT as electrodes, its operation went unexplained and was origi-

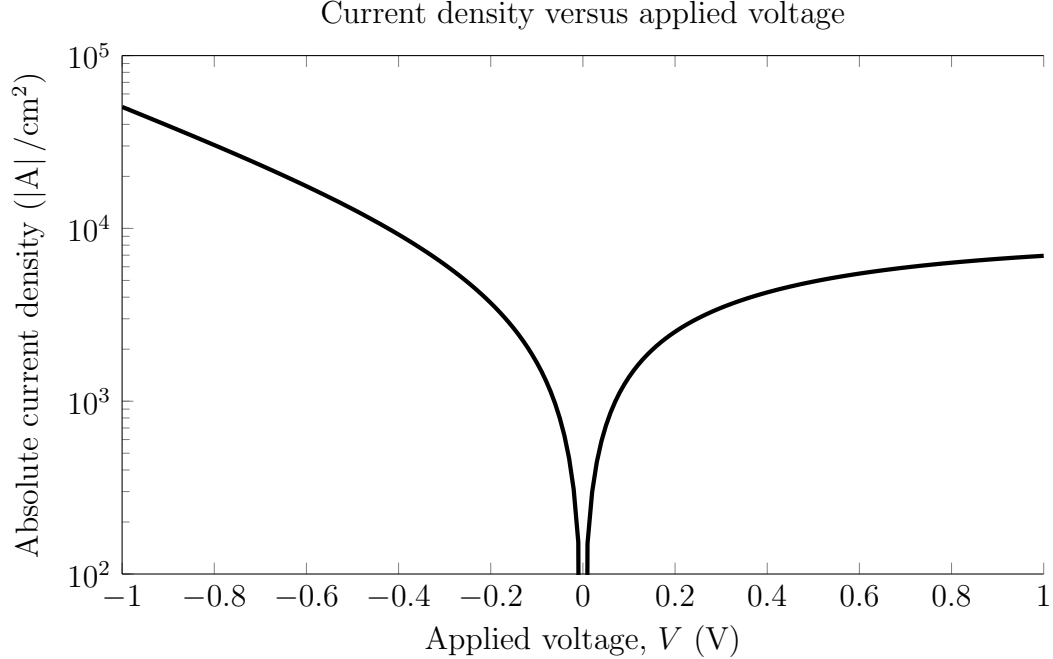


**Figure 4.2:** The Fowler-Nordheim tunneling current of an MIM with material properties listed in Section 4.1.

nally published purely as a dissemination of experimental results. [3] It was not until 2005 that the phenomenon was explained by Zhuravlev et. al, who postulated that the ferroelectric polarization,  $P$ , induces equal and opposite surface charge densities,  $\sigma_p = -P$ , which exist in infinitessimally thin sheets at the interfaces of each contact and the ferroelectric. Shown in Figure 4.3, the surface charges must then be locally screened by each electrode, thereby inducing screening charge densities,  $\sigma_s$ , as given by Equation 4.3, with screening lengths (or debye lengths) in metal 1,  $\sigma_1$ , and metal 2,  $\sigma_2$ , given by Equation 4.4. Finally, these charges modify the zero-polarization band structure with additional potentials within both electrodes and the ferroelectric, as given by Equation 4.5 and shown in Figure 4.3 by Zhuravlev et. al [4]. Though not explicitly given by the group, it is clear that the additional potential contribution within the ferroelectric is given by Equation 4.6.

$$\sigma_s = \frac{Pd}{\varepsilon_f(\delta_1 + \delta_2) + d} \quad (4.3)$$

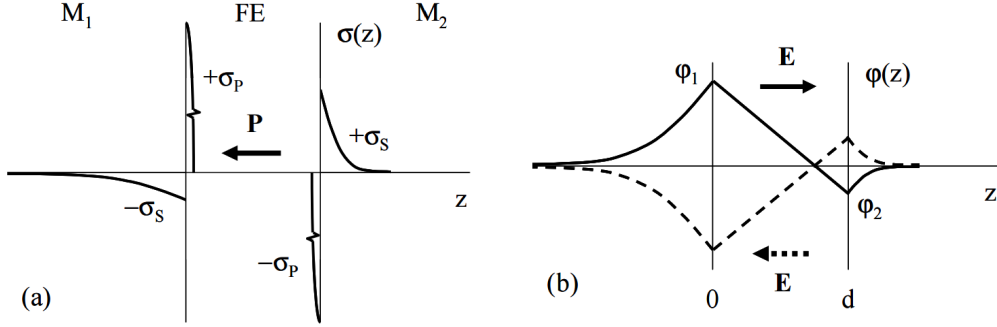


**Figure 4.3:** (a) Diagram of charge densities created for left polarized ferroelectric and (b) corresponding generated potentials across an FTJ, having electrodes with dissimilar screening lengths, from Zhuravlev et. al [4].

$$\delta_x = L_D = \sqrt{\frac{\varepsilon k_B T}{q^2 N_x}} \text{ where, for a metal } N_x = c_0 \quad (4.4)$$

$$\psi(x) = \begin{cases} \frac{\sigma_s \delta_1 \exp(-|x|/\delta_1)}{\varepsilon_0}, & x \leq 0 \\ -\frac{\sigma_s \delta_2 \exp(-|x-d|/\delta_2)}{\varepsilon_0}, & d \leq x \end{cases} \quad (4.5)$$

$$\psi(x) = \begin{cases} \psi(0) + (\psi(d) - \psi(0)) \left(\frac{x}{d}\right), & 0 < x < d \end{cases} \quad (4.6)$$

It's clear to see already that for electrodes with dissimilar screening lengths there will be a non-zero depolarizing field, because of the reduced field contribution from charges further from the interface, and there will be a difference in average potential barriers for polarization towards M1 versus M2. Finally, integrating all the above contributions from polarization-induced charges to the zero-field band structure, an FTJ with material properties consistent with those used in Section 4.1 (and assuming  $P = 10\mu\text{C}/\text{cm}^2$ ,  $\varepsilon_f = 40\varepsilon_0$ ,  $\delta_1 = 0.06\text{ nm}$ , and  $\delta_2 = 0.4\text{ nm}$ ) would exhibit band structures as shown in Figure 4.4.

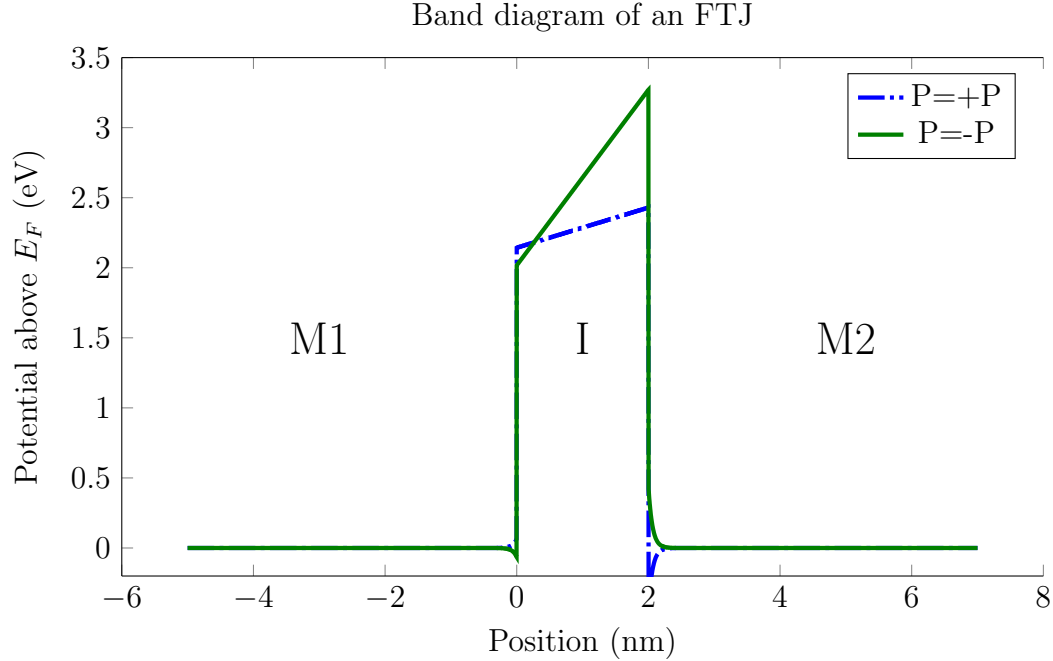


**Figure 4.4:** The energy band diagrams, at  $V = 0$ , of an FTJ with material properties given in Section 4.2, for positive (towards M1) and negative (towards M2) polarization.

### 4.3 Extraction of tunnel Current and (by extension) resistance states

The tunnel current density for each state (positive polarization and negative polarization), is calculated again using Equation 4.2, but now requires the additional potential contributions of equations 4.5 and 4.6. For this case, positive polarization (towards M1) has a lower barrier than negative polarization (towards M2), so we will term each state the LRS and HRS, respectively. The corresponding current density curves are shown in Figure 4.5, and is representative of an FTJ having Al as M1, Al:HfO<sub>2</sub> as ferroelectric, and degenerately doped ( $N_a = 1 \times 10^{20} \text{ cm}^{-3}$ ) p+ Si as M2. Since the resistivity is given by  $\rho = E/J = V/(dJ)$ , the resistance states would correspond directly to the current densities of each state. Lastly, the memory window is a ratio of the device's resistivity (at the same applied voltage, usually the read voltage,  $v_{\text{dda}}$ ) in each state,  $HRS/LRS = \rho_{\text{HRS}}/\rho_{\text{LRS}} = J_{\text{LRS}}/J_{\text{HRS}}$ .

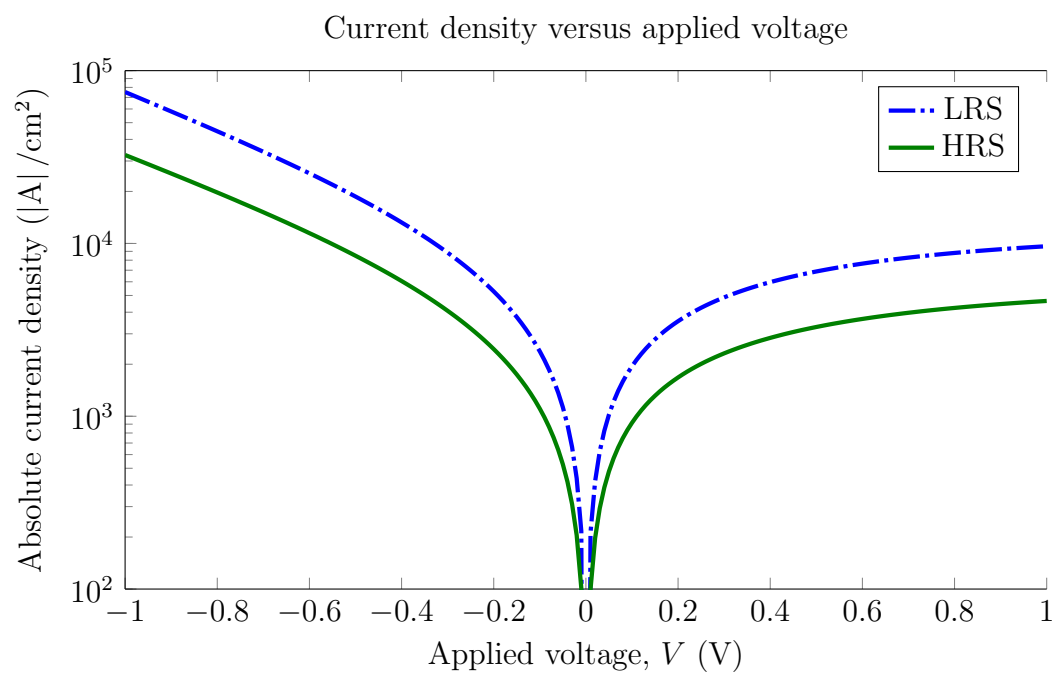


**Figure 4.5:** The Fowler-Nordheim tunneling current of an FTJ with material properties consistent with those used in Figure 4.4, showing a memory window  $HRS/LRS \approx 2.3$ .

# Chapter 5

---

## Design of Ferroelectric HfO<sub>2</sub>-based FTJs and Integration with CMOS Process

For this design, a twin-well polysilicon-gate planar CMOS process flow by Lynn Fuller [34] was modified by the addition of required steps for deposition and patterning of the ferroelectric. If being fabricated at RIT, the author recommends keeping designed CMOS devices at a minimum length of 2  $\mu\text{m}$  to achieve highest yield, though adaptation of these processes to another process with smaller minimum feature size and varying gate material would be relatively straight-forward.

### 5.1 FTJ design

In an effort to keep the FTJ fully CMOS-compatible the electrodes were chosen to be Al and p- doped Si, as shown to be effective in Section 4.3. Each device is designed as a crossbar such that the area of an FTJ is the width of the p- electrode times the width of the Al electrode. This way, a larger array of FTJ devices are designed as horizontal p- lines (in "oxide" mask level) and vertical Al lines.

In order to predict and optimize FTJ performance, all equations from Section 4 were integrated into a flexible python program with user-interface for input of relevant material properties. The code for this program is given in Appendix A.

Interestingly, extracting memory window as a function of increasing screening length in the poor metal (assuming the other metal has a screening length of  $\delta_1 =$

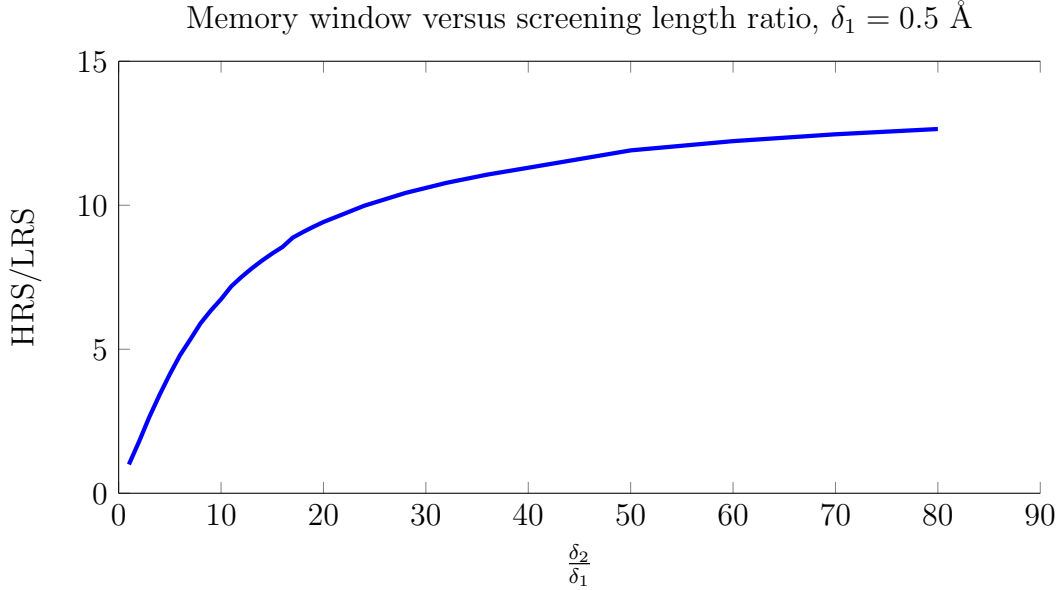


**Figure 5.1:** Simulated HRS/LRS increases with larger screening length ratio before plateauing around  $\frac{\delta_2}{\delta_1} \approx 60$ . For an Al/Al:HfO<sub>2</sub>/p+ Si FTJ with 2 nm ferroelectric.

0.5 Å), as shown in Figure 5.1, shows a saturation starting at around  $60 \approx \delta_2/\delta_1$  (corresponding to  $\delta_2 = 3$  nm, p+ Si  $N_a = 2 \times 10^{18} \text{ cm}^{-3}$ ).

Even more interestingly, varying the screening length in the "good" metal (while keeping the poor metal  $\delta_2 = 3$  nm), as shown in figure 5.2, yields two important conclusions. First, a metal with incredibly high carrier concentration ( $\delta_1 < 0.05 \text{ \AA}$ ) would actually cause a sharp decay in memory window, owing likely to the total screening of the depolarizing field at that interface and (by extension) a removal of its positive effect on introducing dissimilar barriers. Second, the memory window improves with increased screening length but reaches a maximum at  $\delta_1/\delta_2 \approx 0.38$ . This is likely due to increasing total available charges to contribute to depolarizing field until maximizing once charges are located too far away from the interface to contribute (as is the case in materials with a larger screening length). The screening length of the Al electrode could be increased by interface defects, oxide charges, or material impurities. The screening length of AlSi (10% Si) would also be larger than pure Al and approach the ideal value ( $\delta_1 = 1.14$  nm).



**Figure 5.2:** Simulated HRS/LRS for increasing  $\delta_1$ , showing a maximum. For an Al/Al:HfO<sub>2</sub>/p+ Si FTJ with 2 nm ferroelectric.

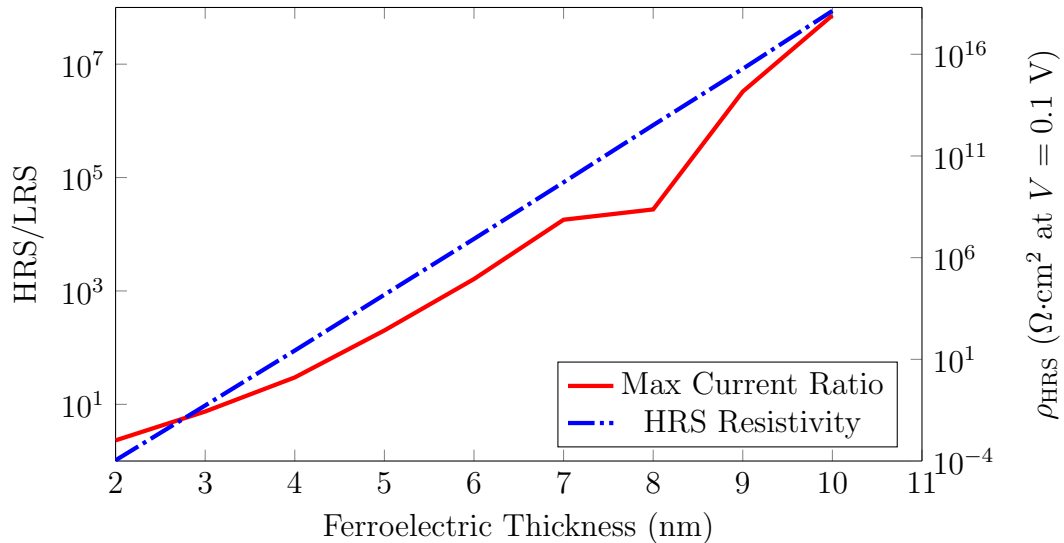


**Figure 5.3:** Simulated HRS/LRS and HRS resistivity for an Al/Al:HfO<sub>2</sub>/p+ Si FTJ with varying ferroelectric thickness.

## 5.2 State of the art FTJs

For this study, it is best to assume the Al electrode will behave non-optimally (having no impurities) and therefore, the FTJ design for the Al/Al:HfO<sub>2</sub>/p-Si device presented in this work has material properties  $\delta_1 = 0.06$  nm,  $X_1 = 4.08$  eV,  $\varepsilon_f = 40\varepsilon_0$ ,  $E_a = 2$  eV,  $P_r = 15\mu\text{C}/\text{cm}^2$ ,  $d = 2, 3$ , or  $5$ ,  $m^* = 0.11m_e$ ,  $\delta_2 = 3$  nm, and  $X_2 = 4.85$  eV. The Al:HfO<sub>2</sub> ferroelectric is adapted from the process used by Polakowski et. Al [35] and is assumed to behave with similar speed, polarization, and endurance performance. A comparison of this device to other state of the art FTJs is shown in Table 5.1. Importantly, the small coercive electric field ( $\mathcal{E}_c$ ) of HfO<sub>2</sub>-based ferroelectrics leads to a lower required program voltage (the coercive voltage,  $V_c$ ), and therefore lower power consumption, compared to BaTiO<sub>3</sub> and BiFeO<sub>3</sub> FTJs. Speed performance between FTJs are mostly similar, though endurance of HfO<sub>2</sub>-based devices is higher than that of BiFeO<sub>3</sub> devices. Most importantly, the Al/Al:HfO<sub>2</sub>/p-Si FTJ can be designed with either a 2, 3, or 5 nm ferroelectric layer; leading to performance with either lower high-state resistivity ( $\rho_{HRS}$ ) than all other FTJs (enabling high speed performance by minimizing  $\tau = RC$ ) while only exhibiting moderate power density (Pd) with a 2 nm ferroelectric or very high  $\rho_{HRS}$  with a potentially huge memory window of  $5 \times 10^5$  and extremely low power performance (2.5 fJ for each 500 nm<sup>2</sup> device) with a 5 nm ferroelectric (more ideal for NMC applications where a large memory window permits more memory states). At a more moderate performance optimization, a 3 nm ferroelectric in the Al/Al:HfO<sub>2</sub>/p-Si FTJ yields a memory window similar to that of the BaTiO<sub>3</sub> FTJ reported by Abuwasib et. Al [9] but achieves lower power consumption by a factor of  $\approx 1 \times 10^{-3}$ . All three of these simulation results indicate that Al:HfO<sub>2</sub>-based FTJs are superior to both alternative technologies and FTJs using competing ferroelectrics for both neuromorphic computing and nonvolatile memory applications, excelling at low-power high-speed performance.

**CHAPTER 5. DESIGN OF FERROELECTRIC HFO<sub>2</sub>-BASED FTJs AND INTEGRATION WITH CMOS PROCESS**

---

Researcher [cite]	Device	Materials	$\mathcal{E}_c$ (V/cm)	Area	CMOS?
Chanthbouala et. Al [36]	FTJ	Co/BaTiO <sub>3</sub> /LSMO	$1\times 10^7$	0.096	No
Abuwasib et. Al [9]	FTJ	Co/BaTiO <sub>3</sub> /LSMO	$1\times 10^7$	0.303	No
Boyn et. Al [12]	FTJ	Co/BiFeO <sub>3</sub> /CCMO	$3.3\times 10^6$	0.125	No
Mueller, Schroeder et. Al [37, 38]	MIM	Pt/TiN/Si-HfO <sub>2</sub> /TiN	$1\times 10^5$	10000	Yes
Polakowski et. Al [35]	MIM	TiN/Al:HfO <sub>2</sub> /TiN	$1\times 10^5$	50	Yes
This Work (Based on Simulations)	FTJ	Al/Al:HfO <sub>2</sub> /p-Si	$1\times 10^5$	0.25	Yes

Research	$d$ (nm)	$\rho_{\text{HRS}}$ ( $\Omega \cdot \text{cm}^2$ )	HRS/LRS	$P_r$	Speed	Endurance	$V_c$	Pd ( $\text{W}/\text{cm}^2$ )
[36]	2	$4.8\times 10^{-2}$	300	-	10 ns	-	2.0	83.3
[9]	2	$4.8\times 10^{-3}$	60	-	-	-	2.0	823
[12]	4.6	$5\times 10^{-2}$	1000	100	100 ns	$4\times 10^6$	1.5	45
[37, 38]	10	-	-	17	10 ns	$1\times 10^{10}$	1.0	
[35]	12	-	-	15	not rep.	$2\times 10^9$	1.2	
This Work	2	$1.8\times 10^{-4}$	6.2				0.2	222
	3	$1.54\times 10^{-1}$	90	15	10 ns		0.3	0.584
	5	$2.3\times 10^5$	500000				0.5	$1\times 10^{-6}$

**Table 5.1:** Tables comparing relevant performance data for this research work to state of the art FTJs. LSMO stands for  $\text{La}_x\text{Sr}_{1-x}\text{MnO}_3$  and CCMO is  $\text{Ca}_{0.96}\text{Ce}_{0.04}\text{MnO}_3$ . Area units are  $\mu\text{m}^2$ . Pd is surface power density and  $P_r$  is remanent polarization in ( $\mu\text{C}/\text{cm}^2$ ).

### 5.3 Designed CMOS-process with FTJ-fabrication steps

Step Number	Step Code	Step Description	Tool	Time (hrs)
1	OX05	pad oxide 500 Å, Tube 4, 45 min at 1000C	Bruce Furnace 4	3
2	CV02	1500 Å Si <sub>3</sub> N <sub>4</sub> LPCVD Deposition, 30 min at 810C	LPCVD Nitride	4
3	PH03	level 1- Oxide - Clear Field	ASML & SSI	1
4	ET29	Plasma etch Nitride, 1500 Å target	LAM 490	0.3
5	ET07	ash all photoresist	Gasonics Asher	0.15
6	CL01	RCA clean	RCA Bench	0.85
7	OX04	First Oxide Tube 1, 3650 Å Bruce 1 Recipe 330, 55 mins at 1000C	Bruce Furnace 1	2.65
8	ET06	Etch Oxide, 3650 Å target, BOE 7tol for 3.6 min	7tol BOE	0.25
9	OX04	2nd Oxide Tube 1, 3650 Å, Bruce 1 Recipe 330, 55 mins at 1000C	Bruce Furnace 1	2.65
10	ET19	Nitride etch, 30s dip 5:1 BHF, 20 min Hot Phosphoric Acid 175C	Hot Phos Bench	1
11	PH03	level 2 Nwell - Dark Field	ASML & SSI	1
12	IM01	Cover bottom of wafer: Nwell top, 3E13, P31, 170 KeV	Varian Implanter	2
13	ET07	ash all photoresist	Gasonics Asher	0.15
14	PH03	level 3 – Pwell - dark field (or clear field Nwell mask with neg resist)	ASML & SSI	1
15	IM01	Cover top of wafer, Pwell bottom, 8E13, B11, 80 KeV	Varian Implanter	2
16	ET07	ash all photoresist	Gasonics Asher	1
17	OX06	Well Drive, Tube 1 Recipe 11, 480 min at 1100C	Bruce Furnace 1	8
18	PH03	level 4 - NMOS Vt - dark field (or clear field Nwell mask with neg resist)	ASML & SSI	1

**CHAPTER 5. DESIGN OF FERROELECTRIC HFO<sub>2</sub>-BASED FTJs AND INTEGRATION WITH CMOS PROCESS**

---

Step Number	Step Code	Step Description	Tool	Time (hrs)
19	IM01	NMOS Vt, 7.95e12, P31, 60KeV	Varian Implanter	6
20	ET07	ash all photoresist	Gasonics Asher	0.15
21	PH03	level 5 – PMOS VT adjust - nwell level - dark field	ASML & SSI	1
22	IM01	PMOS Vt, 3.02e12, B11, 30 KeV	Varian Implanter	6
23	ET07	ash all photoresist	Gasonics Asher	0.15
24	ET06	etch 500 Å pad oxide, 50:1 H <sub>2</sub> O:HF (3.6 mins)	50:1 HF Etch	0.25
25	CL01	pre-gate oxide RCA clean (with extra etch, next stop)	RCA Bench	0.85
26	ET06	etch native oxide (extra 30s 50:1 HF dip)	RCA Bench	0.1
27	OX06	100 Å dry (N <sub>2</sub> O) gate oxide, Bruce Tube 4, Recipe 213, 60 mins at 900C	Bruce Furnace 4	3
28	CV01	LPCVD poly deposition, 4000 Å	LPCVD Polysilicon	4
29	PH03	level 6 – poly gate - clear field	ASML & SSI	1
30	ET08	poly gate plasma etch, 4000 Å target, FACPOLY recipe	Drytek Quad	0.5
31	ET07	ash all photoresist	Gasonics Asher	0.15
32	CL01	RCA clean	RCA Bench	0.85
33	OX05	poly re-ox, 500 Å, Bruce Tube 4 Recipe 250	Bruce Furnace 4	3
34	PH03	level 7 - p-LDD - dark field	ASML & SSI	1
35	IM01	PMOS LDD, 4E13, B11, 50 KeV	Varian Implanter	4
36	ET07	ash all photoresist	Gasonics Asher	0.15

**CHAPTER 5. DESIGN OF FERROELECTRIC HFO<sub>2</sub>-BASED FTJs AND INTEGRATION WITH CMOS PROCESS**

---

Step Number	Step Code	Step Description	Tool	Time (hrs)
37	PH03	level 8 - n-LDD - dark field	ASML & SSI	1
38	IM01	PMOS LDD, 4E13, P31, 60 KeV	Varian Implanter	4
39	ET07	ash all photoresist	Gasonics Asher	0.15
40	CL01	RCA clean	RCA Bench	0.85
41	CV02	LPCVD nitride spacer 3500 Å	LPCVD Nitride	4
42	ET39	sidewall spacer etch, 3500 Å target, FACSPCR 30scm SF6 and CFV3 (125mm/min)	Drytek Quad	0.5
43	PH03	level 9 - N+D/S - dark field	ASML & SSI	1
44	IM01	N+D/S, 4E15, P31, 60 KeV	Varian Implanter	2
45	ET07	ash all photoresist	Gasonics Asher	0.15
46	PH03	level 10 - P+ D/S - Pimp - Dark Field	ASML & SSI	1
47	IM01	P+D/S, 4E15, B11, 50 KeV	Varian Implanter	2
47(2)	IM01	Cover bottom of wafer: P+ top 4E15, B11, 50 KeV	Varian Implanter	2
48	ET07	Cover top half of wafer: N+ bottom 4E15, P31, 60 KeV ash all photoresist	Varian Implanter	2
49	CL01	RCA clean	RCA Bench	0.85
50	OX08	DS Anneal, Bruce 2, 3, Recipe 284, 45 min at 1000C	Bruce Furnace 2	3
51	ET06	silicide pad ox (500A) etch, 50:1 H2O HF	50:1 HF Etch	0.25

Step Number	Step Code	Step Description	Tool	Time (hrs)
52	ME03	HF dip & Ti Sputter	CVC601	3
53	RT01	RTP 1 min, 650C	RTP	1
54	ET11	Unreacted Ti Etch	Etch Bench	1
55	RT02	RTP 1 min, 800C	RTP	1
56	CV03	TEOS, P-5000, 4000 Å Oxide	P5000 TEOS Ch A	0.5
57	PH03	Photoresist mask to remove TEOS for ALD HfO <sub>2</sub> , Thick Resist COAT-FAC and DEVFAC Recipes - FEHfO <sub>2</sub> Level - Dark Field	ASML & SSI	1
58	ET06	TEOS Etch for HfO <sub>2</sub> area FACCUT, follow with 50:1 HF dip	Drytek Quad	0.5
59	ET07	Solvent Strip or Ash	Solvent Strip Bench	0.5
60	CV33	ALD HfO <sub>2</sub> Deposition w/ TiN	ALD	4
61	RT02	RTP 1 min, 800C	RTP	1
62	PH03	(optional) Half wafer protect	Karl Suss Contact Aligner Stepper	0.5
63	ET06	TiN wet etch with RCA 1 NH <sub>4</sub> OH:H <sub>2</sub> O <sub>2</sub> :H <sub>2</sub> O = 1:2:5 (APM) solution at 60 C. (1nm/s, [39])	Hot Plate with Pyrex Dish	1

**CHAPTER 5. DESIGN OF FERROELECTRIC HFO<sub>2</sub>-BASED FTJs AND INTEGRATION WITH CMOS PROCESS**

---

Step Number	Step Code	Step Description	Tool	Time (hrs)
64	ET07	(optional) Solvent Strip or Ash	Solvent Strip Bench	0.5
65	PH03	Photoresist mask to remove HfO <sub>2</sub> if not selective growth (Negative Resist) - FEHfO <sub>2</sub> Level - Dark Field	ASML & SSI	1
66	ET06	HfO <sub>2</sub> etch, 50:1 H <sub>2</sub> O:HF appx. 97s for 3nm HfO <sub>2</sub> , assuming 1:10 HfO <sub>2</sub> :SiO <sub>2</sub> selectivity. [40]	50:1 HF Etch	0.25
67	ET07	Solvent Strip or Ash	Gasonics Asher	0.15
68	PH03	level 11 - CC, Thick Resist COATFAC and DEVFAC Recipes - Cont level - dark field	ASML & SSI	1
69	ET06	CC etch, FACCUT, 200 W, 100 mT, 50 sccm CHF <sub>3</sub> , 10 sccm CF <sub>4</sub> , 100 sccm Ar	Drytek Qquad	0.5
70	ET07	ash all photoresist	Gasonics Asher	0.15
71	CL01	RCA clean	RCA Bench	0.85
72	ME01	Aluminum Sputter 7500 Å	CVC601	1
73	PH03	level 12 - Metal1, Thick resist, COATMTL and DEVMTL recipes, clear field plasma 125W, Al Etch, BCl, Cl <sub>2</sub> , Chloroform, Target 7500 Å	ASML & SSI	1
74	ET15		LAM4600	1.5

Step Number	Step Code	Step Description	Tool	Time (hrs)
75	ET07	ash all photoresist	Gasonics Asher	0.15
76	CV03	TEOS, P-5000, 4000 ÅOxide	P5000 TEOS Ch A	0.5
77	PH03	Vial - dark field	ASML & SSI	1
78	ET26	Via Etch	Drytek Quad	0.5
79	ME01	Al Deposition	CVC601	1
80	PH03	Metal 2 - clear field	ASML & SSI	1
81	ET15	plasma 125W, Al Etch, BC <sub>l</sub> , Cl <sub>2</sub> , Chloroform, Target 7500 Å	LAM4600	1.5
82	ET07	ash all photoresist	Gasonics Asher	0.15
83	CV03	TEOS, P-5000, 4000 ÅOxide	P5000 TEOS Ch A	0.5
84	PH03	Via2 - dark field	ASML & SSI	1
85	ET26	Via Etch	Drytek Quad	0.5

Step Number	Step Code	Step Description	Tool	Time (hrs)
86	ME01	Al Deposition	CVC601	1
87	PH03	Metal 3 - clear field	ASML & SSI	1
88	ET15	plasma 125W, Al Etch, BCl, Cl <sub>2</sub> , Chloroform, Target 7500 Å	LAM4600	1.5
89	ET07	ash all photoresist	Gasonics Asher	0.15
90	CV03	TEOS, P-5000, 4000 Å Oxide	P5000 TEOS Ch A	0.5
91	PH03	Via3 - dark field	ASML & SSI	1
92	ET26	Via Etch	Drytek Quad	0.5
93	ME01	Al Deposition	CVC601	1
94	PH03	Metal 4 - clear field	ASML & SSI	1
95	ET15	plasma 125W, Al Etch, BCl, Cl <sub>2</sub> , Chloroform, Target 7500 Å	LAM4600	1.5
96	ET07	ash all photoresist	Gasonics Asher	0.15
97	SI01	sinter	Bruce	2

To minimize additional process steps, the p-Si electrode is defined by the pseudo-STI field oxide growth (steps 3-9) which also defines the active areas of transistors. This process does exhibit some feature thinning, so a 2  $\mu\text{m}$  line on mask (transferred to nitride) yields approximately a 250 nm line width of exposed silicon for the electrode. The p- doping is introduced during the implant for PMOS-device source/drain, step 47. A modified version of step 47, called step 47(2), can be used to study the affect of n-doping instead of p-doping the lower (M2) electrode, but cannot be used with full CMOS integration. To confine Al:HfO<sub>2</sub> to FTJ areas, the same tetra-ethyl orthosilicate (TEOS) oxide used as an interlevel dielectric (ILD) below each metal layer is deposited, step 56, and patterned, step 57, to open windows to FTJ areas before Al:HfO<sub>2</sub> deposition by ALD, step 60. The Al:HfO<sub>2</sub> is also capped in-situ with TiN before being annealed in RTP (to form the ferroelectric state), step 61. The TiN must then be removed, since it is conducting and would cause device shorts, and is selectively removed, in step 63, by the SC1 chemistry used in a standard RCA clean (at a rate of 1nm/s), as shown by Liu et. al [39]. This must be done in a pyrex dish on a hot plate in a wet etch bench, not in the RCA bench, to avoid contamination. Finally, the same mask used to open windows in the TEOS can be used with negative resist, in step 65, to create a soft mask protecting the FTJ areas and then etch the Al:HfO<sub>2</sub>, in step 66, from unwanted areas (though this is not necessary). Having already deposited the TEOS oxide, the contact cuts can be etched, step 69, and metal 1 (Al) deposited, step 72, and patterned, steps 73 and 74. The metal 1 mask is therefore also defining the Al electrodes for the FTJs! In whole, the only extra steps for FTJ-fabrication are the TEOS oxide etch, ferroelectric deposition and anneal, and TiN/ferroelectric etching only requiring one extra mask. A shortened version of this process, with only the required steps to fabricate FTJ devices, is given in Appendix B.

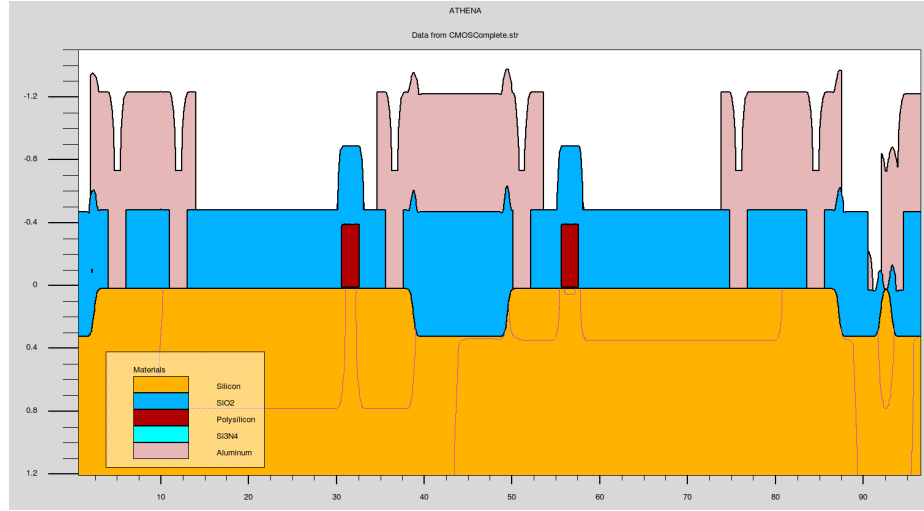


**Figure 5.4:** Athena simulation of CMOS devices tuned for low threshold voltages (left) and FTJ device (right).

## 5.4 Process simulation

*Silvaco* is a semiconductor simulation tool used often in both academic and industry research. It has modules for process simulation, *Athena*, and electrical simulation of a simulated process, *Atlas*; though electrical simulations are more suited to transistor performance and related connections. In order to verify the proposed process design, from Section 5.3, it was simulated using *Athena*. The code is included in Appendix C and important figures are shown in this section. Importantly, the CMOS devices are shown in Figure 5.4, showing appropriate wells and junction depths for source/drain. The window opened in TEOS is shown to be appropriate for isolating ferroelectric to desired areas, shown in Figure 5.5 with SiO<sub>2</sub> substituted for HfO<sub>2</sub> since *Athena* does not have it. This simulation platform was also used to fine tune the use of wet etch before HfO<sub>2</sub> deposition to accurately reach 250 nm device width, shown in Figure 5.6.

For implementation within another process node or with transistors of differing threshold voltage, *Athena* simulation should be repeated with corrected well, threshold adjust, and source/drain implants. Surface doping of the FTJ region should be extracted and used for recalculation of  $\delta_2$  and corresponding memory window.

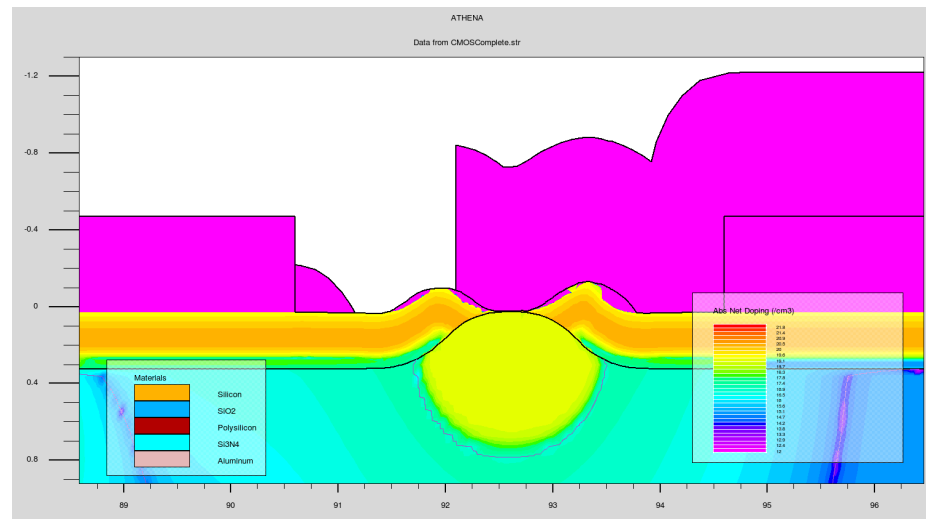


**Figure 5.5:** Athena simulation of FTJ device (SiO<sub>2</sub> substituted for ferroelectric).

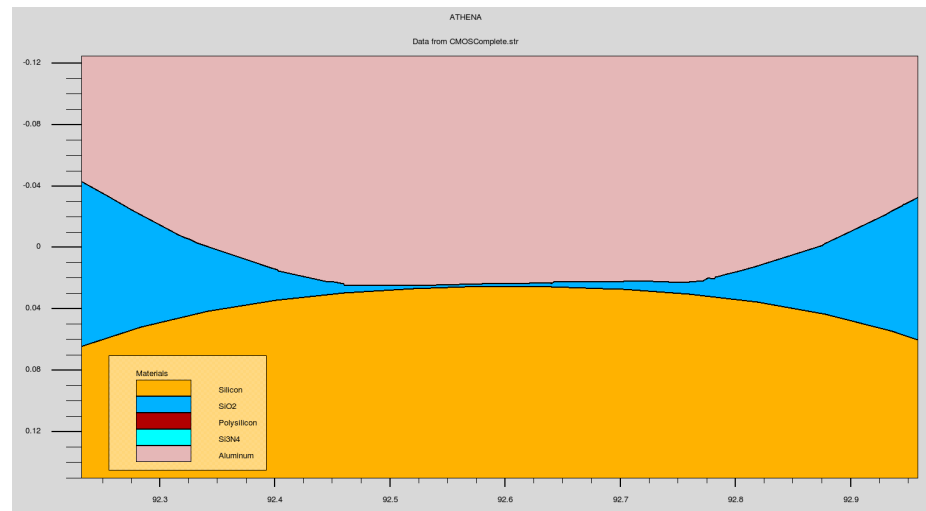


**Figure 5.6:** Zoom of FTJ device showing  $\approx 250$  nm device width.

# Chapter 6

---

## System Design and Simulations for Digital Memory Applications

The designs of all circuits were performed in *Cadence Virtuoso* using a 45 nm CMOS PDK. The design rules of this PDK are consistent with those required for the 2 um process to be performed at RIT but allowed for easier use of the DRC and LVS tools native to this PDK. Additionally, this allowed for performance simulation representative of implementation with fairly modern devices. When implemented in the 2 um CMOS process at RIT, the mask file from *Virtuoso* was simply scaled up (from 45 nm to 2 um, a factor of 44.44) before mask printing.

### 6.1 Read/Write scheme

When writing an FTJ, the bias applied across it must meet or exceed the coercive voltage,  $V_c$ , in order to flip the polarization to the desired direction (over any reasonable amount of time). While reading, the bias must be less than  $V_c$  in order to prevent state disturbance. Let's take, for example, an FTJ with  $V_c = 0.5$  V. As shown in Figure 6.1, these schemes would work to write the HRS and LRS as shown and to read the device (since read will always be performed in the same direction).

However, FTJs are often (if not always) designed in an array (like most memory). Within this array, the positive terminals are connected to rows and the negative terminals to columns, as shown in Figure 6.2. Using the address scheme from before,

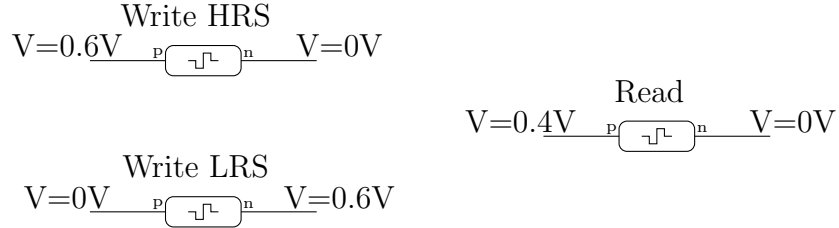


**Figure 6.1:** An address scheme which, though appropriate for a stand-alone device, would be inappropriate for devices in an array.

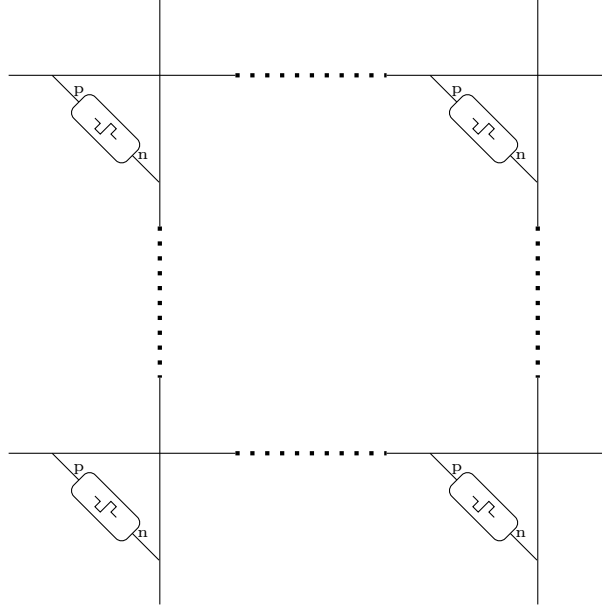


**Figure 6.2:** A simple schematic showing the typical connectivity of FTJ devices in an array, for both memory or neuromorphic logic applications. Lines and columns only connect through FTJ devices and do not connect at intersections. Dotted lines indicate an arbitrary number of repeated lines and columns.

other non-addressed devices in that row or column would experience the same bias as the addressed device!

Ultimately, the best solution to this will be one of two options and will be up to the system designer. The first option is to have rails centered around ground such that the write rails are (for our example)  $V_{DD}=0.3$  V and  $V_{SS}=-0.3$  V, read rails are  $v_{dda}=0.2$  V and  $v_{ssa}=-0.2$  V and whenever a column or row is not being addressed it should be grounded. That way, the write scheme follows Figure 6.3 for addressed devices and non-addressed devices, shown in Figure 6.4 (in same row), are not disturbed during

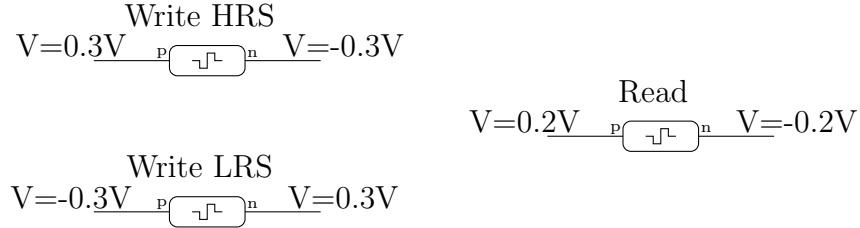


**Figure 6.3:** An address scheme appropriate for FTJs in an array.

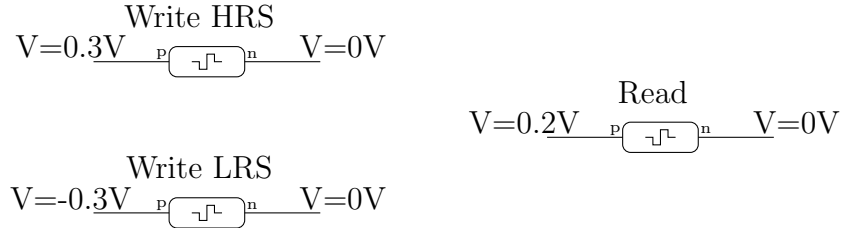


**Figure 6.4:** Non-addressed devices in the same row, for various write/read states. Non-addressed devices in the same column would experience the opposite bias. In this way, these devices will not be disturbed.

read or write.

Though this address choice does allow non-addressed devices to stay at ground, preventing current flow through the FTJ devices to the bulk silicon (which is typically grounded) it does require CMOS devices with near-zero threshold voltage. If this is undesirable, another option is to shift all rails by  $+V_{DD}$ , leaving the write rail low at 0V but requiring all non-addressed lines to be held (for our example) at 0.3V. Ultimately, this is the decision of the system designer and depends on related process constraints.

## 6.2 Linear resistance change simulation

The most simple way to model the changing resistance of an FTJ is to first calculate, using equations from Chapter 4, the resistance of each state (at the read bias) using material properties appropriate for the chosen device. The model written in *Verilog-A*, given in Appendix D.1.1, assumes that the resistance would change linearly over some chosen "transition time" while biased above  $|V_c|$  towards the corresponding

state and saturate once reaching the resistance of that state. Simulation results using CMOS devices from the 45nm PDK of *Cadence Virtuoso* (used for ease of DRC and LVS, and for results more representative of a modern CMOS process) are shown in Figure 6.10 and are useful for digital memory applications, with write times of  $\approx 0.6$  ns for HRS and  $\approx 0.3$  ns for LRS and read times of  $\approx 10$  ns for HRS and  $\approx 4$  ns for LRS. However, brain-inspired computing systems, which require precise control as the device transitions from one state to the other, need a more complicated simulation which models polarization change versus time and corresponding resistance.

### 6.3 Timing-based simulation

Working with data for polarization versus program time from Schroeder et. al [41], piece-wise polynomial models were fit to the data and used to direct further study of the general phenomena of timing in ferroelectrics. Some modeled curves are given in Figure 6.5 and the equation and relevant model fit parameters are given by Equation 6.1. Though these curves suggest switching times close to 1  $\mu$ s, the group posits that this data was influenced by the test setup delay and that realistic switching times are in the 1 ns range [41].

$$2Pr(V, t) = \text{MIN} \left( \begin{array}{l} \text{MIN}(13.071 * V^{2.929}, 6.339 * V + 27.357) \\ , \text{MAX}(\text{MIN}(D + E * \ln(t), \text{MAX}(A + B \log(t) + C \log^2(t), 0)), 0) \end{array} \right)$$

$$A = \text{MAX}(445.4V - 416.102, 22V)$$

$$B = \text{MAX}(118.125V - 112.071, 5.8V)$$

$$C = \text{MAX}(7.782V - 7.525, 0.26V)$$

$$D = \text{MIN}(9.904V + 17.865, 19.375V^2 - 6.3V + 1.4)$$

$$E = \text{MAX}(9.105V - 5.152 - 3.387V^2, 0.217)$$
(6.1)

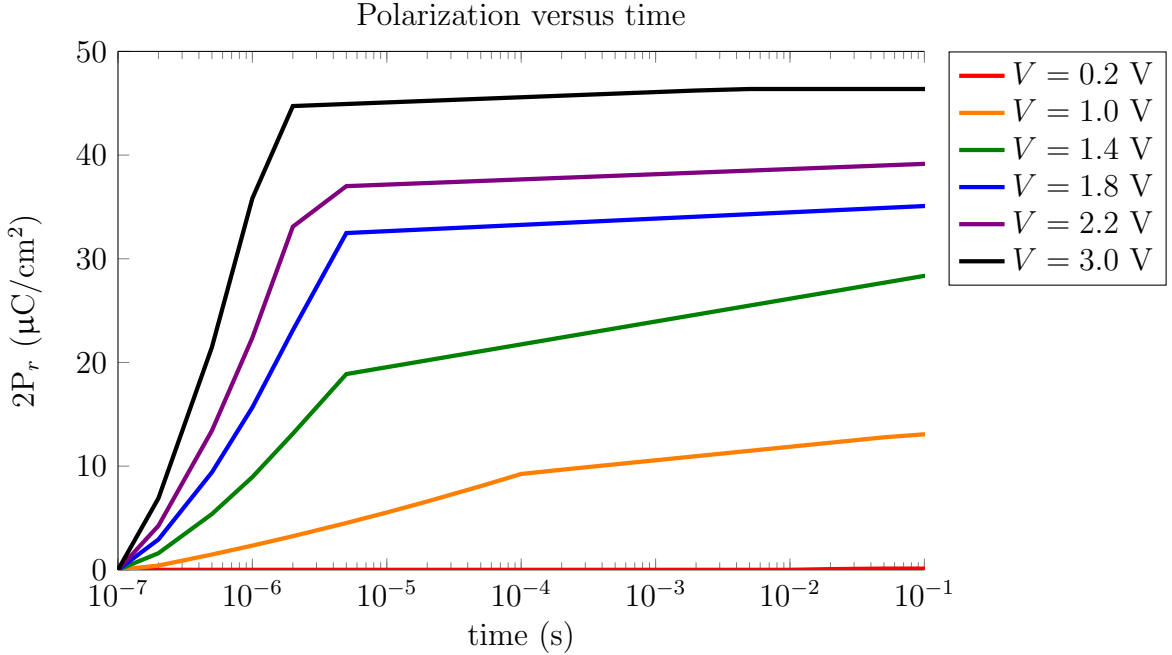


**Figure 6.5:** Changing polarization as a function of time for varying applied voltages for a sample with  $V_c \approx 0.9$  V.

As discussed in Section 2.4, total polarization in ferroelectric materials is the aggregate contribution of many domains, each having their own switching voltages and times depending upon their orientation (referenced to the applied field). As such, the model was binned into domains by subtracting a total curve of  $V = V_a - 0.2$  from  $V = V_a$ , therefore giving the polarization contribution for ferroelectric domains having switching voltages  $V_a - 0.2 < V_c < V_a$ . These curves were modified by capping at maximum (removing decreasing polarization for increasing time) and are shown in Figure 6.6.

One would logically expect a normal distribution of domains; with very few having low coercive voltage, very many switching at some moderate voltage, and very few being oriented so close to  $90^\circ$  from the applied field to have very high coercive voltage. Though a bit noisy, owing likely to the multiple normalizations performed on the curves in previous model steps, the maximum domain contributions shown in Figure 6.7 do suggest this type of normal distribution, centered around  $V_c = 0.9$  V but

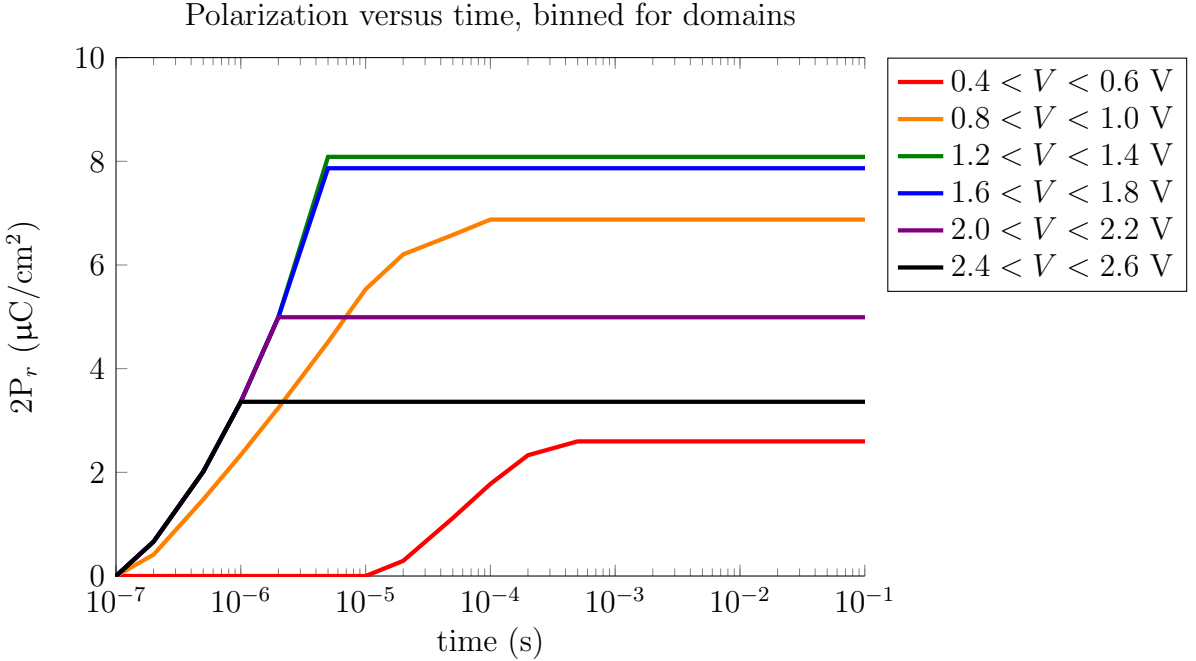


**Figure 6.6:** Changing polarization as a function of time binned for domains existing in 0.2V intervals for a sample with  $V_c \approx 0.9$  V. Only a subset of curves are plotted. The models work best when binned from 0.2V to 3V in 0.2V intervals.

having a very long right-sided tail. Further, Figure 6.8 plots switching times binned for domains and shows that for higher voltages the switching times decrease. This should make some sense, considering domains which require larger voltages to switch have more excess energy while switching and therefore transition faster.

Finally, the model equations for polarization versus time binned for domains were implemented in a *Verilog-A* model, given in Appendix D.2.1, which keeps track of each domain's contribution based on applied voltage and aggregate time. The model then calculates corresponding resistance based on the current total polarization, given material constants, using equations from Section 4.3.

## 6.4 Address systems

The interconnectivity described is shown in Figure 6.9 connected to a single FTJ which uses the linear resistance *Verilog-A* model, from Appendix D.1.1. Systems for

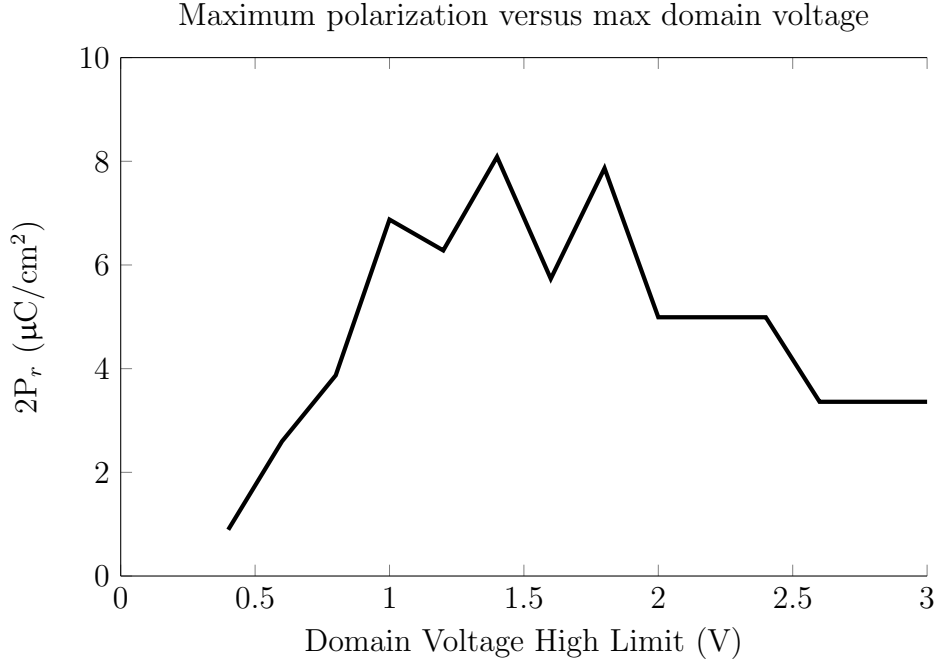


**Figure 6.7:** Maximum polarization for domains binned to 0.2V intervals, resembling a noisy normal distribution with a long right-sided tail.

addressing FTJ devices, following the read/write scheme given in Section 6.1, were designed as tristate CMOS cells using both 45 nm devices and 2  $\mu\text{m}$  devices, though only 45 nm system performance will be examined here (since those results more closely describe the capabilities of these memories). The tristate devices, shown in Appendices D.3 through D.7, accept read enable (Ren), write enable (Wen), and write line (W) signals and toggle the output to desired voltages. SAP\_ADDRESS\_ROW\_W and SAP\_ADDRESS\_COLUMN\_W are used to toggle a connected row and column (positive and negative FTJ terminal) to high ( $V_{DD}$ ) and low ( $V_{SS}$ ) write voltages, respectively when Wen is high and W is high (writing the HRS). When Wen is high but W is low (writing LRS) the row is pulled to low write voltage and column to high. Read voltages applied by SAP\_ADDRESS\_ROW\_R and SAP\_ADDRESS\_COLUMN\_R, when Ren is high, always bring the row to read high ( $v_{dda}$ ) and the column to read low ( $v_{ssa}$ ). The column read voltage is applied to a reference resistor in series with the FTJ (and the rest of the column) and output is taken from an inverter taking its

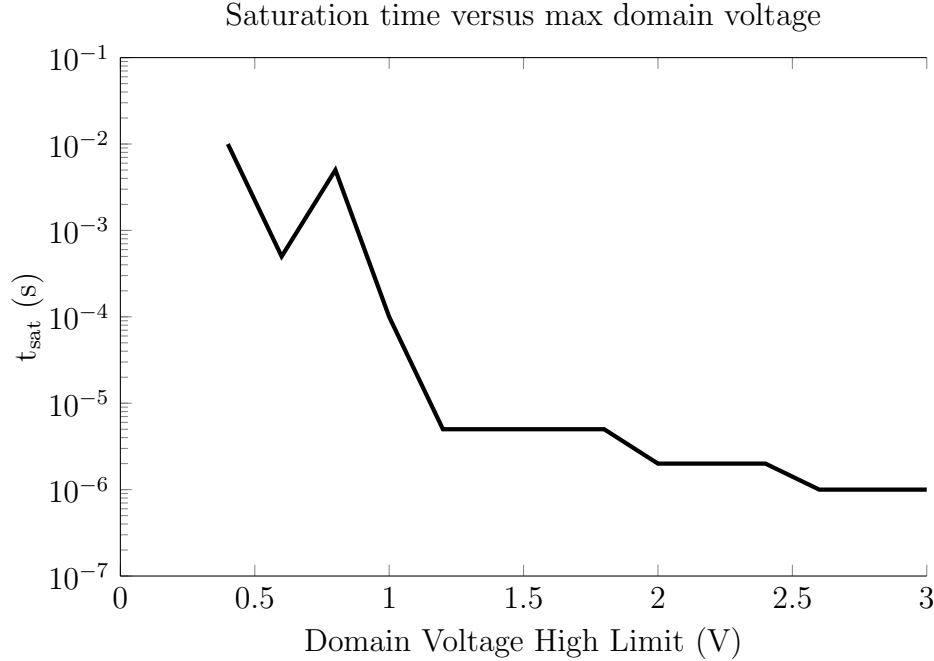


**Figure 6.8:** Time until polarization saturation for domains binned to 0.2V intervals. Higher energy domains (oriented less parallel to the applied field) switch faster due to excess energy.

input from the node ( $V_o$ ) between the reference resistor and the FTJ. In this way, if  $R_{FTJ} > R_{ref}$  then  $V_o$  pulls to  $v_{ssa}$  and the inverter pulls to  $V_{DD}$ . If  $R_{FTJ} < R_{ref}$ , then  $V_o$  pulls to  $v_{dda}$  and the inverter transitions to  $V_{SS}$ . SAP\_ADDRESS\_GND\_vcc is used to hold rows and/or columns at vcc whenever not being written or read, to prevent write/read disturbs. To ensure all of the write voltage and vcc makes it to the FTJ, a pass transistor is connected in series with the reference resistor and is set to be off only while reading. Shown in figures 6.10 and 6.11 are simulation outputs of this system, showing read times of 10 ns and write times as short as 0.3 ns.

## 6.5 Simulation results - $4 \times 4$ Array

A testbench, code given in Appendix D.10, was written in *Verilog* which programs a  $4 \times 4$  array of FTJ, as shown in Appendix D.9, all to HRS and then writes binary numbers 0 through 15 on the first row. Writing devices in an array is a two-step

process; one step writes devices to HRS and the next step to LRS. After writing each number, the row is read to check for write errors, then the row below it is read to check for write disturbs, and finally the original row is read again to check for read disturbs. A small portion of waveforms are shown in Figure 6.12, showing 10ns read and write pulses separated by 10ns guard times for relaxation of excess voltage from capacitive discharging. This system exhibits no write errors, write disturbs, or read disturbs.

A series of tests writing random binary numbers from 0 to 15 to random rows of the array exhibits 100% accuracy, shown in Figure 6.13, but often causes *Spectre* simulation to crash by not converging. Minor modifications may need to be made to the *Verilog-A* model to smooth edges and prevent convergence issues.

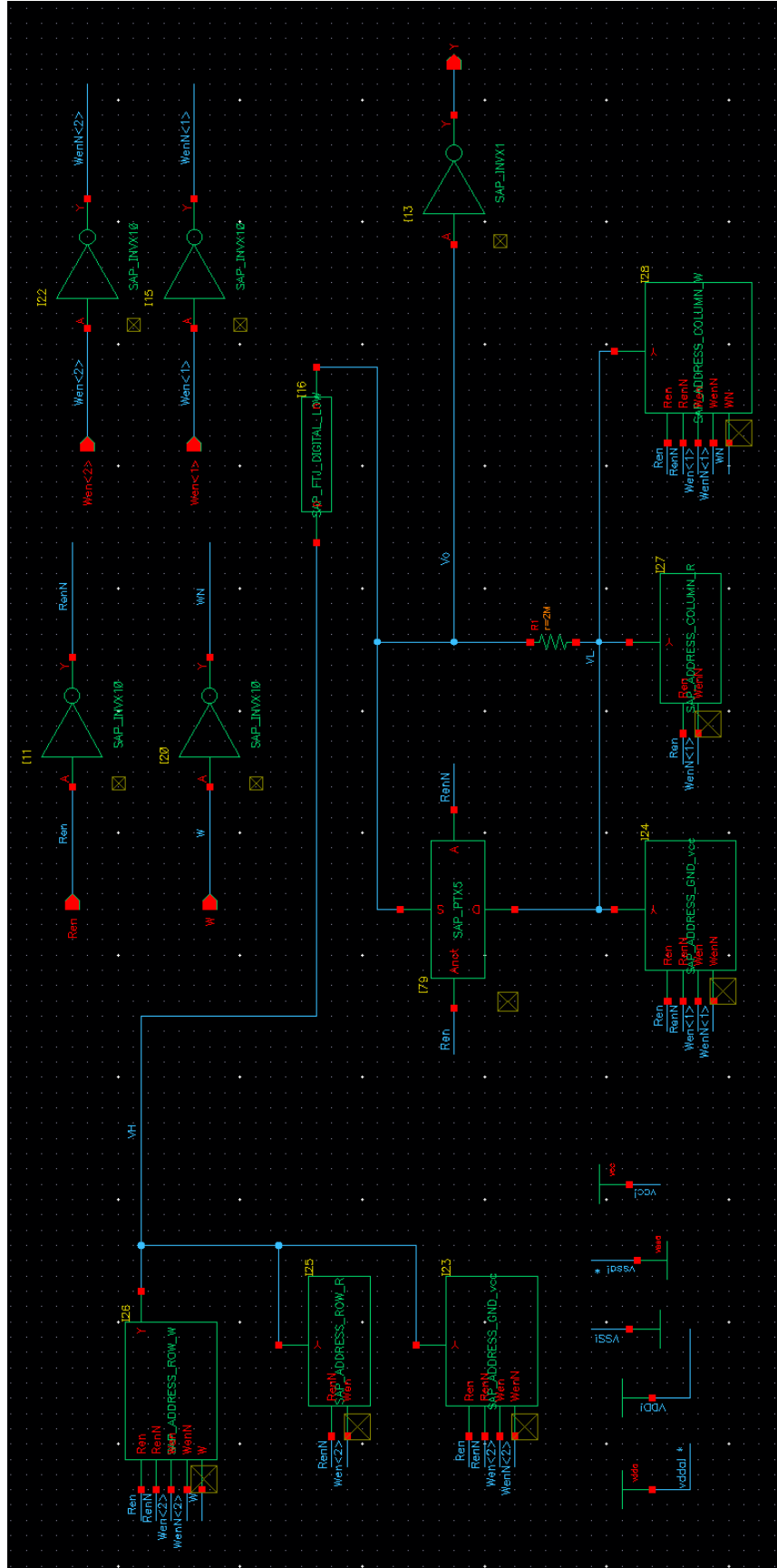


**Figure 6.9:** Schematic of address systems connected to a single FTJ. Note the inverted output taken above the reference resistor and the pass transistor to bypass that resistor while writing and applying vcc. The FTJ simulates with a LRS of 300 K $\Omega$  and HRS of 10 M $\Omega$ . The reference resistor is 2 M $\Omega$ .

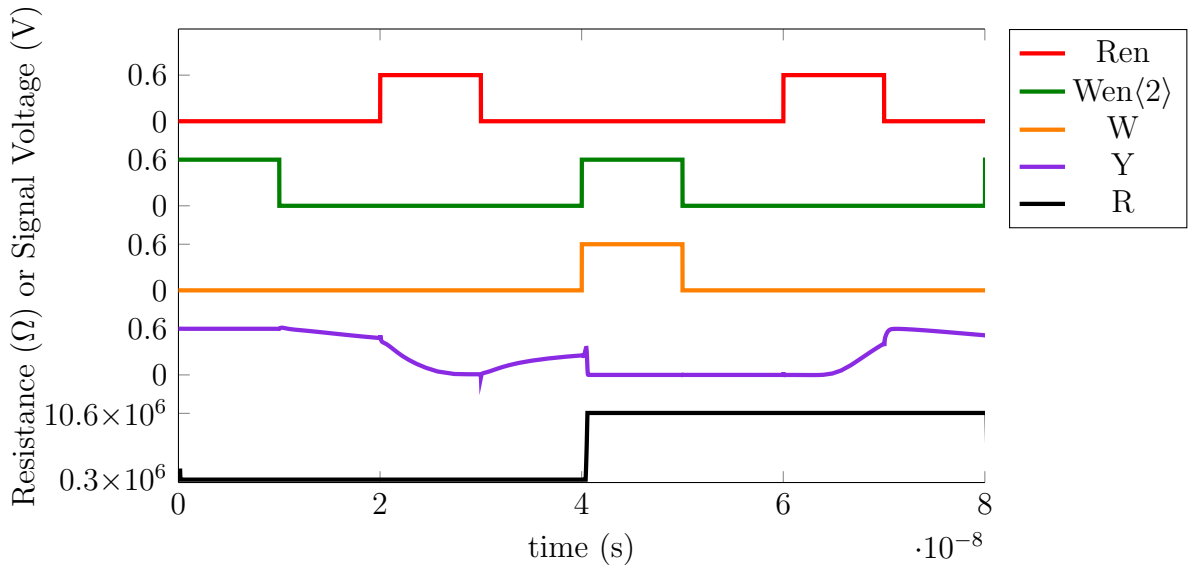


**Figure 6.10:** Simulation results from a single FTJ device connected to address circuitry designed with 45 nm CMOS.  $\text{Wen}\langle 1 \rangle$  follows the same curve as  $\text{Wen}\langle 2 \rangle$  in this simulation. Notice that the output,  $Y$ , transitions low when reading (Ren high) an FTJ in LRS and transitions high when reading an HRS FTJ. Write and read times are 10 ns.

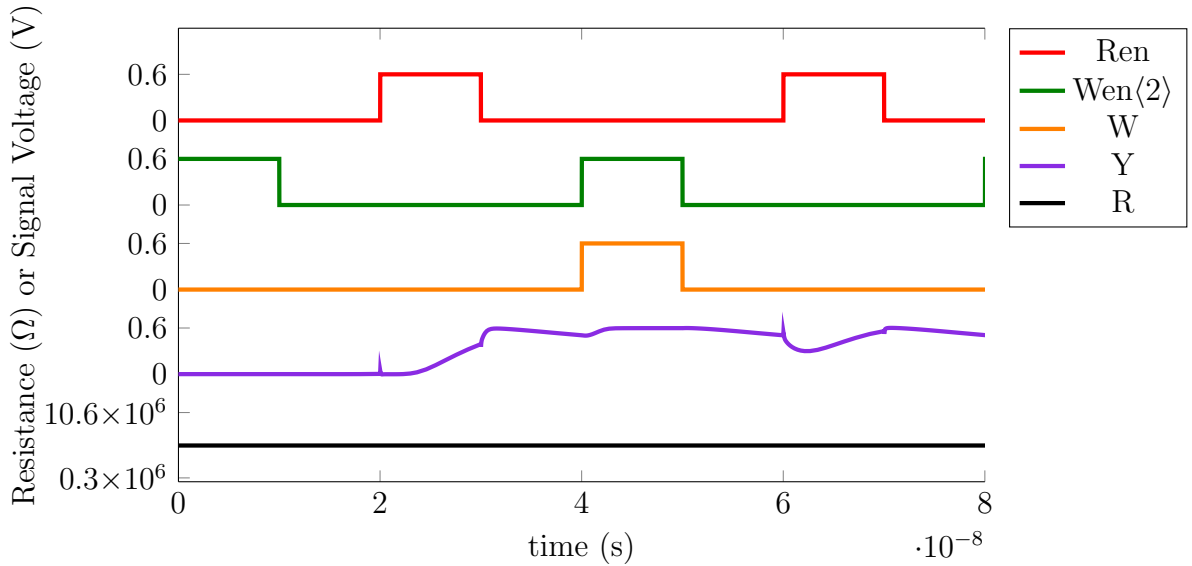


**Figure 6.11:** Simulation results from a single FTJ device connected to address circuitry designed with 45 nm CMOS.  $\text{Wen}\langle 1 \rangle$  is constantly off in this simulation; testing for write disturb when programming a different device in the same row, once in an array. The FTJ state remains unchanged even after write enable toggles for high and low writes, verifying that this system is robust against write disturbs of non-addressed devices.



**Figure 6.12:** Small portion of waveform while writing binary 0 to 15 in one row while all other FTJ in the  $4 \times 4$  array are in HRS.

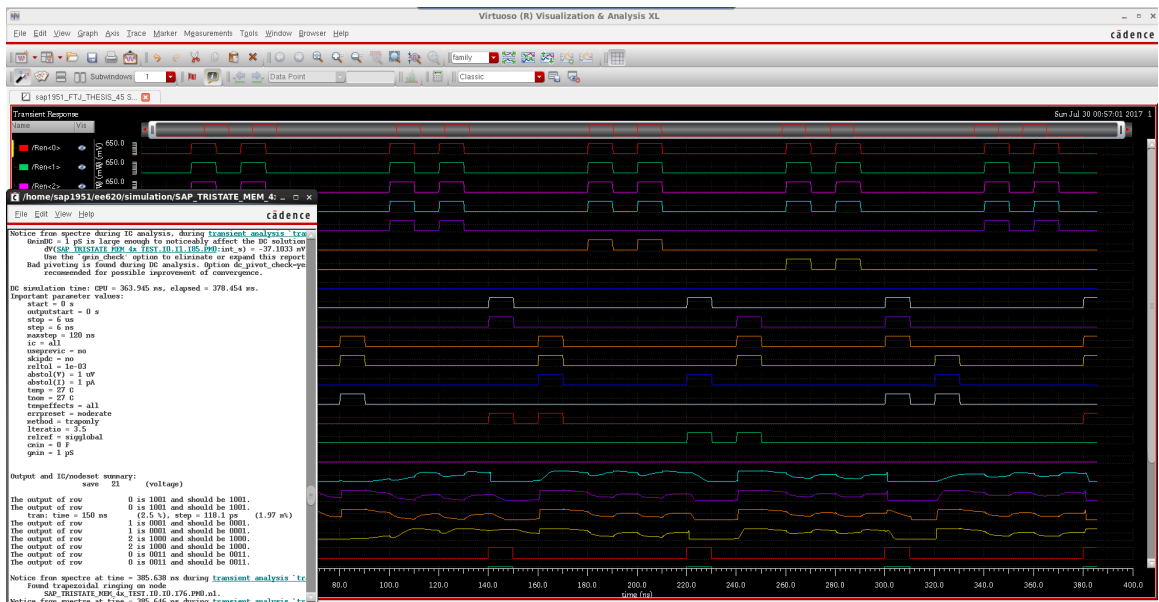


**Figure 6.13:** Waveform and simulation log for random binary numbers being written to random rows of the  $4 \times 4$  array.

# Chapter 7

---

## Conclusions

This work has laid a nearly comprehensive framework for fabrication of FTJ devices with/without connected CMOS devices, from material to architecture. The physical phenomena present within ferroelectric materials was examined as a function of crystal structure and domains. FTJ device structures were modeled as a function of material properties and methods of extracting corresponding performance metrics (using a custom-built python code) were presented and evaluated for the proposed Al/Al:HfO<sub>2</sub>/p-Si FTJ (having  $\delta_1 = 0.06$  nm,  $\chi_1 = 4.08$  eV,  $\varepsilon_f = 40\varepsilon_0$ ,  $E_a = 2$  eV,  $P_r = 15\mu\text{C}/\text{cm}^2$ ,  $d = 2, 3$ , or  $5$ ,  $m^* = 0.11m_e$ ,  $\delta_2 = 3$  nm, and  $\chi_2 = 4.85$  eV) which exhibits a memory window as high as HRS/LRS  $\approx 5 \times 10^5$  with max current density of  $\approx 3 \times 10^{-2}$  A/cm<sup>2</sup> and power density of 1  $\mu\text{W}/\text{cm}^2$  with a 5 nm ferroelectric, enabling ultra-low power computing (compared to 45 W/cm<sup>2</sup> for competing FTJ devices) at high speeds. Using a 2 nm ferroelectric, the FTJ can achieve current density as high as  $8 \times 10^3$  A/cm<sup>2</sup> with a memory window of HRS/LRS  $\approx 6$ , targeting higher speed applications. These devices are therefore capable of lower power and higher speed performance than any alternative memristor technology, shown in sections 3.4 and 5.1, including competing FTJ devices.

The FTJs designed and simulated were then integrated into a new process flow, based on a twin-well polysilicon gate planar-CMOS technology, which was verified by *Silvaco Athena* simulation. Algorithms for read and write of devices in an array were

proposed, implemented by systems designed using a 45nm CMOS process design kit in *Cadence Virtuoso Design Suite*, and successfully simulated (using a Verilog testbench for stimulation) as digital memory storage devices in a  $4 \times 4$  array architecture, with write and read times as low as 0.3 ns and 10ns, respectively.

## 7.1 Future Work

Ten device wafers are currently at step 22 of the FTJ-only process, shown in Appendix B, and will be completed by a future student. These wafers will be split into three groups of three wafers (with one left over), two of which will be sent to NamLAB and UCB for Si:HfO<sub>2</sub> and HfZrO<sub>2</sub> film deposition, respectively, on each wafer at one of three different thicknesses (the author recommends 2, 5, and 8nm). Once samples are completed, experimental results for  $P_r$ ,  $t_{\text{sat}}$ ,  $E_c$ , and resistances/current densities in each state, along with more detailed timing data for switching transitions, should be compiled and implemented in the polarization-timing FTJ model *Verilog-A* code, shown in Appendix D.2.1, which will be stored on the RIT gitlab. Finally, these models based on experimental data should be implemented with a brain-inspired computing system to examine performance of these devices in such an application. These designs could then be fabricated either by RIT (scaled to 2  $\mu\text{m}$  CMOS) or an external foundry.

## References

---

- [1] Y. Shimakawa, M. Azuma, and N. Ichikawa, “Multiferroic Compounds with Double-Perovskite Structures,” *Materials*, vol. 4, no. 1, pp. 153–168, Jan. 2011. [Online]. Available: <http://www.mdpi.com/1996-1944/4/1/153>
- [2] A. B. Kaufman, “An expandable ferroelectric random access memory,” *IEEE Transactions on Computers*, vol. C-22, no. 2, pp. 154–158, Feb 1973.
- [3] J. R. Contreras, J. Schubert, H. Kohlstedt, and R. Waser, “Memory device based on a ferroelectric tunnel junction,” in *Device Research Conference, 2002. 60th DRC. Conference Digest*, June 2002, pp. 97–98.
- [4] M. Zhuravlev, R. Sabirianov, S. Jaswal, and E. Tsymbal, “Giant electroresistance in ferroelectric tunnel junctions,” *PHYSICAL REVIEW LETTERS*, vol. 94, no. 24, JUN 24 2005.
- [5] A. Aziz, N. Shukla, S. Datta, and S. K. Gupta, “Coast: Correlated material assisted stt mrams for optimized read operation,” in *2015 IEEE/ACM International Symposium on Low Power Electronics and Design (ISLPED)*, July 2015, pp. 1–6.
- [6] S. Lee, K. Kim, K. Kim, U. Pi, Y. Jang, U. i. Chung, I. Yoo, and K. Kim, “Highly scalable stt-mram with 3-dimensional cell structure using in-plane magnetic anisotropy materials,” in *2012 Symposium on VLSI Technology (VLSIT)*, June 2012, pp. 65–66.
- [7] I. E. Ebong and P. Mazumder, “Cmos and memristor-based neural network design for position detection,” *Proceedings of the IEEE*, vol. 100, no. 6, pp. 2050–2060, June 2012.

## REFERENCES

---

- [8] S. Kim, H. Wong, Y. Cui, Y. Nishi, and S. U. D. of Electrical Engineering, *Scalability and Reliability of Phase Change Memory*. Stanford University, 2010. [Online]. Available: <https://books.google.com/books?id=4WZq0q4wCAAC>
- [9] M. Abuwasib, H. Lee, P. Sharma, C. B. Eom, A. Gruverman, and U. Singisetti, “Cmos compatible integrated ferroelectric tunnel junctions (ftj),” in *2015 73rd Annual Device Research Conference (DRC)*, June 2015, pp. 45–46.
- [10] Z. Wang, W. Zhao, A. Bouchenak-Khelladi, Y. Zhang, W. Lin, J. O. Klein, D. Ravelosona, and C. Chappert, “Compact modelling for co/bto/lsmo ferroelectric tunnel junction,” in *Nanotechnology (IEEE-NANO), 2013 13th IEEE Conference on*, Aug 2013, pp. 229–232.
- [11] S. Boyn, S. Girod, V. Garcia, S. Fusil, S. Xavier, C. Deranlot, H. Yamada, C. Carrétéro, E. Jacquet, M. Bibes, A. Barthelemy, and J. Grollier, “High-performance ferroelectric memory based on fully patterned tunnel junctions,” vol. 104, p. 052909, 02 2014.
- [12] S. Boyn, “Ferroelectric tunnel junctions: memristors for neuromorphic computing,” Ph.D. dissertation, Paris Saclay, 2016.
- [13] J. Henkel, S. Pagani, H. Amrouch, L. Bauer, and F. Samie, “Ultra-low power and dependability for iot devices (invited paper for iot technologies),” in *Design, Automation Test in Europe Conference Exhibition (DATE), 2017*, March 2017, pp. 954–959.
- [14] J. M. Cruz-Albrecht, M. W. Yung, and N. Srinivasa, “Energy-efficient neuron, synapse and stdp integrated circuits,” *IEEE Transactions on Biomedical Circuits and Systems*, vol. 6, no. 3, pp. 246–256, June 2012.
- [15] R. Serrano-Gotarredona, M. Oster, P. Lichtsteiner, A. Linares-Barranco, R. Paz-Vicente, F. Gomez-Rodriguez, L. Camunas-Mesa, R. Berner, M. Rivas-Perez,

- T. Delbruck, S. C. Liu, R. Douglas, P. Hafliger, G. Jimenez-Moreno, A. C. Balluels, T. Serrano-Gotarredona, A. J. Acosta-Jimenez, and B. Linares-Barranco, “Caviar: A 45k neuron, 5m synapse, 12g connects/s aer hardware sensory-processing-learning-actuating system for high-speed visual object recognition and tracking,” *IEEE Transactions on Neural Networks*, vol. 20, no. 9, pp. 1417–1438, Sept 2009.
- [16] S. B. Furber, F. Galluppi, S. Temple, and L. A. Plana, “The spinnaker project,” *Proceedings of the IEEE*, vol. 102, no. 5, pp. 652–665, May 2014.
- [17] S. Ambrogio, S. Balatti, V. Milo, R. Carboni, Z. Wang, A. Calderoni, N. Ramaswamy, and D. Ielmini, “Novel rram-enabled 1t1r synapse capable of low-power stdp via burst-mode communication and real-time unsupervised machine learning,” in *2016 IEEE Symposium on VLSI Technology*, June 2016, pp. 1–2.
- [18] D. Ielmini, S. Ambrogio, V. Milo, S. Balatti, and Z. Q. Wang, “Neuromorphic computing with hybrid memristive/cmos synapses for real-time learning,” in *2016 IEEE International Symposium on Circuits and Systems (ISCAS)*, May 2016, pp. 1386–1389.
- [19] J. Park, M. Kwak, K. Moon, J. Woo, D. Lee, and H. Hwang, “Tiox-based rram synapse with 64-levels of conductance and symmetric conductance change by adopting a hybrid pulse scheme for neuromorphic computing,” *IEEE Electron Device Letters*, vol. PP, no. 99, pp. 1–1, 2016.
- [20] J.-C. Liu, I.-T. Wang, C. W. Hsu, W. C. Luo, and T.-H. Hou, “Investigating mlc variation of filamentary and non-filamentary rram,” in *Proceedings of Technical Program - 2014 International Symposium on VLSI Technology, Systems and Application (VLSI-TSA)*, April 2014, pp. 1–2.

## REFERENCES

---

- [21] S. Mueller, S. R. Summerfelt, J. Muller, U. Schroeder, and T. Mikolajick, “Ten-nanometer ferroelectric Si:HfO<sub>2</sub> films for next-generation fram capacitors,” *IEEE Electron Device Letters*, vol. 33, no. 9, pp. 1300–1302, Sept 2012.
- [22] M. Lines and A. Glass, *Principles and Applications of Ferroelectrics and Related Materials*, ser. International series of monographs on physics. OUP Oxford, 1977. [Online]. Available: <https://books.google.com/books?id=p6ruJH8C84kC>
- [23] T. S. Boescke, J. Mueller, D. Brauhaus, U. Schroeder, and U. Boettger, “Ferroelectricity in hafnium oxide thin films.” *Applied Physics Letters*, vol. 99, no. 10, p. 102903, 2011. [Online]. Available: <http://ezproxy.rit.edu/login?url=http://search.ebscohost.com/login.aspx?direct=true&db=afh&AN=65503915&zsite=ehost-live>
- [24] D. A. Buck, “Ferroelectrics for digital information storage and switches,” Master’s thesis, Massachusetts Institute of Technology, June 1952.
- [25] L. N. Ridenour, “Computer memories,” *Scientific American*, vol. 192, no. 6, pp. 92–100, 1955. [Online]. Available: <https://www.scientificamerican.com/magazine/sa/1955/06-01/#article-the-amateur-scientist-1955-06>
- [26] H. Kohlstedt, N. Pertsev, J. Contreras, and R. Waser, “Theoretical current-voltage characteristics of ferroelectric tunnel junctions,” *PHYSICAL REVIEW B*, vol. 72, no. 12, SEP 2005.
- [27] H. Takishita, T. Onagi, and K. Takeuchi, “Storage class memory based ssd performance in consideration of error correction capabilities and write/read latencies,” in *2016 IEEE Silicon Nanoelectronics Workshop (SNW)*, June 2016, pp. 92–93.
- [28] V. Mohan, T. Bunker, L. Grupp, S. Gurumurthi, M. R. Stan, and S. Swanson, “Modeling power consumption of nand flash memories using flashpower,”

- IEEE Transactions on Computer-Aided Design of Integrated Circuits and Systems*, vol. 32, no. 7, pp. 1031–1044, July 2013.
- [29] I. Micron Technology, “Tn-29-19: Nand flash 101,” Tech. Rep., 2006. [Online]. Available: [http://www.micron.com/~/media/Documents/Products/Technical%20Note/NAND%20Flash/tn2919\\_nand\\_101.pdf](http://www.micron.com/~/media/Documents/Products/Technical%20Note/NAND%20Flash/tn2919_nand_101.pdf)
- [30] D. S. Chevitarese and M. N. D. Santos, “Real-time face tracking and recognition on ibm neuromorphic chip,” in *2016 IEEE International Symposium on Multimedia (ISM)*, Dec 2016, pp. 667–672.
- [31] D. Liu, H. Cheng, R. Peng, and Y. Yin, “Two resistive switching behaviors in ag/sio<sub>2</sub>/pt memristors,” in *2016 IEEE 16th International Conference on Nanotechnology (IEEE-NANO)*, Aug 2016, pp. 651–654.
- [32] K.-H. Kim, S. Gaba, D. Wheeler, J. M. Cruz-Albrecht, T. Hussain, N. Srinivasa, and W. Lu, “A functional hybrid memristor crossbar-array/cmos system for data storage and neuromorphic applications,” *Nano Letters*, vol. 12, no. 1, pp. 389–395, 2012, pMID: 22141918. [Online]. Available: <http://dx.doi.org/10.1021/nl203687n>
- [33] H. S. P. Wong, S. Raoux, S. Kim, J. Liang, J. P. Reifenberg, B. Rajendran, M. Asheghi, and K. E. Goodson, “Phase change memory,” *Proceedings of the IEEE*, vol. 98, no. 12, pp. 2201–2227, Dec 2010.
- [34] L. Fuller, S. Parikh, and C. Amareshbabu, “Rit’s advanced cmos process  $\lambda = 0.25 \mu\text{m}$ ,  $l_{\text{poly}} = 0.5 \mu\text{m}$ ,  $l_{\text{eff}} = 100 \text{ nm}$ ,” 2014. [Online]. Available: <https://people.rit.edu/lffeee/AdvCmosProcessIntegration.pdf>
- [35] P. Polakowski, S. Riedel, W. Weinreich, M. Rudolf, J. Sundqvist, K. Seidel, and J. Muller, “Ferroelectric deep trench capacitors based on al:hfo<sub>2</sub> for 3d non-

- volatile memory applications,” in *2014 IEEE 6th International Memory Workshop (IMW)*, May 2014, pp. 1–4.
- [36] A. Chanthbouala, A. Crassous, V. Garcia, K. Bouzehouane, S. Fusil, X. Moya, J. Allibe, B. Dlubak, J. Grollier, S. Xavier, C. Deranlot, A. Moshar, R. Proksch, N. D. Mathur, M. Bibes, and A. Barthelemy, “Solid-state memories based on ferroelectric tunnel junctions,” *Nature Nanotechnology*, vol. 7, no. 2, pp. 101–104, 2012.
- [37] S. Mueller, J. Muller, U. Schroeder, and T. Mikolajick, “Reliability characteristics of ferroelectric Si:HfO<sub>2</sub> thin films for memory applications,” *IEEE Transactions on Device and Materials Reliability*, vol. 13, no. 1, pp. 93–97, March 2013.
- [38] U. Schroeder, E. Yurchuk, S. Mueller, J. Mueller, S. Slesazeck, T. Schloesser, M. Trentzsch, and T. Mikolajick, “Non-volatile data storage in hfo2-based ferroelectric fets,” in *2012 12th Annual Non-Volatile Memory Technology Symposium Proceedings*, Oct 2013, pp. 60–63.
- [39] Y. Liu, T. Kamei, K. Endo, S. O’uchi, J. Tsukada, H. Yamauchi, T. Hayashida, Y. Ishikawa, T. Matsukawa, K. Sakamoto, A. Ogura, and M. Masahara, “Nanoscale wet etching of physical-vapor-deposited titanium nitride and its application to sub-30-nm-gate-length fin-type double-gate metal–oxide–semiconductor field-effect transistor fabrication,” *Japanese Journal of Applied Physics*, vol. 49, no. 6S, p. 06GH18, 2010. [Online]. Available: <http://stacks.iop.org/1347-4065/49/i=6S/a=06GH18>
- [40] J. Starzynski, “Selective hafnium oxide etchant,” Mar. 16 2006, uS Patent App. 10/938,191. [Online]. Available: <https://www.google.com/patents/US20060054595>

## REFERENCES

---

- [41] U. Schroeder, E. Yurchuk, S. Mueller, J. Mueller, S. Slesazeck, T. Schloesser, M. Trentzsch, and T. Mikolajick, “Non-volatile data storage in hfo<sub>2</sub>-based ferroelectric fets,” in *2012 12th Annual Non-Volatile Memory Technology Symposium Proceedings*, Oct 2013, pp. 60–63.

# Appendix A: Python Program Code

## A.1 Core Code

---

```
1  #-*- coding: utf-8-*-
2  """
3  Created on Sun May 15 18:23:58 2016
4
5  @author: Spencer Pringle @ Rochester Institute of Technology
6  """
7
8  from pylab import *
9  from PyQt4 import QtGui, QtCore
10 from matplotlib.backends.backend_qt4agg import (
11     FigureCanvasQTAgg as FigureCanvas,
12     NavigationToolbar2QT as NavigationToolbar)
13 from matplotlib.figure import Figure
14 import sys
15 import GUI_NEW
16
17 class ExampleApp(QtGui.QMainWindow, GUI_NEW.Ui_MainWindow):
18     def __init__(self):
19         super(self.__class__, self).__init__()
20         self.setupUi(self)
21
22         self.ModelingProgress.setValue(0)
23
24         self.Metal1Box.addItems(['SrRuO3', 'Co', 'Al', 'Metal 1'])
25
26         self.Metal1Box.setCurrentIndex(0)
```

## APPENDIX A. PYTHON PROGRAM CODE

```
25         self.Metal2Box.addItem(['PZT', 'La_(0.67)Sr_(0.33)MnO_3', 'p+ Silicon',
26                                     , 'Metal 2'])
27
28         self.Metal2Box.setCurrentIndex(0)
29
30         self.FerroBox.addItem(['BaTiO_3', 'Al-HfO_2', 'Ferro'])
31
32         self.FerroBox.setCurrentIndex(0)
33
34
35         self.RunModeling.clicked.connect(self.Model)
36
37         self.Metal1Box.currentIndexChanged.connect(self.Metal1Update)
38
39         self.Metal2Box.currentIndexChanged.connect(self.Metal2Update)
40
41         self.FerroBox.currentIndexChanged.connect(self.FerroelectricUpdate)
42
43
44         self.Metal1Box.setCurrentIndex(2)
45
46         self.Metal2Box.setCurrentIndex(2)
47
48         self.FerroBox.setCurrentIndex(1)
49
50
51
52         self.Metal1Box.setcurrentIndex(2)
53
54         self.Metal2Box.setcurrentIndex(2)
55
56         self.FerroBox.setcurrentIndex(1)
57
58
59     def Model(self):
60
61         self.ModelingProgress.setValue(0)
62
63         self.FrontOutput.clear()
64
65         self.PotentialOutput.clear()
66
67         global sigma_p, sigma_s, q, epsilon_0, phi, sigma, k_1, k_2, a_0, x,
68
69                         y, meshSpace, potentialMesh, phi_2, phi_1, positiveMesh,
70
71                         negativeMesh
72
73         global e0, m0, kT, kb, h, m_0
74
75         global d, E_a, epsilon_f, P, h, h_eV
76
77         global delta_1, a_1, E_f_1
78
79         global delta_2, a_2, E_f_2
```

```

48          global G_2, G_1, x_1, x_2, phi_bar_pos, phi_bar_neg, x_1_index,
49                      x_2_index, m_0, A_tun, J_0, J, v_app, phi_diff
50          global Ath_pos, Jth_pos, Ath_neg, Jth_neg, phi_prime, phi_prime_pos,
51                      phi_prime_neg
50          global Atun_pos, J0_pos, Jtun_pos, Atun_neg, J0_neg, Jtun_neg, V, T,
51                      R_pos, R_neg, m_star
51          global Ran, numchild, i, w, items, WellDir, WellFermi, Bar_Length_Pos
51                      , Bar_Length_Neg, x_1_pos, x_2_pos, V, h_bar
52
53          epsilon_0=8.854E-12 #free space perm [F/m]
54          T=300 #Temperature (K)
55          #Non-adjustable Constants
56          e0=8.854E-14 #Permittivity of free space [F/cm]
57          m_0=9.11E-31 #Electron rest mass (kg)
58          h=6.626E-34 #Planck's constant (m^2*kg/sec)
59          q=1.6E-19 #Electron charge (C)
60          kb=1.38E-23 #Boltzman constant(J/K)
61          kT=(kb/q)*T           #[eV]
62          a_0=5.291E-11
63          h=6.626E-34
64          h_bar=h/(2*pi)
65          h_eV=4.13E-15
66          meshSpace=2/1000
67          v_app=.1
68
69          #Initialize Ferroelectric Material Values
70          epsilon_f=self.FerroDielectricConst.value()

```

## APPENDIX A. PYTHON PROGRAM CODE

---

```
71         E_a=self.FerroEA.value()
72
73         m_star=self.FerroEMass.value()
74
75         P=self.FerroPolarization.value()
76
77         d=self.FerroThick.value()*1E-9
78
79
80         #Initialize Metal 1 Values
81
82         E_f_1=self.Metal1FermiEnergy.value()
83
84         if self.Metal1ScreenLength.value()==0:
85
86             delta_1=(E_f_1/(4*pi*q*self.Metal1Lattice.value())*1E-10)
87
88             **(1/2)
89
90         else:
91
92             delta_1=self.Metal1ScreenLength.value()*1E-9
93
94
95         #Initialize Metal 2 Values
96
97         #if self.Metal2Box.currentIndex()==2
98
99         E_f_2=self.Metal2FermiEnergy.value()
100
101        #else:
102
103        #    E_f_2=self.Metal2FermiEnergy.value()
104
105        if self.Metal2ScreenLength.value()==0:
106
107            delta_2=(E_f_2/(4*pi*q*self.Metal2Lattice.value())*1E-10)
108
109            **(1/2)
110
111        else:
112
113            delta_2=self.Metal2ScreenLength.value()*1E-9
114
115
116        #Calculate and store charges and wave vector magnitudes...
117
118        sigma_p=P*1E-2
119
120        sigma_s=sigma_p*d/(epsilon_f*(delta_1+delta_2)+d)
```

```

96
97     V=np.linspace(-1,1,201)
98
99     self.Potential()
100
101    x_1_pos=x_1
102
103    x_2_pos=x_2
104
105    positiveMesh=potentialMesh
106
107    phi_prime_pos=phi_prime
108
109    Ath_pos=(4*pi*m_0*(kb**2)*q)/((h**3))
110
111    Jth_pos = Ath_pos*1E-4*(T**2)*exp(-phi_prime_pos/kT)*(1-exp(-abs(V)/
112
113    phi_diff=phi_1-phi_2
114
115    Bar_Length_Pos=x_2-x_1
116
117    phi_bar_pos=mean(y[x_1_index:x_2_index])
118
119    Atun_pos=((2*m_0*q*m_star)**(1/2))*(Bar_Length_Pos)*(2e-9)/h_bar
120
121    #Atun_pos=(4*pi*(x_2-x_1)*1e-9*(2*m_0)**(1/2))/h
122
123    #J0_pos=(q)/(2*pi*h*((x_2-x_1)*1E-9)**2)
124
125    J0_pos=(6.08e8)/((Bar_Length_Pos)**2)
126
127    Jtun_pos=J0_pos*((phi_bar_pos)*exp(-Atun_pos*((phi_bar_pos)**(1/2))))
128
129    -(phi_bar_pos+V)*exp(-Atun_pos*((phi_bar_pos+V)**(1/2))))
130
131    R_pos=np.zeros(size(V))
132
133    for i in range(0, size(V)):
134
135        if Jtun_pos[i]!=0 and Jtun_pos[i]!='nan':
136
137            R_pos[i]=V[i]/Jtun_pos[i]
138
139        else:
140
141            R_pos[i]='nan'
142
143    np.nanmean(abs(R_pos))
144
145    Jtun_pos=abs(Jtun_pos)

```

## APPENDIX A. PYTHON PROGRAM CODE

---

```
121     Itun_pos=Jtun_pos[np.where(V==.5)[0]]*(250e-7)**2
122     Itun_pos_1_250=Jtun_pos[[110][0]]*(250e-7)**2
123     Itun_pos_2_250=Jtun_pos[[120][0]]*(250e-7)**2
124     Itun_pos_1_500=Jtun_pos[[110][0]]*(500e-7)**2
125     Itun_pos_2_500=Jtun_pos[[120][0]]*(500e-7)**2
126     Rtun_pos_250=.5/Itun_pos
127     Rtun_pos_1_250=.1/Itun_pos_1_250
128     Rtun_pos_1_500=.1/Itun_pos_1_500
129     Rtun_pos_2_250=.2/Itun_pos_2_250
130     Rtun_pos_2_500=.2/Itun_pos_2_500
131     rho_pos=.5/Jtun_pos[np.where(V==.5)]
132     rho_pos_1=.1/Jtun_pos[[110][0]]
133     self.FrontOutput.insertPlainText('Under Positive Polarization (toward
134                                         Metal 1), at .5V bias:')
135     self.FrontOutput.insertPlainText('\n')
136     self.FrontOutput.insertPlainText('\t J_th='+'%.2e'%Jth_pos[np.where(V
137 ==.5)[0]] +' A/cm^2')
138     self.FrontOutput.insertPlainText('\n')
139     self.FrontOutput.insertPlainText('\t I_tun='+'%.2e'%Jtun_pos[np.where(V
140 ==.5)[0]] +' A/cm^2')
141     self.FrontOutput.insertPlainText('\n')
142     self.FrontOutput.insertPlainText('Under Positive Polarization (toward
143                                         Metal 1), at .2V bias:')
```

## APPENDIX A. PYTHON PROGRAM CODE

---

```
143         self.FrontOutput.insertPlainText('\n')
144         self.FrontOutput.insertPlainText('t J_th='+'%.2e'%Jth_pos[[120][0]]
145                                         +' A/cm^2')
146         self.FrontOutput.insertPlainText('\n')
147         self.FrontOutput.insertPlainText('t J_tun='+'%.2e'%Jtun_pos
148                                         [[120][0]] +' A/cm^2')
149         self.FrontOutput.insertPlainText('\n')
150         self.FrontOutput.insertPlainText('\n')
151         self.FrontOutput.insertPlainText('Under Positive Polarization (toward
152                                         Metal 1), at .1V bias:')
153         self.FrontOutput.insertPlainText('\n')
154         self.FrontOutput.insertPlainText('t J_th='+'%.2e'%Jth_pos[[110][0]]
155                                         +' A/cm^2')
156         self.FrontOutput.insertPlainText('\n')
157         self.FrontOutput.insertPlainText('t J_tun='+'%.2e'%Jtun_pos
158                                         [[110][0]] +' A/cm^2')
159         self.FrontOutput.insertPlainText('\n')
160         P=P
161         sigma_p=P*1E-2
162         sigma_s=sigma_p*d/(epsilon_f*(delta_1+delta_2)+d)
```

---

## APPENDIX A. PYTHON PROGRAM CODE

```
163         self.Potential()
164
165         x_1_neg=x_1
166
167         x_2_neg=x_2
168
169         negativeMesh=potentialMesh
170
171         phi_prime_neg=phi_prime
172
173         Ath_neg=(4*pi*m_0*(kb**2)*q)/((h**3))
174
175         Jth_neg = Ath_neg*1E-4*(T**2)*exp(-phi_prime_neg/kT)*(1-exp(-abs(V)/
176
177         kT))
178
179         Bar_Length_Neg=x_2-x_1
180
181         phi_bar_neg=mean(y[x_1_index:x_2_index])
182
183         Atun_neg=((2*m_0*q*m_star)**(1/2))*(Bar_Length_Neg)*(2e-9)/h_bar
184
185         J0_neg=(6.08e8)/((Bar_Length_Neg)**2)
186
187         Jtun_neg=J0_neg*((phi_bar_neg)*exp(-Atun_neg*((phi_bar_neg)**(1/2)))
188
189         -((phi_bar_neg)+V)*exp(-Atun_neg*((phi_bar_neg)+V)**(1/2)))
190
191         R_neg=np.zeros(size(V))
192
193         for i in range(0, size(V)):
194
195             if Jtun_neg[i]!=0 and Jtun_neg[i]!='nan':
196
197                 R_neg[i]=V[i]/Jtun_neg[i]
198
199             else:
200
201                 R_neg[i]='nan'
202
203         Jtun_neg=abs(Jtun_neg)
204
205         Itun_neg=Jtun_neg[np.where(V==.5)[0]]*(250e-7)**2
206
207         Itun_neg_1_250=Jtun_neg[[110][0]]*(250e-7)**2
208
209         Itun_neg_1_500=Jtun_neg[[110][0]]*(500e-7)**2
210
211         Itun_neg_2_250=Jtun_neg[[120][0]]*(250e-7)**2
212
213         Itun_neg_2_500=Jtun_neg[[120][0]]*(500e-7)**2
```

## APPENDIX A. PYTHON PROGRAM CODE

---

```
188     Rtun_neg_250=.5/Itun_neg
189
190     Rtun_neg_1_250=.1/Itun_neg_1_250
191
192     Rtun_neg_1_500=.1/Itun_neg_1_500
193
194     Rtun_neg_2_250=.2/Itun_neg_2_250
195
196     Rtun_neg_2_500=.2/Itun_neg_2_500
197
198     rho_neg=.5/Jtun_neg[np.where(V==.5)[0]]
199
200     rho_neg_1=.1/Jtun_neg[[110][0]]
201
202     self.FrontOutput.insertPlainText('\n')
203
204     self.FrontOutput.insertPlainText('Under Negative Polarization (toward
205
206
207
208
209
210
211
212
213
214
215
216
217
218
219
220
221
222
223
224
225
226
227
228
229
230
231
232
233
234
235
236
237
238
239
240
241
242
243
244
245
246
247
248
249
250
251
252
253
254
255
256
257
258
259
260
261
262
263
264
265
266
267
268
269
270
271
272
273
274
275
276
277
278
279
280
281
282
283
284
285
286
287
288
289
290
291
292
293
294
295
296
297
298
299
300
301
302
303
304
305
306
307
308
309
310
311
312
313
314
315
316
317
318
319
320
321
322
323
324
325
326
327
328
329
330
331
332
333
334
335
336
337
338
339
340
341
342
343
344
345
346
347
348
349
350
351
352
353
354
355
356
357
358
359
360
361
362
363
364
365
366
367
368
369
370
371
372
373
374
375
376
377
378
379
380
381
382
383
384
385
386
387
388
389
390
391
392
393
394
395
396
397
398
399
400
401
402
403
404
405
406
407
408
409
410
411
412
413
414
415
416
417
418
419
420
421
422
423
424
425
426
427
428
429
430
431
432
433
434
435
436
437
438
439
440
441
442
443
444
445
446
447
448
449
450
451
452
453
454
455
456
457
458
459
460
461
462
463
464
465
466
467
468
469
470
471
472
473
474
475
476
477
478
479
480
481
482
483
484
485
486
487
488
489
490
491
492
493
494
495
496
497
498
499
500
501
502
503
504
505
506
507
508
509
510
511
512
513
514
515
516
517
518
519
520
521
522
523
524
525
526
527
528
529
530
531
532
533
534
535
536
537
538
539
540
541
542
543
544
545
546
547
548
549
550
551
552
553
554
555
556
557
558
559
559
560
561
562
563
564
565
566
567
568
569
570
571
572
573
574
575
576
577
578
579
579
580
581
582
583
584
585
586
587
588
589
589
590
591
592
593
594
595
596
597
598
599
599
600
601
602
603
604
605
606
607
608
609
609
610
611
612
613
614
615
616
617
618
619
619
620
621
622
623
624
625
626
627
628
629
629
630
631
632
633
634
635
636
637
638
639
639
640
641
642
643
644
645
646
647
648
649
649
650
651
652
653
654
655
656
657
658
659
659
660
661
662
663
664
665
666
667
668
669
669
670
671
672
673
674
675
676
677
678
679
679
680
681
682
683
684
685
686
687
688
689
689
690
691
692
693
694
695
696
697
698
699
699
700
701
702
703
704
705
706
707
708
709
709
710
711
712
713
714
715
716
717
718
719
719
720
721
722
723
724
725
726
727
728
729
729
730
731
732
733
734
735
736
737
738
739
739
740
741
742
743
744
745
746
747
748
749
749
750
751
752
753
754
755
756
757
758
759
759
760
761
762
763
764
765
766
767
768
769
769
770
771
772
773
774
775
776
777
778
779
779
780
781
782
783
784
785
786
787
788
789
789
790
791
792
793
794
795
796
797
798
799
799
800
801
802
803
804
805
806
807
808
809
809
810
811
812
813
814
815
816
817
818
819
819
820
821
822
823
824
825
826
827
828
829
829
830
831
832
833
834
835
836
837
838
839
839
840
841
842
843
844
845
846
847
848
849
849
850
851
852
853
854
855
856
857
858
859
859
860
861
862
863
864
865
866
867
868
869
869
870
871
872
873
874
875
876
877
878
879
879
880
881
882
883
884
885
886
887
888
889
889
890
891
892
893
894
895
896
897
898
899
899
900
```

## APPENDIX A. PYTHON PROGRAM CODE

---

```
209         self.FrontOutput.insertPlainText('t J_tun='+'%.2e'%Jtun_neg  
210                                         [[120][0]] +' A/cm^2')  
  
211         self.FrontOutput.insertPlainText('\n')  
  
211         self.FrontOutput.insertPlainText('t I_tun(250nm x 250nm)='+'%.2e'%  
211                                         Itun_neg_2_250 +' A')  
  
212         self.FrontOutput.insertPlainText('\n')  
  
213         self.FrontOutput.insertPlainText('t I_tun(500nm x 500nm)='+'%.2e'%  
213                                         Itun_neg_2_500 +' A')  
  
214         self.FrontOutput.insertPlainText('\n')  
  
215         self.FrontOutput.insertPlainText('\n')  
  
216         self.FrontOutput.insertPlainText('Under Negative Polarization (toward  
216                                         Metal 2), at .1V bias:')  
  
217         self.FrontOutput.insertPlainText('\n')  
  
218         self.FrontOutput.insertPlainText('t J_th='+'%.2e'%Jth_neg[[110][0]]  
218                                         +' A/cm^2')  
  
219         self.FrontOutput.insertPlainText('\n')  
  
220         self.FrontOutput.insertPlainText('t J_tun='+'%.2e'%Jtun_neg  
220                                         [[110][0]] +' A/cm^2')  
  
221         self.FrontOutput.insertPlainText('\n')  
  
222         self.FrontOutput.insertPlainText('t I_tun(250nm x 250nm)='+'%.2e'%  
222                                         Itun_neg_1_250 +' A')  
  
223         self.FrontOutput.insertPlainText('\n')  
  
224         self.FrontOutput.insertPlainText('t I_tun(500nm x 500nm)='+'%.2e'%  
224                                         Itun_neg_1_500 +' A')  
  
225         self.FrontOutput.insertPlainText('\n')  
  
226  
  
227         phi_diff=abs(phi_bar_pos-phi_bar_neg)
```

## APPENDIX A. PYTHON PROGRAM CODE

---

```
228         if Jtun_neg[np.where(V==.5)[0]]>Jtun_pos[np.where(V==.5)[0]]:
229             Jtun_Ratio=Jtun_neg[np.where(V==.5)[0]]/Jtun_pos[np.where(V
230 ==.5)[0]]
231             LRSR=np.nanmean(abs(R_neg))
232             HRSR=np.nanmean(abs(R_pos))
233         else:
234             Jtun_Ratio=Jtun_pos[np.where(V==.5)[0]]/Jtun_neg[np.where(V
235 ==.5)[0]]
236             LRSR=np.nanmean(abs(R_pos))
237             HRSR=np.nanmean(abs(R_neg))
238             self.FrontOutput.insertPlainText('Difference in Average Potential
239                                         Barriers:\n')
240             self.FrontOutput.insertPlainText('t'+'%.3f'%phi_bar_pos+'-'+'%.3f'%phi_bar_neg+'='+'%.3f'%phi_diff+' eV\n')
241             self.FrontOutput.insertPlainText('\n')
242             self.FrontOutput.insertPlainText('Ratio of Tunnel Current at .5V Bias
243                                         in HRS vs. LRS:\n')
244             self.FrontOutput.insertPlainText('t'+'%.3f'%Jtun_Ratio+'\n')
245             self.FrontOutput.insertPlainText('\n')
246             self.FrontOutput.insertPlainText('LRS and HRS Resistances (250nm x
247                                         250nm, at .5V):\n')
248             self.FrontOutput.insertPlainText('t Pos:'+'%.3e'%Rtun_pos_250+' Ohm
249                                         \n t Neg:'+'%.3e'%Rtun_neg_250+' Ohm\n')
250             self.FrontOutput.insertPlainText('\n')
251             self.FrontOutput.insertPlainText('LRS and HRS Resistivity @ .5V:\n')
```

## APPENDIX A. PYTHON PROGRAM CODE

---

```
248     self.FrontOutput.insertPlainText('t Pos:'+'%.3e'%rho_pos +' Ohm cm  
249                                         ^2\n\t Neg:'+'%.3e'%rho_neg +' Ohm cm^2\n')  
250     self.FrontOutput.insertPlainText('\n')  
251     self.FrontOutput.insertPlainText('\n')  
252     self.FrontOutput.insertPlainText('LRS and HRS Resistivity @ .1V:\n')  
253     self.FrontOutput.insertPlainText('t Pos:'+'%.3e'%rho_pos_1 +' Ohm cm  
254                                         ^2\n\t Neg:'+'%.3e'%rho_neg_1 +' Ohm cm^2\n')  
255     self.FrontOutput.insertPlainText('\n')  
256     self.FrontOutput.insertPlainText('LRS and HRS Resistances (250nm x  
257                                         250nm, at .2V):\n')  
258     self.FrontOutput.insertPlainText('t Pos:'+'%.3e'%Rtun_pos_2_250 +'  
259                                         Ohm\n\t Neg:'+'%.3e'%Rtun_neg_2_250 +' Ohm\n')  
260     self.FrontOutput.insertPlainText('\n')  
261     self.FrontOutput.insertPlainText('\n')  
262     self.FrontOutput.insertPlainText('LRS and HRS Resistances (500nm x  
263                                         500nm, at .2V):\n')  
264     self.FrontOutput.insertPlainText('t Pos:'+'%.3e'%Rtun_pos_2_500 +'  
265                                         Ohm\n\t Neg:'+'%.3e'%Rtun_neg_2_500 +' Ohm\n')  
266     self.FrontOutput.insertPlainText('\n')  
267     self.FrontOutput.insertPlainText('LRS and HRS Resistances (250nm x  
268                                         250nm, at .1V):\n')  
269     self.FrontOutput.insertPlainText('t Pos:'+'%.3e'%Rtun_pos_1_250 +'  
270                                         Ohm\n\t Neg:'+'%.3e'%Rtun_neg_1_250 +' Ohm\n')  
271     self.FrontOutput.insertPlainText('\n')  
272     self.FrontOutput.insertPlainText('LRS and HRS Resistances (500nm x  
273                                         500nm, at .1V):\n')
```

## APPENDIX A. PYTHON PROGRAM CODE

---

```
266             self.FrontOutput.insertPlainText('t Pos:'+'%.3e'%Rtun_pos_1_500 +'  
267                                         Ohm\n\t Neg:'+'%.3e'%Rtun_neg_1_500 +' Ohm\n')  
268  
269             self.FrontOutput.insertPlainText('\n')  
270  
271             Jtunratio=max(np.nan_to_num(np.divide(Jtun_pos, Jtun_neg)))  
272  
273             self.closeall()  
274  
275             fig1 = Figure()  
276  
277             ax1f1 = fig1.add_subplot(111)  
278             ax1f1.plot(positiveMesh[0,:], positiveMesh[1,:])  
279             ax1f1.plot(negativeMesh[0,:], negativeMesh[1,:])  
280             ExampleApp.addmpl(self,fig1)  
281  
282             fig2=Figure()  
283  
284             ax1f2 = fig2.add_subplot(111)  
285             ax1f2.plot(V, Jth_pos)  
286             ax1f2.plot(V, Jth_neg)  
287             ExampleApp.addmpl(self,fig2)  
288  
289             fig3=Figure()  
290  
291             ax1f3 = fig3.add_subplot(111)  
292             ax1f3.plot(V, Jtun_pos)  
293             ax1f3.plot(V, Jtun_neg)  
294             ax1f3.set_yscale('log')  
295             ExampleApp.addmpl(self,fig3)
```

## APPENDIX A. PYTHON PROGRAM CODE

```
291         self.PotentialOutput.insertPlainText('V\tJtunpos\tJtunneg\n')
292
293     for i in range(0, size(V)):
294
295         self.PotentialOutput.insertPlainText('.3f'%V[i] + '\t' +
296
297         %.3e'%Jtun_pos[i] + '\t' + '.3e'%Jtun_neg[i] + '\n')
298
299     self.PotentialOutput.insertPlainText('X\tV1pos\tV2neg\n')
300
301     for p in range(0, size(x)):
302
303         self.PotentialOutput.insertPlainText('.3f'%x[p] + '\t' +
304
305         %.3f'%positiveMesh[1,p] + '\t' + '%.3f'%negativeMesh[1,p]
306
307         + '\n')
308
309     def unfill(self):
310
311         global numchild, i, w, items
312
313         numchild=self.PotentialMPlay.count()
314
315         items = (self.PotentialMPlay.itemAt(i) for i in range(self.
316
317             PotentialMPlay.count()))
318
319         for w in items:
320
321             try:
322
323                 self.PotentialMPlay.removeWidget(w.widget())
324
325             except AttributeError:
326
327                 pass
328
329             try:
330
331                 self.PotentialMPlay.removeItem(w.item())
332
333             except AttributeError:
334
335                 pass
```

## APPENDIX A. PYTHON PROGRAM CODE

---

```
313     def closeall(self): #solution found on http://python.6.x6.nabble.com/
Completely-removing-items-from-a-layout-td1924202.html
314         def deleteItems(layout):
315             if layout is not None:
316                 while layout.count():
317                     item = layout.takeAt(0)
318                     widget = item.widget()
319                     if widget is not None:
320                         widget.deleteLater()
321                 else:
322                     deleteItems(item.layout())
323             deleteItems(self.PotentialMPay)
324
325     def Potential(self):
326         global P, x, index, y, x_prime, potentialMesh, delta_1, delta_2,
327             E_f_1, E_f_2, phi_2, phi_1, x_1, x_2, x_1_index, x_2_index,
328             phi_prime, WellDir, WellFermi
329
330         x = np.linspace(-5,5+(d*1E9),(5+(d*1E9))/meshSpace)
331         y = np.zeros(size(x))
332         index = 0
333         flag = 0
334         if delta_1<delta_2:
335             WellFermi=E_f_2
336             WellDir=-1
```

```

337         else:
338             WellFermi=E_f_1
339             WellDir=1
340
341         for x_prime in x:
342             if x_prime<=0:
343                 y[index]=(sigma_s*delta_1/epsilon_0)*exp(-abs(x_prime
344                                         *1E-9)/(delta_1))
345
346             elif x_prime>=(d*1E9):
347                 y[index]=(-sigma_s*delta_2/epsilon_0)*exp(-abs(
348                                         x_prime*1E-9)-d)/(delta_1))
349
350             if x_prime<=0:
351                 phi_1=y[index]
352
353             if x_prime>=(d*1E9) and flag==0:
354                 phi_2=y[index]
355
356             flag=1
357
358             index=index+1
359
360             self.ModelingProgress.setValue(index*50/size(x))
361             index = 0
362
363             for x_u in x:
364                 if x_u>0 and x_u<(d*(1E9)):
365
366                     y[index]=phi_1-((x_u/(d*1E9))*(phi_1-phi_2))
367
368                     index=index+1
369
370                     self.ModelingProgress.setValue(50+(index*25/size(x)))
371
372             index = 0
373
374             for x_u in x:
375                 if x_u>0 and x_u<(d*(1E9)):
```

## APPENDIX A. PYTHON PROGRAM CODE

---

```
362                     y[index]=y[index]+(E_f_1-E_a)+((x_u/(d*1E9))*(E_f_2-
363                                         E_f_1))
364
365                                         if x_u<=0:
366                                         phi_1=y[index]
367                                         if x_u>=(d*1E9) and flag==0:
368                                         phi_2=y[index]
369                                         flag=1
370                                         index=index+1
371                                         self.ModelingProgress.setValue(50+(index*25/size(x)))
372                                         phi_prime=max(y)
373                                         index=0
374                                         for x_u in x:
375                                         if y_flag==0 and y[index]>phi_prime/10:
376                                         x_1=x_u
377                                         x_1_index=index
378                                         y_flag=1
379                                         if y_flag==1 and y[index]<phi_prime/10:
380                                         x_2=x_u
381                                         x_2_index=index-1
382                                         y_flag=2
383                                         index=index+1
384                                         self.ModelingProgress.setValue(75+(index*25/size(x)))
385                                         potentialMesh=vstack((x,y))
386                                         def addmpl(self, fig):
387                                         for clos in range(self.PotentialMPlay.count()):
388                                         try:
```

## APPENDIX A. PYTHON PROGRAM CODE

---

```
388                     self.canvas.close()
389
390             except AttributeError:
391
392                 pass
393
394                 self.canvas = FigureCanvas(fig)
395
396                 self.PotentialMPlay.addWidget(self.canvas)
397
398
399             def Metal1Update(self):
400
401                 if self.Metal1Box.currentIndex()==0:
402
403                     self.Metal1ScreenLength.setValue(.6)
404
405                     self.Metal1FermiEnergy.setValue(1.5)
406
407                     self.Metal1Lattice.setValue(0)
408
409                 elif self.Metal1Box.currentIndex()==1:
410
411                     self.Metal1ScreenLength.setValue(.05)
412
413                     self.Metal1FermiEnergy.setValue(5)
414
415                     self.Metal1Lattice.setValue(0)
416
417                 elif self.Metal1Box.currentIndex()==2:
418
419                     self.Metal1ScreenLength.setValue(.06)
420
421                     self.Metal1FermiEnergy.setValue(4.08)
422
423                     self.Metal1Lattice.setValue(0)
424
425             def FerroelectricUpdate(self):
426
427                 if self.FerroBox.currentIndex()==0:
428
429                     self.FerroDielectricConst.setValue(2000)
```

## APPENDIX A. PYTHON PROGRAM CODE

---

```
415             self.FerroEA.setValue(2.5)
416             self.FerroPolarization.setValue(20)
417             self.FerroThick.setValue(2)
418             self.FerroEMass.setValue(1)
419         elif self.FerroBox.currentIndex()==1:
420             self.FerroDielectricConst.setValue(40)
421             self.FerroEA.setValue(2.0)#http://e-citations.ethbib.ethz.ch/
422             self.FerroPolarization.setValue(10)
423             self.FerroThick.setValue(2)#http://e-citations.ethbib.ethz.ch/
424             self.FerroEMass.setValue(.11)
425     def Metal2Update(self):
426         if self.Metal2Box.currentIndex()==0:
427             self.Metal2ScreenLength.setValue(.07)
428             self.Metal2FermiEnergy.setValue(3.5)
429             self.Metal2Lattice.setValue(0)
430         elif self.Metal2Box.currentIndex()==1:
431             self.Metal2ScreenLength.setValue(.1)
432             self.Metal2FermiEnergy.setValue(4.8)#From Abuwasib_15
433             self.Metal2Lattice.setValue(0)
434         elif self.Metal2Box.currentIndex()==2:
435             self.Metal2ScreenLength.setValue(.4)
436             self.Metal2FermiEnergy.setValue(4.85)
437             self.Metal2Lattice.setValue(0)
438
439
```

```

440  def main():
441      if QtCore.QCoreApplication.instance() != None:
442          app = QtCore.QCoreApplication.instance()
443      else:
444          app = QtGui.QApplication(sys.argv) #A new instance of QApplication
445      form = ExampleApp()                  #We set the form to be our
446      form.show()                         #Show the form
447      app.exec_()                          #and execute the app
448
449
450  if __name__ == '__main__':           # if we're running file directly and not
451      main()                           #run the main function

```

---

## A.2 GUI Code

---

```

1  #-*- coding: utf-8 -*-
2
3  #Form implementation generated from reading ui file 'FTJ_GUILPringleSinglePage.ui'
4  #
5  # Created by: PyQt4 UI code generator 4.11.4
6  #
7  #WARNING All changes made in this file will be lost!
8
9  from PyQt4 import QtCore, QtGui
10

```

## APPENDIX A. PYTHON PROGRAM CODE

---

```
11  try:
12      _fromUtf8 = QtCore.QString.fromUtf8
13
14  except AttributeError:
15      def _fromUtf8(s):
16          return s
17
18  try:
19      _encoding = QtGui.QApplication.UnicodeUTF8
20
21      def _translate(context, text, disambig):
22          return QtGui.QApplication.translate(context, text, disambig,
23                                              _encoding)
24
25  class Ui_MainWindow(object):
26
27      def setupUi(self, MainWindow):
28
29          MainWindow.setObjectName(_fromUtf8("MainWindow"))
30
31          MainWindow.resize(941, 739)
32
33          self.centralwidget = QtGui.QWidget(MainWindow)
34
35          self.centralwidget.setObjectName(_fromUtf8("centralwidget"))
36
37          self.gridLayout = QtGui.QGridLayout(self.centralwidget)
38
39          self.gridLayout.setObjectName(_fromUtf8("gridLayout"))
40
41          self.splitter_5 = QtGui.QSplitter(self.centralwidget)
42
43          self.splitter_5.setOrientation(QtCore.Qt.Vertical)
44
45          self.splitter_5.setObjectName(_fromUtf8("splitter_5"))
46
47          self.splitter = QtGui.QSplitter(self.splitter_5)
```

## APPENDIX A. PYTHON PROGRAM CODE

---

```
37         self.splitter.setOrientation(QtCore.Qt.Horizontal)
38
39         self.layoutWidget = QtGui.QWidget(self.splitter)
40
41         self.verticalLayout_7 = QtGui.QVBoxLayout(self.layoutWidget)
42
43         self.verticalLayout_7.setObjectName(_fromUtf8("verticalLayout_7"))
44
45         self.verticalLayout_4 = QtGui.QVBoxLayout()
46
47         self.verticalLayout_4.setObjectName(_fromUtf8("verticalLayout_4"))
48
49         self.verticalLayout = QtGui.QVBoxLayout()
50
51         self.verticalLayout.setObjectName(_fromUtf8("verticalLayout"))
52
53         self.gridLayout_3 = QtGui.QGridLayout(self.groupBox)
54
55         self.gridLayout_3.setObjectName(_fromUtf8("gridLayout_3"))
56
57         self.verticalLayout_3 = QtGui.QVBoxLayout()
58
59         self.verticalLayout_3.setObjectName(_fromUtf8("verticalLayout_3"))
60
61         self.horizontalLayout_2 = QtGui.QHBoxLayout()
62
63         self.horizontalLayout_2.setObjectName(_fromUtf8("horizontalLayout_2"))
64
65         self.groupBox.setLayout(self.verticalLayout)
66
67         self.label = QtGui.QLabel(self.groupBox)
68
69         self.label.setObjectName(_fromUtf8("label"))
70
71         self.horizontalLayout_2.addWidget(self.label)
72
73         self.label_2 = QtGui.QLabel(self.groupBox)
74
75         self.label_2.setObjectName(_fromUtf8("label_2"))
76
77         self.horizontalLayout_2.addWidget(self.label_2)
78
79         self.label_3 = QtGui.QLabel(self.groupBox)
80
81         self.label_3.setObjectName(_fromUtf8("label_3"))
82
83         self.horizontalLayout_2.addWidget(self.label_3)
```

## APPENDIX A. PYTHON PROGRAM CODE

---

```
63         self.horizontalLayout_2.addWidget(self.label_3)
64
65         self.verticalLayout_3.addLayout(self.horizontalLayout_2)
66
67         self.horizontalLayout = QtGui.QHBoxLayout()
68
69         self.horizontalLayout.setObjectName(_fromUtf8("horizontalLayout"))
70
71         self.Metal1Box = QtGui.QComboBox(self.groupBox)
72
73         self.Metal1Box.setObjectName(_fromUtf8("Metal1Box"))
74
75         self.horizontalLayout.addWidget(self.Metal1Box)
76
77         self.FerroBox = QtGui.QComboBox(self.groupBox)
78
79         self.FerroBox.setObjectName(_fromUtf8("FerroBox"))
80
81         self.horizontalLayout.addWidget(self.FerroBox)
82
83         self.Metal2Box = QtGui.QComboBox(self.groupBox)
84
85         self.Metal2Box.setObjectName(_fromUtf8("Metal2Box"))
86
87         self.horizontalLayout.addWidget(self.Metal2Box)
88
89         self.verticalLayout_3.addLayout(self.horizontalLayout)
90
91         self.gridLayout_3.setLayout(self.verticalLayout_3, 0, 0, 1, 1)
92
93         self.verticalLayout.addWidget(self.groupBox)
94
95         self.verticalLayout_4.setLayout(self.verticalLayout)
96
97         self.verticalLayout_7.setLayout(self.verticalLayout_4)
98
99         self.splitter_4 = QtGui.QSplitter(self.layoutWidget)
100
101        self.splitter_4.setOrientation(QtCore.Qt.Vertical)
102
103        self.splitter_4.setObjectName(_fromUtf8("splitter_4"))
104
105        self.layoutWidget1 = QtGui.QWidget(self.splitter_4)
106
107        self.layoutWidget1.setObjectName(_fromUtf8("layoutWidget1"))
108
109        self.verticalLayout_12 = QtGui.QVBoxLayout(self.layoutWidget1)
110
111        self.verticalLayout_12.setObjectName(_fromUtf8("verticalLayout_12"))
112
113        self.label_14 = QtGui.QLabel(self.layoutWidget1)
114
115        self.label_14.setObjectName(_fromUtf8("label_14"))
```

## APPENDIX A. PYTHON PROGRAM CODE

---

```
90         self.verticalLayout_12.addWidget(self.label_14)
91
92         self.horizontalLayout_4 = QtGui.QHBoxLayout()
93
94         self.horizontalLayout_4.setObjectName(_fromUtf8("horizontalLayout_4"))
95
96         )
97
98         self.Metal1Group = QtGui.QGroupBox(self.layoutWidget1)
99
100        self.Metal1Group.setObjectName(_fromUtf8("Metal1Group"))
101
102        self.horizontalLayout_3 = QtGui.QHBoxLayout(self.Metal1Group)
103
104        self.horizontalLayout_3.setObjectName(_fromUtf8("horizontalLayout_3"))
105
106        )
107
108        self.verticalLayout_9 = QtGui.QVBoxLayout()
109
110        self.verticalLayout_9.setObjectName(_fromUtf8("verticalLayout_9"))
111
112        self.Metal1ScreenLength = QtGui.QDoubleSpinBox(self.Metal1Group)
113
114        self.Metal1ScreenLength.setDecimals(5)
115
116        self.Metal1ScreenLength.setProperty("value", 0.6)
117
118        self.Metal1ScreenLength.setObjectName(_fromUtf8("Metal1ScreenLength"))
119
120        )
121
122        self.verticalLayout_9.addWidget(self.Metal1ScreenLength)
123
124        self.label_5 = QtGui.QLabel(self.Metal1Group)
125
126        self.label_5.setObjectName(_fromUtf8("label_5"))
127
128        self.verticalLayout_9.addWidget(self.label_5)
129
130        self.Metal1FermiEnergy = QtGui.QDoubleSpinBox(self.Metal1Group)
131
132        self.Metal1FermiEnergy.setProperty("value", 1.5)
133
134        self.Metal1FermiEnergy.setObjectName(_fromUtf8("Metal1FermiEnergy"))
135
136        self.verticalLayout_9.addWidget(self.Metal1FermiEnergy)
```

## APPENDIX A. PYTHON PROGRAM CODE

---

```
114         self.label_7 = QtGui.QLabel(self.Metal1Group)
115
116         self.label_7.setObjectName(_fromUtf8("label_7"))
117
118         self.Metal1Lattice = QtGui.QDoubleSpinBox(self.Metal1Group)
119
120         self.Metal1Lattice.setDecimals(5)
121
122         self.Metal1Lattice.setObjectName(_fromUtf8("Metal1Lattice"))
123
124         self.verticalLayout_9.addWidget(self.Metal1Lattice)
125
126         self.horizontalLayout_3.addWidget(self.verticalLayout_9)
127
128         self.horizontalLayout_4.addWidget(self.Metal1Group)
129
130         self.FerroGroup = QtGui.QGroupBox(self.layoutWidget1)
131
132         self.FerroGroup.setObjectName(_fromUtf8("FerroGroup"))
133
134         self.horizontalLayout_5 = QtGui.QHBoxLayout(self.FerroGroup)
135
136         self.horizontalLayout_5.setObjectName(_fromUtf8("horizontalLayout_5"))
137
138         )
139
140         self.verticalLayout_11 = QtGui.QVBoxLayout()
141
142         self.verticalLayout_11.setObjectName(_fromUtf8("verticalLayout_11"))
143
144         self.label_12 = QtGui.QLabel(self.FerroGroup)
145
146         self.label_12.setObjectName(_fromUtf8("label_12"))
147
148         self.verticalLayout_11.addWidget(self.label_12)
149
150         self.FerroDielectricConst = QtGui.QDoubleSpinBox(self.FerroGroup)
151
152         self.FerroDielectricConst.setMaximum(500000.0)
153
154         self.FerroDielectricConst.setProperty("value", 2000.0)
155
156         self.FerroDielectricConst.setObjectName(_fromUtf8("FerroDielectricConst"))
157
158         self.verticalLayout_11.addWidget(self.FerroDielectricConst)
159
160         self.label_6 = QtGui.QLabel(self.FerroGroup)
161
162         self.label_6.setObjectName(_fromUtf8("label_6"))
```

## APPENDIX A. PYTHON PROGRAM CODE

---

```
139         self.verticalLayout_11.addWidget(self.label_6)
140
141         self.FerroBandgap = QtGui.QDoubleSpinBox(self.FerroGroup)
142
143         self.FerroBandgap.setProperty("value", 2.3)
144
145         self.FerroBandgap.setObjectName(_fromUtf8("FerroBandgap"))
146
147         self.verticalLayout_11.addWidget(self.FerroBandgap)
148
149         self.label_9 = QtGui.QLabel(self.FerroGroup)
150
151         self.label_9.setObjectName(_fromUtf8("label_9"))
152
153         self.verticalLayout_11.addWidget(self.label_9)
154
155         self.FerroPolarization = QtGui.QDoubleSpinBox(self.FerroGroup)
156
157         self.FerroPolarization.setProperty("value", 20.0)
158
159         self.FerroPolarization.setObjectName(_fromUtf8("FerroPolarization"))
160
161         self.verticalLayout_11.addWidget(self.FerroPolarization)
162
163         self.label_13 = QtGui.QLabel(self.FerroGroup)
164
165         self.label_13.setObjectName(_fromUtf8("label_13"))
166
167         self.verticalLayout_11.addWidget(self.label_13)
168
169         self.FerroThick = QtGui.QDoubleSpinBox(self.FerroGroup)
170
171         self.FerroThick.setProperty("value", 2.0)
172
173         self.FerroThick.setObjectName(_fromUtf8("FerroThick"))
174
175         self.verticalLayout_11.addWidget(self.FerroThick)
176
177         self.horizontalLayout_5.setLayout(self.verticalLayout_11)
178
179         self.horizontalLayout_4.addWidget(self.FerroGroup)
180
181         self.Metal2Group = QtGui.QGroupBox(self.layoutWidget1)
182
183         self.Metal2Group.setObjectName(_fromUtf8("Metal2Group"))
184
185         self.horizontalLayout_6 = QtGui.QHBoxLayout(self.Metal2Group)
186
187         self.horizontalLayout_6.setObjectName(_fromUtf8("horizontalLayout_6"))
188
189
190     )
191
192     self.verticalLayout_10 = QtGui.QVBoxLayout()
```

## APPENDIX A. PYTHON PROGRAM CODE

---

```
165         self.verticalLayout_10.setObjectName(_fromUtf8("verticalLayout_10"))
166
167         self.label_11 = QtGui.QLabel(self.Metal2Group)
168
169         self.label_11.setObjectName(_fromUtf8("label_11"))
170
171         self.verticalLayout_10.addWidget(self.label_11)
172
173         self.Metal2ScreenLength = QtGui.QDoubleSpinBox(self.Metal2Group)
174
175         self.Metal2ScreenLength.setDecimals(5)
176
177         self.Metal2ScreenLength.setProperty("value", 0.07)
178
179         self.Metal2ScreenLength.setObjectName(_fromUtf8("Metal2ScreenLength"))
180
181     )
182
183     self.verticalLayout_10.addWidget(self.Metal2ScreenLength)
184
185     self.label_8 = QtGui.QLabel(self.Metal2Group)
186
187     self.label_8.setObjectName(_fromUtf8("label_8"))
188
189     self.verticalLayout_10.addWidget(self.label_8)
190
191     self.Metal2FermiEnergy = QtGui.QDoubleSpinBox(self.Metal2Group)
192
193     self.Metal2FermiEnergy.setProperty("value", 3.5)
194
195     self.Metal2FermiEnergy.setObjectName(_fromUtf8("Metal2FermiEnergy"))
196
197     self.verticalLayout_10.addWidget(self.Metal2FermiEnergy)
198
199     self.label_10 = QtGui.QLabel(self.Metal2Group)
200
201     self.label_10.setObjectName(_fromUtf8("label_10"))
202
203     self.verticalLayout_10.addWidget(self.label_10)
204
205     self.Metal2Lattice = QtGui.QDoubleSpinBox(self.Metal2Group)
206
207     self.Metal2Lattice.setDecimals(5)
208
209     self.Metal2Lattice.setObjectName(_fromUtf8("Metal2Lattice"))
210
211     self.verticalLayout_10.addWidget(self.Metal2Lattice)
212
213     self.horizontalLayout_6.setLayout(self.verticalLayout_10)
214
215     self.horizontalLayout_4.addWidget(self.Metal2Group)
216
217     self.verticalLayout_12.setLayout(self.horizontalLayout_4)
```

## APPENDIX A. PYTHON PROGRAM CODE

---

```
191         self.splitter_3 = QtGui.QSplitter(self.splitter_4)
192
193         self.splitter_3.setOrientation(QtCore.Qt.Horizontal)
194
195         self.RunModeling = QtGui.QPushButton(self.splitter_3)
196
197         self.RunModeling.setObjectName(_fromUtf8("RunModeling"))
198
199         self.FrontOutput = QtGui.QTextBrowser(self.splitter_3)
200
201         self.FrontOutput.setMaximumSize(QtCore.QSize(16777215, 16777215))
202
203         self.FrontOutput.setObjectName(_fromUtf8("FrontOutput"))
204
205         self.verticalLayout_7.addWidget(self.splitter_4)
206
207         self.layoutWidget2 = QtGui.QWidget(self.splitter)
208
209         self.layoutWidget2.setObjectName(_fromUtf8("layoutWidget2"))
210
211         self.verticalLayout_14 = QtGui.QVBoxLayout(self.layoutWidget2)
212
213         self.verticalLayout_14.setObjectName(_fromUtf8("verticalLayout_14"))
214
215         self.splitter_2 = QtGui.QSplitter(self.layoutWidget2)
216
217         self.splitter_2.setOrientation(QtCore.Qt.Vertical)
218
219         self.splitter_2.setObjectName(_fromUtf8("splitter_2"))
220
221         self.verticalWidget_6 = QtGui.QWidget(self.splitter_2)
222
223         self.verticalWidget_6.setObjectName(_fromUtf8("verticalWidget_6"))
224
225         self.verticalLayout_8 = QtGui.QVBoxLayout(self.verticalWidget_6)
226
227         self.verticalLayout_8.setObjectName(_fromUtf8("verticalLayout_8"))
228
229         self.PotentialMPlay = QtGui.QVBoxLayout()
230
231         self.PotentialMPlay.setObjectName(_fromUtf8("PotentialMPlay"))
232
233         self.verticalLayout_8.addLayout(self.PotentialMPlay)
234
235         self.PotentialOutput = QtGui.QTextBrowser(self.splitter_2)
236
237         self.PotentialOutput.setMaximumSize(QtCore.QSize(16777215, 16777215))
238
239         self.PotentialOutput.setObjectName(_fromUtf8("PotentialOutput"))
240
241         self.verticalLayout_14.addWidget(self.splitter_2)
```

## APPENDIX A. PYTHON PROGRAM CODE

---

```
218         self.widget = QtGui.QWidget(self.splitter_5)
219
220         self.widget.setObjectName(_fromUtf8("widget"))
221
222         self.verticalLayout_2 = QtGui.QVBoxLayout(self.widget)
223
224         self.ModelingProgress = QtGui.QProgressBar(self.widget)
225
226         self.ModelingProgress.setProperty("value", 24)
227
228         self.ModelingProgress.setObjectName(_fromUtf8("ModelingProgress"))
229
230         self.verticalLayout_2.addWidget(self.ModelingProgress)
231
232         self.horizontalLayout_7 = QtGui.QHBoxLayout()
233
234         self.horizontalLayout_7.setSizeConstraint(QtGui.QLayout.
235
236             SetDefaultConstraint)
237
238         self.horizontalLayout_7.setObjectName(_fromUtf8("horizontalLayout_7"))
239
240         self.label_16 = QtGui.QLabel(self.widget)
241
242         self.label_16.setObjectName(_fromUtf8("label_16"))
243
244         self.horizontalLayout_7.addWidget(self.label_16)
245
246         self.label_15 = QtGui.QLabel(self.widget)
247
248         self.label_15.setObjectName(_fromUtf8("label_15"))
249
250         self.horizontalLayout_7.addWidget(self.label_15)
251
252         self.verticalLayout_2.addLayout(self.horizontalLayout_7)
253
254         self.gridLayout.addWidget(self.splitter_5, 0, 0, 1, 1)
255
256         MainWindow.setCentralWidget(self.centralwidget)
257
258         self.statusbar = QtGui.QStatusBar(MainWindow)
259
260         self.statusbar.setObjectName(_fromUtf8("statusbar"))
261
262         MainWindow.setStatusBar(self.statusbar)
263
264         self.retranslateUi(MainWindow)
```

## APPENDIX A. PYTHON PROGRAM CODE

---

```
243     QtCore.QMetaObject.connectSlotsByName(MainWindow)
244
245     def retranslateUi(self, MainWindow):
246
247         MainWindow.setWindowTitle(_translate("MainWindow", "MainWindow", None
248
249             self.groupBox.setTitle(_translate("MainWindow", "Materials", None))
250
251             self.label.setText(_translate("MainWindow", "Metal 1", None))
252             self.label_2.setText(_translate("MainWindow", "Ferroelectric", None))
253             self.label_3.setText(_translate("MainWindow", "Metal 2", None))
254
255             self.label_14.setText(_translate("MainWindow", "If you know the metal
256
257                 screening lengths, enter them below and leave lattice constant
258
259                 as 0.\n"
260
261             " Otherwise, leave them as 0 and enter the lattice constant, and the program will
262             calculate an approx. screening length.", None))
263
264             self.Metal1Group.setTitle(_translate("MainWindow", "Metal 1", None))
265
266             self.label_4.setText(_translate("MainWindow", "Screening Length (nm)"
267
268                 , None))
269
270             self.label_5.setText(_translate("MainWindow", "Fermi Energy (eV)",
271
272                 None))
273
274             self.label_7.setText(_translate("MainWindow", "Lattice Constant (
275
276                 Angstrom)", None))
277
278             self.FerroGroup.setTitle(_translate("MainWindow", "Ferroelectric",
279
280                 None))
281
282             self.label_12.setText(_translate("MainWindow", "Dielectric Constant (
283
284                 E_f/E_0)", None))
285
286             self.label_6.setText(_translate("MainWindow", "Bandgap (eV)", None))
```

```

260             self.label_9.setText(_translate("MainWindow", "Polarization (micro C/
cm^2)", None))

261             self.label_13.setText(_translate("MainWindow", "Thickness (nm)", None
))

262             self.Metal2Group.setTitle(_translate("MainWindow", "Metal 2", None))

263             self.label_11.setText(_translate("MainWindow", "Screening Length (nm)
", None))

264             self.label_8.setText(_translate("MainWindow", "Fermi Energy (eV)", None))

265             self.label_10.setText(_translate("MainWindow", "Lattice Constant (
Angstrom)", None))

266             self.RunModeling.setText(_translate("MainWindow", "Model This!\n"
267             "\n"))

268             "Output values\n"
269             "will appear to the\n"
270             " right →\n"
271             "\n"
272             "Energy band is plotted\n"
273             "at far right.\n"
274             "\n"
275             "Further plots will be found\n"
276             " on other tabs.", None))

277             self.label_16.setText(_translate("MainWindow", "May 2016, sap1951@rit
.edu, (585) 236—9510", None))

278             self.label_15.setText(_translate("MainWindow", "Created by Spencer
Pringle for Rochester Institute of Technology, 1 Lomb Drive,
Rochester, NY 14623", None))

```

---

## Appendix B: Partial Process - FTJ-devices only

Step Full Step	Num/ Step	Step Code	Step Description	Tool	Time (hrs)
1/1		OX05	pad oxide 500 Å, Tube 4, 45 min at 1000C	Bruce Furnace 4	3
2/2		CV02	1500 Å Si3N4 LPCVD Deposition, 30 min at 810C	LPCVD Nitride	4
3/3		PH03	level 1- Oxide - Clear Field	ASML & SSI	1
4/4		ET29	Plasma etch Nitride, 1500 Å target	LAM 490	0.3
5/5		ET07	ash all photoresist	Gasonics Asher	0.15
6/6		CL01	RCA clean	RCA Bench	0.85
7/7		OX04	First Oxide Tube 1, 3650 Å Bruce 1 Recipe 330, 55 mins at 1000C	Bruce Furnace 1	2.65
8/8		ET06	Etch Oxide, 3650 Å target, BOE 7tol for 3.6 min	7tol BOE	0.25
9/9		OX04	2nd Oxide Tube 1, 3650 Å, Bruce 1 Recipe 330, 55 mins at 1000C	Bruce Furnace 1	2.65
10/10		ET19	Nitride etch, 30s dip 5:1 BHF, 20 min Hot Phosphoric Acid 175C	Hot Phos Bench	1
11/11		PH03	level 2 Nwell - Dark Field	ASML & SSI	1
12/12		IM01	Cover bottom of wafer: Nwell top, 3E13, P31, 170 KeV	Varian Implanter	2
13/15		IM01	Cover top of wafer, Pwell bottom, 8E13, B11, 80 KeV	Varian Implanter	2
14/16		ET07	ash all photoresist	Gasonics Asher	1
15/17		OX06	Well Drive, Tube 1 Recipe 11, 480 min at 1100C	Bruce Furnace 1	8
16/24		ET06	etch 500 Å pad oxide, 50:1 H <sub>2</sub> O:HF (3.6 mins)	50:1 HF Etch	0.25
17/46		PH03	level 10 - P+ D/S - Pimp - Dark Field	ASML & SSI	1

---

**APPENDIX B. PARTIAL PROCESS - FTJ-DEVICES ONLY**


---

Step Num/ Full Step	Step Code	Step Description	Tool	Time (hrs)
18/47(2)	IM01	Cover bottom of wafer: P+ top 4E15, B11, 50 KeV	Varian Implanter	2
18/47(2)	IM01	Cover top half of wafer: N+ bottom 4E15, P31, 60 KeV	Varian Implanter	2
19/48	ET07	ash all photoresist	Gasonics Asher	0.15
20/49	CL01	RCA clean	RCA Bench	0.85
21/50	OX08	DS Anneal, Bruce 2, 3, Recipe 284, 45 min at 1000C	Bruce Furnace 2	3
22/56	CV03	TEOS, P-5000, 4000 ÅOxide	P5000 TEOS Ch A	0.5
23/57	PH03	Photoresist mask to remove TEOS for ALD HfO <sub>2</sub> , Thick Resist COATFAC and DEVFAC Recipes - FEHfO <sub>2</sub> Level - Dark Field	ASML & SSI	1
24/58	ET06	TEOS Etch for HfO <sub>2</sub> area FACCUT, follow with 50:1 HF dip	Drytek Quad	0.5
25/59	ET07	Solvent Strip or Ash	Solvent Strip Bench	0.5
26/60	CV33	ALD HfO <sub>2</sub> Deposition w/ TiN	ALD	4
27/61	RT02	RTP 1 min, 800C	RTP	1
28/62	PH03	(optional) Half wafer protect	Karl Suss Contact	0.5
29/63	ET06	TiN wet etch with RCA 1 NH4OH:H <sub>2</sub> O <sub>2</sub> :H <sub>2</sub> O = 1:2:5 (APM) solution at 60 C. (1nm/s, [39])	Aligner Stepper Hot Plate with Pyrex Dish	1

**APPENDIX B. PARTIAL PROCESS - FTJ-DEVICES ONLY**

---

<b>Step Num/ Full Step</b>	<b>Step Code</b>	<b>Step Description</b>	<b>Tool</b>	<b>Time (hrs)</b>
30/64	ET07	(optional) Solvent Strip or Ash	Solvent Strip Bench	0.5
31/65	PH03	Photoresist mask to remove HfO <sub>2</sub> if not selective growth (Negative Resist) - FEHfO <sub>2</sub> Level - Dark Field	ASML & SSI	1
32/66	ET06	HfO <sub>2</sub> etch, 50:1 H <sub>2</sub> O:HF appx. 97s for 3nm HfO <sub>2</sub> , assuming 1:10 HfO <sub>2</sub> :SiO <sub>2</sub> selectivity. [40]	50:1 HF Etch	0.25
33/67	ET07	Solvent Strip or Ash	Gasonics Asher	0.15
34/68	PH03	level 11 - CC, Thick Resist COATFAC and DEVFAC Recipes - Cont level - dark field	ASML & SSI	1
35/69	ET06	CC etch, FACCUT, 200 W, 100 mT, 50 sccm CHF <sub>3</sub> , 10 sccm CF <sub>4</sub> , 100 sccm Ar	Drytek Qquad	0.5
36/70	ET07	ash all photoresist	Gasonics Asher	0.15
37/71	CL01	RCA clean	RCA Bench	0.85
38/72	ME01	Aluminum Sputter 7500 Å	CVC601	1
39/73	PH03	level 12 - Metal1, Thick resist, COATMTL and DEVMTL recipes, clear field	ASML & SSI	1
40/74	ET15	plasma 125W, Al Etch, BCl, Cl <sub>2</sub> , Chloroform, Target 7500 Å	LAM4600	1.5
41/75	ET07	ash all photoresist	Gasonics Asher	0.15

## Appendix C: Athena code

```

1  #Full process for CMOS portion of Thesis
2
3 go athena
4
5 line x loc=0.0 spac=0.02
6 line x loc=96.6 spac=0.02
7 #
8 line y loc=0.00 spac=0.02
9 line y loc=2 spac=0.02
10 line y loc=3 spac=0.1
11 line y loc=5 spac=0.1
12
13 method grid.oxide=.01 gridinit.ox=.01
14
15 # INITIALIZE MATERIAL
16 #
-----#
17 #
18 init silicon boron resistivity=10 orientation=100
    space.mult=3.0
20
21 #OX05
22 diffus time=27 temp=25 t.final=800 nitro
23 diffus time=20 temp=800 t.final=1000 f.o2=5
24 diffus time=50 temp=1000 f.o2=10
25 diffus time=5 temp=1000 f.n2=15
26 diffus time=40 temp=1000 t.final=800 f.n2=10
27 diffus time=15 temp=800 t.final=25 f.n2=5
28
29 #CV02
30 deposit nitride thick=0.15
31
32 #PH03
33 deposit photoresist thick=1.00
34 etch photoresist start x=39.10 y=-2.00
35 etch cont x=49.10 y=-2.00
36 etch cont x=49.10 y=3.00
37 etch cont x=39.10 y=3.00
38 etch done x=39.10 y=-2.00
39 etch photoresist start x=87.60 y=-2.00
40 etch cont x=91.60 y=-2.00
41 etch cont x=91.60 y=3.00
42 etch cont x=87.60 y=3.00
43 etch done x=87.60 y=-2.00
44 etch photoresist left p1.x=2
45 etch photoresist right p1.x=93.6
46
47 #ET29
48 etch nitride right p1.x=93.6
49 etch nitride start x=39.10 y=-2.00
50 etch cont x=49.10 y=-2.00
51 etch cont x=49.10 y=3.00
52 etch cont x=39.10 y=3.00
53 etch done x=39.10 y=-2.00
54 etch nitride start x=87.60 y=-2.00
55 etch cont x=91.60 y=-2.00
56 etch cont x=91.60 y=3.00
57 etch cont x=87.60 y=3.00
58 etch done x=87.60 y=-2.00
59 etch nitride left p1.x=2
60
61 #ET07
62 etch photoresist all
63
64 #CL01
65
66
67 #OX04
68 diffus time=27 temp=25 t.final=800 nitro
69 diffus time=20 temp=800 t.final=1000 f.n2=5
70 diffus time=5 temp=1000 f.o2=2
71 diffus time=50 temp=1000 f.h2=3.6 f.o2=2
72 diffus time=5 temp=1000 f.n2=15
73 diffus time=40 temp=1000 t.final=800 f.n2=10
74 diffus time=15 temp=800 t.final=25 f.n2=5
75
76 #ET06
77 rate.etch machine=BOE(7to1) oxide u.m wet.etch
    isotropic=0.1
78 etch machine=BOE(7to1) time=3.6 minutes
79
80 #OX04
81 diffus time=27 temp=25 t.final=800 nitro
82 diffus time=20 temp=800 t.final=1000 f.n2=5
83 diffus time=5 temp=1000 f.o2=2
84 diffus time=50 temp=1000 f.h2=3.6 f.o2=2
85 diffus time=5 temp=1000 f.n2=15
86 diffus time=40 temp=1000 t.final=800 f.n2=10
87 diffus time=15 temp=800 t.final=25 f.n2=5
88
89 #ET19
90 etch nitride all
91
92 #PH03
93 deposit photoresist thick=1.00
94 etch photoresist start x=0.00 y=-2.00
95 etch cont x=44.10 y=-2.00
96 etch cont x=44.10 y=3.00
97 etch cont x=0.00 y=3.00
98 etch done x=0.00 y=-2.00
99 etch photoresist start x=90.60 y=-2.00
100 etch cont x=94.6 y=-2.00
101 etch cont x=94.6 y=3.00

```

## APPENDIX C. ATHENA CODE

---

```

102 | etch cont x=90.6 y=3.00
103 | etch done x=0.00 y=-2.00
104 |
105 | #IM01
106 |
107 | implant phosphor dose=3.0e13 energy=170 tilt=0
108 |     rotation=0 crystal
109 | #ET07
110 | etch photoresist all
111 |
112 | #PH03
113 | deposit photoresist thick=1.00
114 | etch photoresist start x=44.1 y=-2.00
115 | etch cont x=88.6 y=-2.00
116 | etch cont x=88.6 y=3.00
117 | etch cont x=44.1 y=3.00
118 | etch done x=44.1 y=-2.00
119 |
120 | #IM01
121 | implant boron dose=8.0e13 energy=80 tilt=0
122 |     rotation=0 crystal
123 | #ET07
124 | etch photoresist all
125 |
126 | #OX06
127 | diffus time=27 temp=25 t.final=800 nitro
128 | diffus time=30 temp=800 t.final=1100 f.n2=10
129 | diffus time=360 temp=1100 f.n2=10
130 | diffus time=5 temp=1100 f.n2=10
131 | diffus time=60 temp=1100 t.final=800 f.n2=10
132 | diffus time=12 temp=800 t.final=25 f.n2=5
133 |
134 | #PH03
135 | deposit photoresist thick=1.00
136 | etch photoresist start x=44.1 y=-2.00
137 | etch cont x=88.6 y=-2.00
138 | etch cont x=88.6 y=3.00
139 | etch cont x=44.1 y=3.00
140 | etch done x=44.1 y=-2.00
141 | etch photoresist left p1.x=2
142 |
143 | #IM01
144 | implant phosphor dose=7.95e12 energy=60 tilt=0
145 |     rotation=0 crystal
146 | #ET07
147 | etch photoresist all
148 |
149 | #PH03
150 | deposit photoresist thick=1.00
151 | etch photoresist start x=2.00 y=-2.00
152 | etch cont x=44.10 y=-2.00
153 | etch cont x=44.10 y=3.00
154 | etch cont x=2.00 y=3.00
155 | etch done x=2.00 y=-2.00
156 |
157 | #IM01
158 | implant boron dose=3.02e12 energy=30 tilt=0
159 |     rotation=0 crystal
160 | #ET07
161 | etch photoresist all
162 |
163 | struct outfile = CMOSWellandVt.str
164 | #tonyplot CMOSWellandVt.str
165 |
166 | #ET06
167 | rate.etch machine=H2O_HF(50to1) oxide n.m wet.etch
168 |     isotropic=18.7
169 | etch machine=H2O_HF(50to1) time=3.6 minutes
170 | #CL01
171 |
172 | #ET06
173 | #ET06
174 |
175 |
176 | #OX06
177 | deposit oxide thick=0.01
178 |
179 | #CV01
180 | deposit polysilicon thick=0.40
181 |
182 | #PH03
183 | deposit photoresist thick=1.00
184 | etch photoresist left p1.x=30.6
185 | etch photoresist start x=32.60 y=-2.00
186 | etch cont x=55.60 y=-2.00
187 | etch cont x=55.60 y=3.00
188 | etch cont x=32.60 y=3.00
189 | etch done x=32.60 y=-2.00
190 | etch photoresist right p1.x=57.60
191 |
192 | #ET08
193 | etch polysilicon left p1.x=30.6
194 | etch polysilicon start x=32.60 y=-2.00
195 | etch cont x=55.60 y=-2.00
196 | etch cont x=55.60 y=3.00
197 | etch cont x=32.60 y=3.00
198 | etch done x=32.60 y=-2.00
199 | etch polysilicon right p1.x=57.60
200 |
201 | #ET07
202 | etch photoresist all
203 |
204 | #CL01
205 |
206 |
207 | #OX05
208 | diffus time=27 temp=25 t.final=800 nitro

```

## APPENDIX C. ATHENA CODE

---

```

209 | deposit oxide thick=0.05
210 | diffus time=20 temp=800 t.final=1000 f.n2=5
211 | diffus time=50 temp=1000 f.n2=10
212 | diffus time=5 temp=1000 f.n2=15
213 | diffus time=40 temp=1000 t.final=800 f.n2=10
214 | diffus time=15 temp=800 t.final=25 f.n2=5
215 |
216 | #PH03
217 | deposit photoresist thick=4.00
218 | etch photoresist start x=10.00 y=-6.00
219 | etch cont x=44.30 y=-6.00
220 | etch cont x=44.30 y=3.00
221 | etch cont x=10.00 y=3.00
222 | etch done x=10.00 y=-6.00
223 | etch photoresist start x=80.60 y=-6.00
224 | etch cont x=88.6 y=-6.00
225 | etch cont x=88.6 y=3.00
226 | etch cont x=80.6 y=3.00
227 | etch done x=80.6 y=-6.00
228 |
229 | #IM01
230 | implant boron dose=4e14 energy=50 tilt=0 rotation
231 | =0 crystal
232 | #ET07
233 | etch photoresist all
234 |
235 | #PH03
236 | deposit photoresist thick=4.00
237 | etch photoresist start x=44.30 y=-6.00
238 | etch cont x=80.60 y=-6.00
239 | etch cont x=80.60 y=3.00
240 | etch cont x=44.30 y=3.00
241 | etch done x=44.30 y=-6.00
242 | etch photoresist left p1.x=10
243 |
244 | #IM01
245 | implant phosphor dose=4e14 energy=60 tilt=0
246 | rotation=0 crystal
247 | #ET07
248 | etch photoresist all
249 |
250 | #CL01
251 | struct outfile = CMOSPostNitride.str
252 |
253 | #CV02
254 | deposit nitride thick=0.35
255 |
256 | #ET39
257 | etch nitride dry thick=0.40
258 |
259 | #PH03
260 | deposit photoresist thick=4.00
261 | etch photoresist start x=44.30 y=-6.00
262 | etch cont x=80.60 y=-6.00
263 | etch cont x=80.60 y=3.00
264 | etch cont x=44.30 y=3.00
265 | etch done x=44.30 y=-6.00
266 | etch photoresist left p1.x=10
267 |
268 | #IM01
269 | implant phosphor dose=2.7e13 energy=60 tilt=0
270 | rotation=0 crystal
271 | #ET07
272 | etch photoresist all
273 |
274 | #PH03
275 | deposit photoresist thick=4.00
276 | etch photoresist start x=10.00 y=-6.00
277 | etch cont x=44.30 y=-6.00
278 | etch cont x=44.30 y=3.00
279 | etch cont x=10.00 y=3.00
280 | etch done x=10.00 y=-6.00
281 | etch photoresist start x=80.60 y=-6.00
282 | etch cont x=88.6 y=-6.00
283 | etch cont x=88.6 y=3.00
284 | etch cont x=80.6 y=3.00
285 | etch done x=80.6 y=-6.00
286 | etch photoresist start x=90.60 y=-2.00
287 | etch cont x=94.6 y=-2.00
288 | etch cont x=94.6 y=3.00
289 | etch cont x=90.6 y=3.00
290 | etch done x=0.00 y=-2.00
291 |
292 | #IM01
293 | implant boron dose=2.7e13 energy=50 tilt=0
294 | rotation=0 crystal
295 | #ET07
296 | etch photoresist all
297 |
298 | #CL01
299 | struct outfile = CMOSPostNitride.str
300 |
301 | #OX08
302 | diffus time=27 temp=25 t.final=800 nitro
303 | diffus time=20 temp=800 t.final=1000 f.n2=5
304 | diffus time=20 temp=1000 f.n2=10
305 | diffus time=5 temp=1000 f.n2=15
306 | diffus time=40 temp=1000 t.final=800 f.n2=10
307 | diffus time=15 temp=800 t.final=25 f.n2=5
308 |
309 | #ET06
310 | rate.etch machine=H2O_HF(50to1) oxide n.m wet.etch
311 | isotropic=18.7
312 | etch machine=H2O_HF(50to1) time=3 minutes
313 | #was 3.6 minutes
314 |
315 | struct outfile = CMOSSD2.str

```

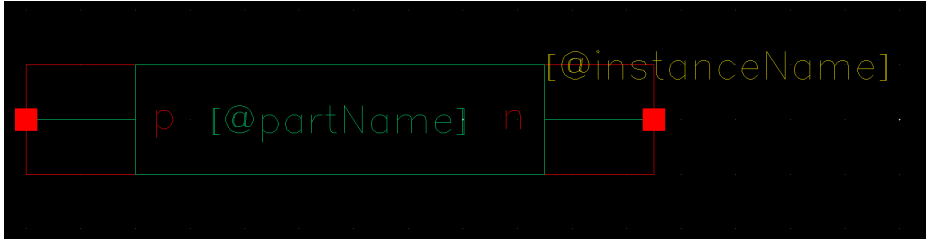
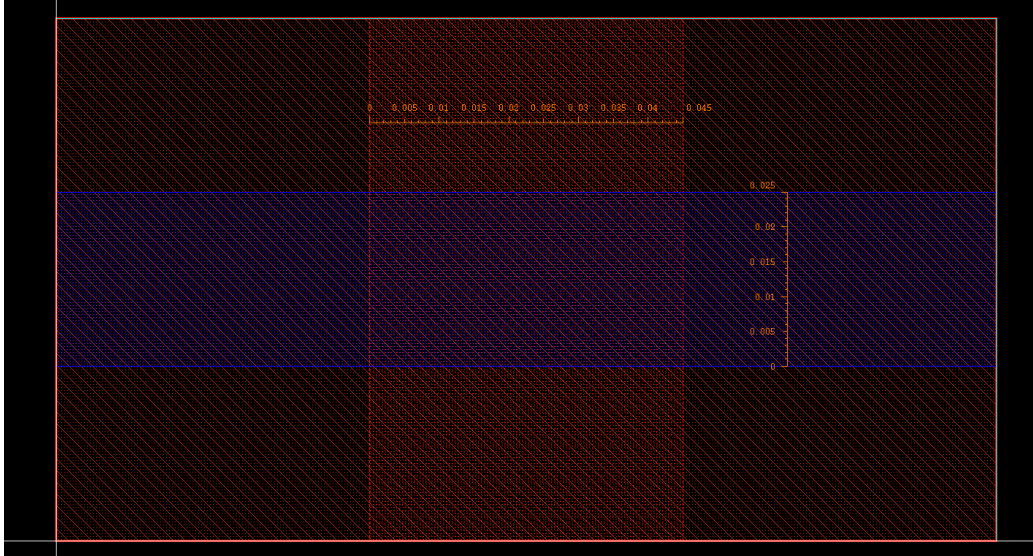
## APPENDIX C. ATHENA CODE

---

316	#tonyplot CMOSSD.str	365	etch done x=83.60 y=-6.00
317		366	etch photoresist start x=90.60 y=-6.00
318	#ME03	367	etch cont x=94.60 y=-6.00
319		368	etch cont x=94.60 y=3.00
320		369	etch cont x=90.60 y=3.00
321	#RT01	370	etch done x=90.60 y=-6.00
322		371	
323		372	
324	#ET11	373	#ET06
325		374	etch oxide dry thick=0.5
326		375	
327	#RT02	376	#ET07
328		377	etch photoresist all
329		378	
330	#CV03	379	#CL01
331	deposit oxide thick=0.50 divisions=20	380	
332	#added the divisions=20	381	
333		382	#ME01
334	#PH03	383	deposit aluminum thick=0.75
335	deposit photoresist thick=1.00	384	
336	etch photoresist start x=4.00 y=-6.00	385	#PH03
337	etch cont x=6.00 y=-6.00	386	deposit photoresist thick=1.30
338	etch cont x=6.00 y=3.00	387	etch photoresist left p1.x=2.00
339	etch cont x=4.00 y=3.00	388	etch photoresist start x=14.00 y=-6.00
340	etch done x=4.00 y=-6.00	389	etch cont x=34.60 y=-6.00
341	etch photoresist start x=11.00 y=-6.00	390	etch cont x=34.60 y=3.00
342	etch cont x=13.00 y=-6.00	391	etch cont x=14.00 y=3.00
343	etch cont x=13.00 y=3.00	392	etch done x=14.00 y=-6.00
344	etch cont x=11.00 y=3.00	393	etch photoresist start x=53.60 y=-6.00
345	etch done x=11.00 y=-6.00	394	etch cont x=73.80 y=-6.00
346	etch photoresist start x=35.60 y=-6.00	395	etch cont x=73.80 y=3.00
347	etch cont x=37.60 y=-6.00	396	etch cont x=53.60 y=3.00
348	etch cont x=37.60 y=3.00	397	etch done x=53.60 y=-6.00
349	etch cont x=35.60 y=3.00	398	etch photoresist start x=87.60 y=-6.00
350	etch done x=35.60 y=-6.00	399	etch cont x=92.10 y=-6.00
351	etch photoresist start x=50.10 y=-6.00	400	etch cont x=92.10 y=3.00
352	etch cont x=52.10 y=-6.00	401	etch cont x=87.60 y=3.00
353	etch cont x=52.10 y=3.00	402	etch done x=87.60 y=-6.00
354	etch cont x=50.10 y=3.00	403	
355	etch done x=50.10 y=-6.00	404	#ET15
356	etch photoresist start x=74.80 y=-6.00	405	etch aluminum dry thick=1.00
357	etch cont x=76.80 y=-6.00	406	
358	etch cont x=76.80 y=3.00	407	#ET07
359	etch cont x=74.80 y=3.00	408	etch photoresist all
360	etch done x=74.80 y=-6.00	409	
361	etch photoresist start x=83.60 y=-6.00	410	struct outfile = CMOSComplete2.str
362	etch cont x=85.60 y=-6.00	411	tonyplot CMOSComplete2.str
363	etch cont x=85.60 y=3.00	412	
364	etch cont x=83.60 y=3.00	413	quit

## Appendix D: sap1951\_FTJ\_THESES\_45

### D.1 Linear Resistance FTJ Model

Library Name:	sap1951_FTJ_THESES_45
Cell Name:	SAP_FTJ_DIGITAL_LOW
Layout Area:	(45nm CMOS) $0.135\mu\text{m} \times 0.075\mu\text{m} = W \times H$ (Scaled 2um CMOS) $6 \mu\text{m} \times 3.3 \mu\text{m} = W \times H$
Symbol with Port Names:	
	
Layout:	
	

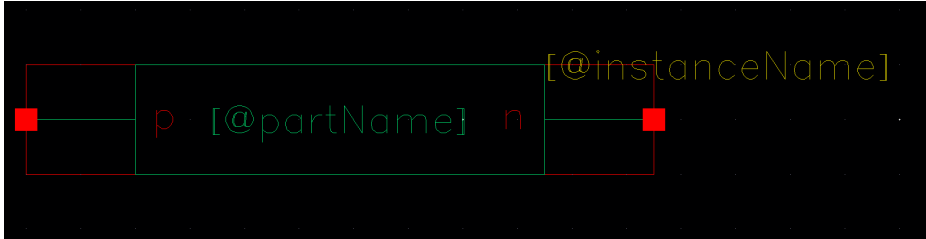
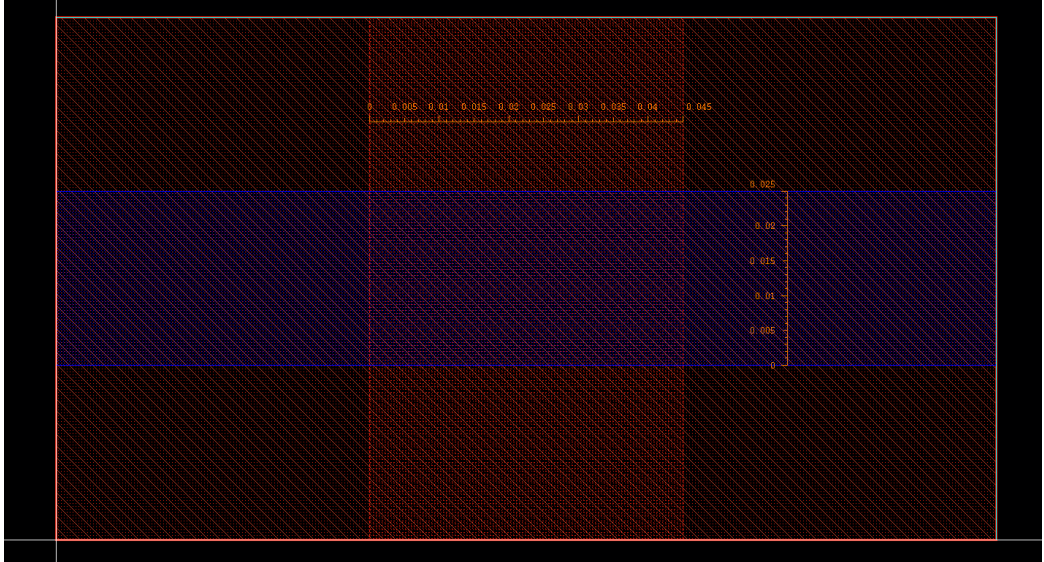
### D.1.1 Verilog Model

```
1          // VerilogA for sap1951_FTJ_THESES_45,
2          SAP_FTJ_DIGITAL_LOW, veriloga
3
4          'include "constants.vams"
5          'include "disciplines.vams"
6          'timescale 10ps/1fs
7
8
9          module SAP_FTJ_DIGITAL_LOW(p, n);
10
11
12          inout p;
13          electrical p;
14          inout n;
15          electrical n;
16
17
18          parameter R_pos = 1e6;           // On
19          resistance 9e6
20
21          parameter R_neg = 1e7;         // Off resistance
22          1.4e8
23
24          parameter dr = 34.35e6;       // abs(R_pos -
25          R_neg) 1.31e8
26
27          parameter dt = 40; //20
28
29          parameter x0 = 0.5;
30
31          parameter v_pos = 0.3;        //
32
33          parameter v_neg = -0.3;       //
```

```
22         real Rm;
23         real Vm;
24         real Im;
25         integer voltages;           // voltages
26                         file pointer
27         integer currents;          // currents
28                         file pointer
29
30         analog begin
31             @initial_step begin
32                 voltages = $fopen("voltages.out");
33                 currents = $fopen("currents.out");
34                 Rm = (1-x0)*R_neg + x0*R_pos;
35             end
36
37             // Get the terminal voltage
38             Vm = V(p,n);
39
40             // Change the memristance
41             if ((Rm > R_pos)&&(Vm>=v_pos))
42                 begin
43                     Rm=Rm-(dr/dt);
44                 end
45             if ((Rm < R_neg)&&(Vm<=v_neg))
46                 begin
47                     Rm=Rm+(dr/dt);
48                 end
```

```
47
48           Im = Vm / Rm;
49           I(p,n) <+ Im;
50
51           $fstroke(voltages,"%g",Vm);
52           $fstroke(currents,"%g",Im);
53
54           @(final_step)
55           begin
56               $fclose(voltages);
57               $fclose(currents);
58           end
59       end
60
61   endmodule
```

## D.2 Polarization-Timing FTJ Model

<b>Library Name:</b>	sap1951_FTJ_THESES_45
<b>Cell Name:</b>	SAP_FTJ_DIGITAL_LOW_TIMING
<b>Layout Area:</b>	(45nm CMOS) $0.135\mu\text{m} \times 0.075\mu\text{m} = W \times H$ (Scaled 2um CMOS) $6 \mu\text{m} \times 3.3 \mu\text{m} = W \times H$
<b>Symbol with Port Names:</b>	
	
<b>Layout:</b>	
	

### D.2.1 Verilog Model

```
1          // VerilogA for sap1951_FTJ_THESES ,
2
3          'include "constants.vams"
4
5          'include "disciplines.vams"
6
7          'timescale 1ns/1ps
8
9
10         module SAP_FTJ_DIGITAL_LOW_TIMING(p, n);
11
12         inout p;
13
14         electrical p;
15
16         inout n;
17
18         electrical n;
19
20
21         parameter Vc=0.4;    //0.3
22
23         parameter Vc0=0.9;
24
25         parameter kb=1.38e-23;
26
27         parameter pi=3.14159;
28
29         parameter m0=9.11e-31;
30
31         parameter mstar=0.11;
32
33         parameter q=1.6e-19;
34
35         parameter h=6.626e-34;
36
37         real hbar=h/(2*pi);
38
39         parameter heV=4.13e-15;
40
41         parameter T=300;
```

```
25         real kT=(kb/q)*T;
26
27         real Rm;
28         real Vm;
29         real Vd;
30         real Im;
31         real sigmap;
32         real sigmas;
33         real Pot1;
34         real Pot2;
35         real Pot;
36
37         parameter AA=445.402;
38         parameter AB=118.125;
39         parameter AC=7.782;
40         parameter BA=-416.102;
41         parameter BB=-112.071;
42         parameter BC=-7.525;
43         parameter ALA=22;
44         parameter ALB=5.8;
45         parameter ALC=0.26;
46         real d=10*Vc*1e-9;
47         parameter delta1=0.06*1e-9;
48         parameter delta2=3.0*1e-9; //0.4*1e-9
49         parameter epsilonnf=40;
50         parameter epsilon0=8.854e-12;
51         parameter Ea=2;
```

```
52          parameter Ef1=4.08;
53          parameter Ef2=5.12;
54          real Atun=sqrt((2*m0*q*mstar))*(d)*(2)/
55              hbar;
56          real J0=(6.08e8)/((d*1e9)**2);
57          parameter Dim=500; //dimension of FTJ (in
58              nm) assuming area of Dim^2
59
60          real A;
61          real Av1;
62          real Av2;
63          real B;
64          real Bv1;
65          real Bv2;
66          real C;
67          real Cv1;
68          real Cv2;
69          real D;
70          real Dv1;
71          real Dv2;
72          real E;
73          real Pr1;
74          real Pr2;
75          real Pr3;
76          real Pr4;
```

```
77      real Pr5;
78      real Pr6;
79      real Pr7;
80
81      real Pr21;
82      real Pr22;
83      real Pr23;
84      real Pr24;
85      real Pr25;
86      real Pr26;
87      real Pr27;
88
89      real time0;
90      real time1;
91      real currenttime;
92
93
94      real tPr[0:13];
95      real Pr[0:13];
96      real tSat[0:13] = '{1e-2, 5e-4, 5e-3, 1e
-4, 5e-6, 5e-6, 5e-6, 5e-6, 2e-6, 2e-6,
2e-6, 1e-6, 1e-6, 1e-6};
97
98      real Prtotal;
99      real Jtun;
100
101     integer voltages;
```

```
102          integer currents;
103          integer i;
104
105          analog begin
106              @ (initial_step) begin
107                  voltages = $fopen("voltages.out");
108                  currents = $fopen("currents.out");
109                  Rm = 1.3e7;
110                  time0 = 1e-13;
111                  // $display ("The coercive voltage is
112                  // currently %e at %e seconds", Vc,
113                  // $abstime);
114
115                  // $display ("J0 is %e and Atun is %e", J0,
116                  // Atun);
117
118                  // $display ("4 is %e and 4**2 is %e", 4,
119                  // 4**2);
120
121                  end
122
123                  // Get terminal voltage
124
125                  Vm=V(p,n);
126
127
128                  // Move along time values of applicable
129                  // polarization domains
130
131
132                  Vd=0.4;
133
134
135                  time1 = $abstime;
```

```
123 // $display("time1 became %e at %e", time1,
124 // $abstime);
125 for (i=0;i<14;i=i+1)
126 begin
127 if (abs(Vm)>(Vd*Vc/Vc0))
128 begin
129
130 if ((Vm<0) && (tPr[i]>(0-tSat[i])))
131 begin
132 tPr[i] = tPr[i]-(time1-time0);
133 end
134 else if ((Vm>0) && (tPr[i]<tSat[i]))
135 tPr[i] = tPr[i]+(time1-time0);
136 //if (Vd>1.7)
137 // $display("Current time is %e while
138 // the saturation time is %e for voltage
139 // of %e", tPr[i], tSat[i], Vd);
140 // $display("The polarization time for
141 // domain between %e and %e is %e at time
142 // %e", Vd-0.2, Vd, tPr[i], $abstime);
143 //Calculate A value for Pr .4
144 Av1 = AA*Vd+BA;
145 Av2 = ALA*Vd;
146 if (Av1>Av2)
147 A=Av1;
148 else
```

```
145      A=A*v2;
146      // $display("A = %e",A);
147      // Calculate B value for Pr .4
148      Bv1 = AB*Vd+BB;
149      Bv2 = ALB*Vd;
150      if (Bv1>Bv2)
151          B=Bv1;
152      else
153          B=Bv2;
154      // $display("B = %e",B);
155      // Calculate C value for Pr .4
156      Cv1 = AC*Vd+BC;
157      Cv2 = ALC*Vd;
158      if (Cv1>Cv2)
159          C=Cv1;
160      else
161          C=Cv2;
162      // $display("C = %e",C);
163      // Calculate D value for Pr .4
164      Dv1 = 9.904*Vd+17.865;
165      Dv2 = 19.375*(Vd**2)-6.3*Vd+1.4;
166      if (Dv1>Dv2)
167          D=Dv2;
168      else
169          D=Dv1;
170      // $display("D = %e",D);
171      // Calculate E value for Pr .4
```

```
172          E = 9.105*Vd-5.152-3.387*(Vd**2);  
173          if (E<0.217)  
174              E=0.217;  
175          //\$display("E = %e",E);  
176          Pr4 = A+B*log((Vc0/Vc)*abs(tPr[i]))+C*(log  
177                  ((Vc0/Vc)*abs(tPr[i]))**2);  
178          Pr3 = D+E*ln((Vc0/Vc)*abs(tPr[i]));  
179          Pr2 = 6.339*Vd+27.357;  
180          Pr1 = 13.071*(Vd**2.929);  
181          if (Pr4<0)  
182              Pr4 = 0;  
183          if (Pr3<Pr4)  
184              Pr5 = Pr3;  
185          else  
186              Pr5 = Pr4;  
187          if (Pr5<0)  
188              Pr5 = 0;  
189          if (Pr1<Pr2)  
190              Pr6 = Pr1;  
191          else  
192              Pr6 = Pr2;  
193          if (Pr5<Pr6)  
194              Pr7 = Pr5;
```

```
198         else
199             Pr7 = Pr6;
200
201             //Calculate A value for Pr .2
202             Av1 = AA*(Vd-0.2)+BA;
203             Av2 = ALA*(Vd-0.2);
204             if (Av1>Av2)
205                 A=Av1;
206             else
207                 A=Av2;
208             //Calculate B value for Pr .2
209             Bv1 = AB*(Vd-0.2)+BB;
210             Bv2 = ALB*(Vd-0.2);
211             if (Bv1>Bv2)
212                 B=Bv1;
213             else
214                 B=Bv2;
215             //Calculate C value for Pr .2
216             Cv1 = AC*(Vd-0.2)+BC;
217             Cv2 = ALC*(Vd-0.2);
218             if (Cv1>Cv2)
219                 C=Cv1;
220             else
221                 C=Cv2;
222             //Calculate D value for Pr .2
223             Dv1 = 9.904*(Vd-0.2)+17.865;
```

```
224      Dv2 = 19.375*((Vd-0.2)**2)-6.3*(Vd-0.2)
              +1.4;
225      if (Dv1>Dv2)
226          D=Dv2;
227      else
228          D=Dv1;
229      //Calculate E value for Pr .2
230      E = 9.105*(Vd-0.2)-5.152-3.387*((Vd-0.2)
              **2);
231      if (E<0.217)
232          E=0.217;
233
234      Pr24 = A+B*log((Vc0/Vc)*abs(tPr[i]))+C*(
              log((Vc0/Vc)*abs(tPr[i]))**2);
235      Pr23 = D+E*ln((Vc0/Vc)*abs(tPr[i]));
236      Pr22 = 6.339*(Vd-0.2)+27.357;
237      Pr21 = 13.071*((Vd-0.2)**2.929);
238
239      if (Pr24<0)
240          Pr24 = 0;
241      if (Pr23<Pr24)
242          Pr25 = Pr23;
243      else
244          Pr25 = Pr24;
245
246      if (Pr25<0)
247          Pr25 = 0;
```

```
248
249         if  (Pr21<Pr22)
250             Pr26 = Pr21;
251         else
252             Pr26 = Pr22;
253
254         if  (Pr25<Pr26)
255             Pr27 = Pr25;
256         else
257             Pr27 = Pr26;
258
259         Pr[i] = Pr7 - Pr27;
260
261         if  (tPr[i]<0)
262             Pr[i] = 0-Pr[i];
263
264         //$/display("Polarization values used were
265             (in order) %e %e %e %e %e %e %e %e %
266             e %e %e %e %e",Pr1,Pr2,Pr3,Pr4,Pr5,Pr6,
267             Pr7,Pr21,Pr22,Pr23,Pr24,Pr25,Pr26,Pr27)
268             ;
269
270         end
271
272         //$/display("The for loop just completed Vd
273             = %e, at time %e", Vd, time1);
274
275         Vd = Vd+0.2;
276
277     end
```

```
270
271     Prtotal =0.5*( Pr[0] + Pr[1] + Pr[2] + Pr
272                         [3] + Pr[4] + Pr[5] + Pr[6] + Pr[7] +
273                         Pr[8] + Pr[9] + Pr[10] + Pr[11] + Pr
274                         [12] + Pr[13]);;
275
276 // $display("The total polarization is
277 // currently %e at %e seconds", Prtotal,
278 // $abstime);
279
280 sigmap=Prtotal*1e-2;
281 // $display("sigma_p is %e", sigmap);
282 sigmas=sigmap*d/(epsilonf*(delta1+delta2)+d);
283 // $display("sigma_s is %e", sigmas);
284
285 Pot1=(sigmas*delta1/epsilon0)+Ea;
286 // $display("Pot1 is %e", Pot1);
287 Pot2=Ea+Ef2-Ef1-(sigmas*delta2/epsilon0);
288 // $display("Pot2 is %e", Pot2);
289 Pot=(Pot1+Pot2)/2;
290 // $display("Average potential barrier is %
291 // %e", Pot);
292 Jtun=J0*((Pot)*exp(-Atun*sqrt(Pot))-(Pot+
293 Vm)*exp(-Atun*sqrt(Pot+Vm)));
294 // $display("Current density in A/cm^2 is %
295 // %e", Jtun);
```

```
288
289          Rm = Vm / ( Jtun * ((Dim*1e-7)**2));
290
291          time0 = $abstime;
292          // $display("time0 became %e at %e", time0,
293          //           $abstime);
294          Im = Vm / Rm;
295          I(p,n) <+ Im;
296
297          $fstroke(voltages, "%g", Vm);
298          $fstroke(currents, "%g", Im);
299
300          @ (final_step)
301          begin
302              $fclose(voltages);
303              $fclose(currents);
304          end
305          // $display("The total polarization is
306          // currently %e at %e seconds", Prtotal,
307          //           $abstime);
308
309
310      endmodule
```

### D.3 SAP\_ADDRESS\_COLUMN\_R

<b>Library Name:</b>	sap1951_FTJ_THESES_45
<b>Cell Name:</b>	SAP_ADDRESS_COLUMN_R

**Function/Truth Table:**

<i>Ren</i>	<i>WenN</i>	<i>Y</i>
0	0	X
0	1	X
1	0	X
1	1	<i>v<sub>ssa</sub></i>

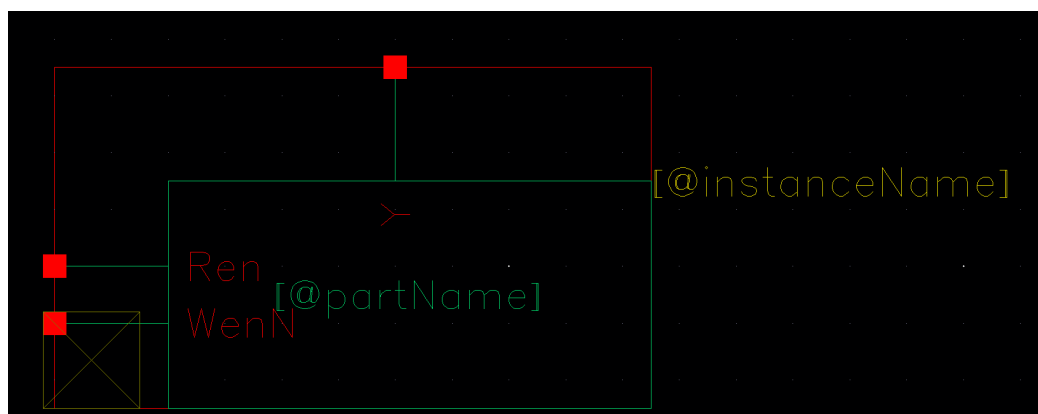
**Propagation Delay ( $t_{pdf}$  and  $t_{pdr}$ ) and Output Rise/Fall Time ( $t_f$  and  $t_r$ ):**

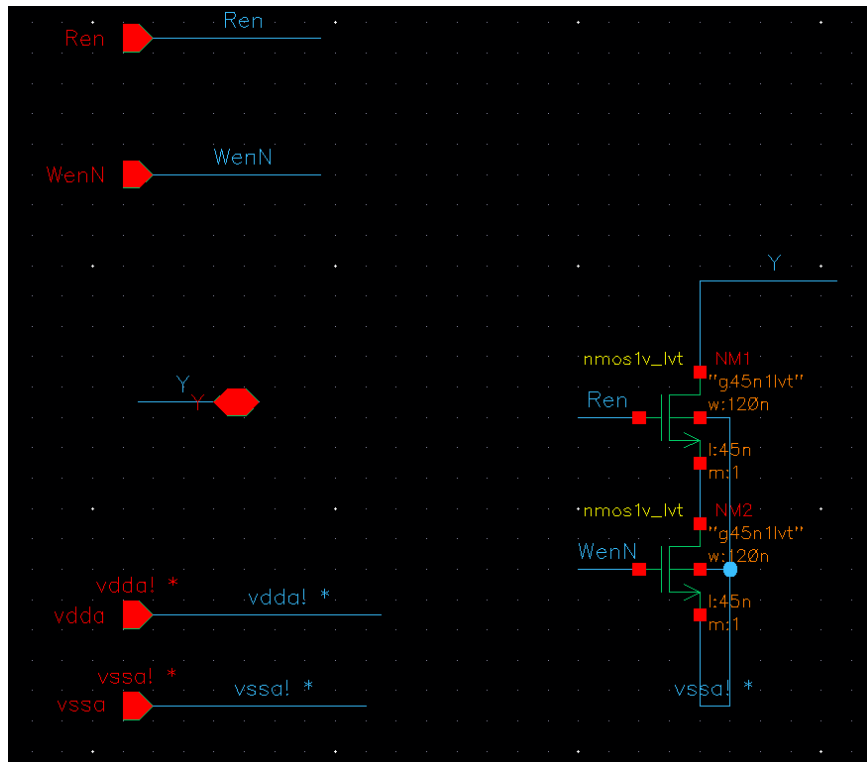
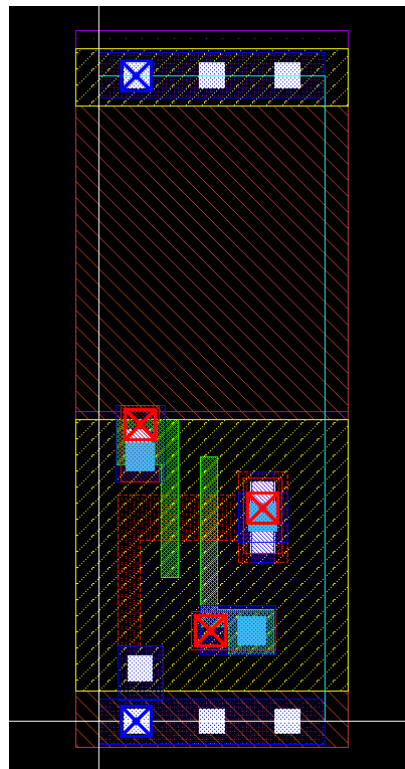
In	Out	$t_{pdf}$	$t_{pdr}$	$t_f$	$t_r$
Ren	Y	$561.8 \times 10^{-12}$	$603.1 \times 10^{-12}$	$473.3 \times 10^{-12}$	$1.498 \times 10^{-9}$
WenN	Y	$552.2 \times 10^{-12}$	$701.6 \times 10^{-12}$	$464.5 \times 10^{-12}$	$1.746 \times 10^{-9}$

Notice long  $t_r$  because this device doesn't drive the output high, it can only drag it down to  $v_{ssa}$ .

**Layout Area:**  $0.6\mu\text{m} \times 1.71\mu\text{m} = W \times H$

**Symbol with Port Names:**



**Schematic:****Layout:**

Functional Simulation Waveforms:



Comments/Notes:

## D.4 SAP\_ADDRESS\_COLUMN\_W

<b>Library Name:</b>	sap1951_FTJ_THESES_45
<b>Cell Name:</b>	SAP_ADDRESS_COLUMN_W

### Function/Truth Table:

<i>Wen</i>	<i>WenN</i>	<i>WN</i>	<i>Ren</i>	<i>RenN</i>	<i>Y</i>
0	1	0	1	0	X
0	1	1	1	0	X
0	1	0	0	1	X
0	1	1	0	1	X
1	0	0	1	0	X
1	0	1	1	0	X
1	0	0	0	1	VDD
1	0	1	0	1	VSS

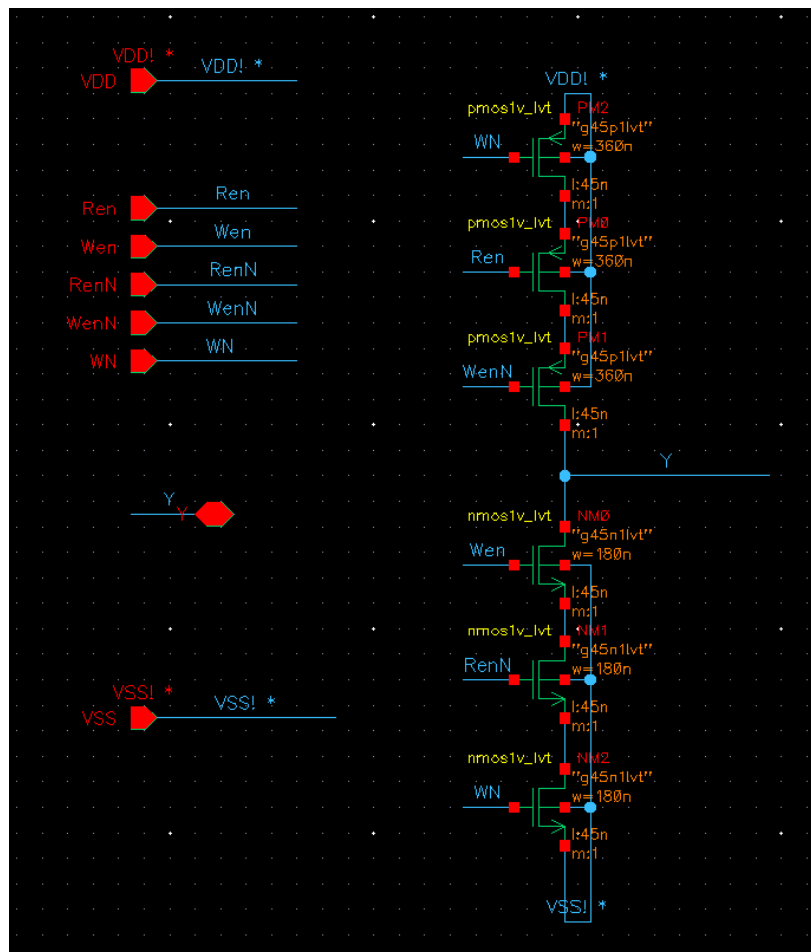
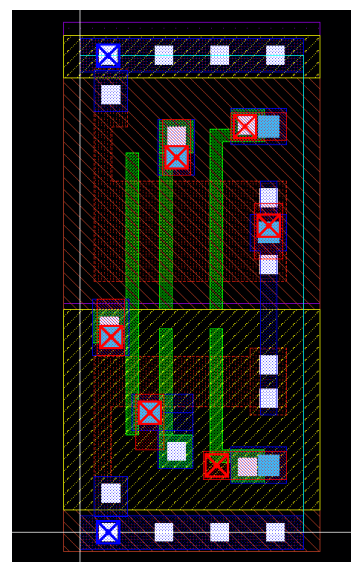
**Propagation Delay ( $t_{\text{pdf}}$  and  $t_{\text{pdr}}$ ) and Output Rise/Fall Time ( $t_f$  and  $t_r$ ):**

In	Out	$t_{\text{pdf}}$	$t_{\text{pdr}}$	$t_f$	$t_r$
Wen	Y	$208 \times 10^{-12}$	$75.14 \times 10^{-12}$	$122.4 \times 10^{-12}$	$97.83 \times 10^{-12}$
WN	Y	$66.89 \times 10^{-12}$	$177.0 \times 10^{-12}$	$54.9 \times 10^{-12}$	$94.81 \times 10^{-12}$
Ren	Y	$102.8 \times 10^{-12}$	$99.16 \times 10^{-12}$	$191.4 \times 10^{-12}$	$82.92 \times 10^{-12}$

**Layout Area:**  $0.8\mu\text{m} \times 1.71\mu\text{m} = W \times H$

### Symbol with Port Names:



**Schematic:****Layout:**

Functional Simulation Waveforms:



Comments/Notes:

## D.5 SAP\_ADDRESS\_ROW\_R

<b>Library Name:</b>	sap1951_FTJ_THESES_45
<b>Cell Name:</b>	SAP_ADDRESS_ROW_R

**Function/Truth Table:**

<i>RenN</i>	<i>Wen</i>	<i>Y</i>
0	0	$v_{dda}$
0	1	X
1	0	X
1	1	X

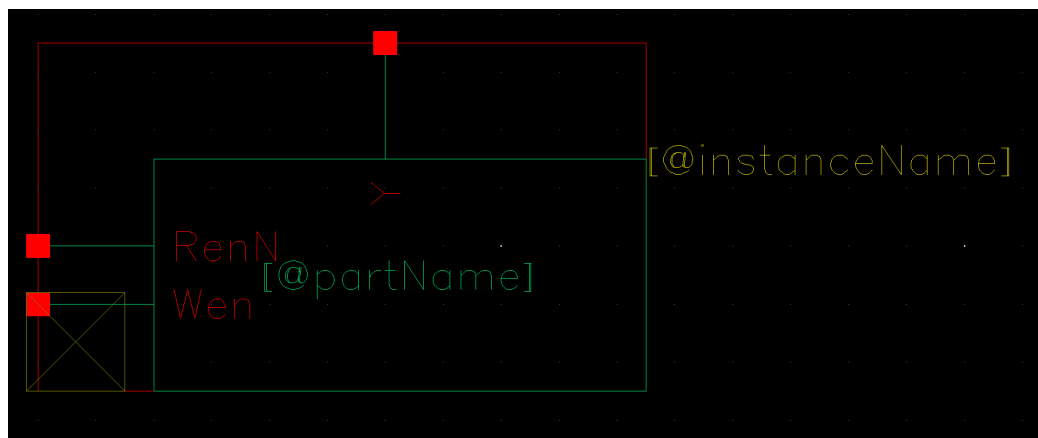
**Propagation Delay ( $t_{pdf}$  and  $t_{pdr}$ ) and Output Rise/Fall Time ( $t_f$  and  $t_r$ ):**

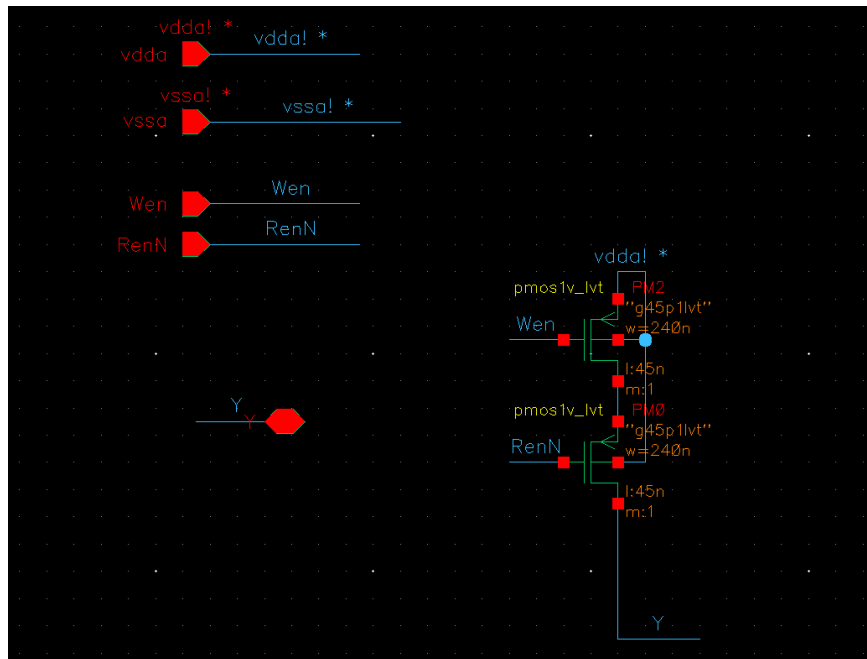
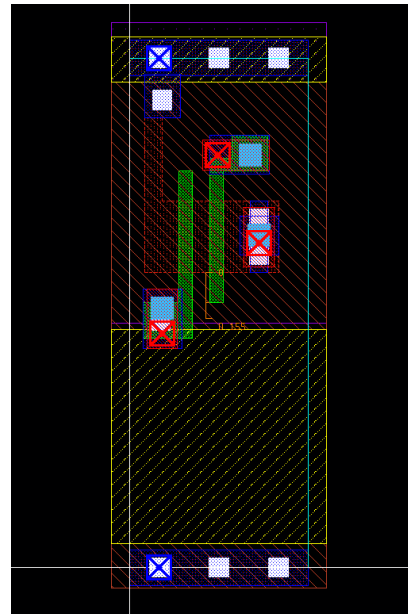
In	Out	$t_{pdf}$	$t_{pdr}$	$t_f$	$t_r$
RenN	Y	-	$513.9 \times 10^{-12}$	-	$433.7 \times 10^{-9}$
Wen	Y	-	$465.7 \times 10^{-12}$	-	$451.3 \times 10^{-9}$

Notice long  $t_r$  because this device doesn't drive the output high, it can only drag it down to  $v_{ssa}$ .

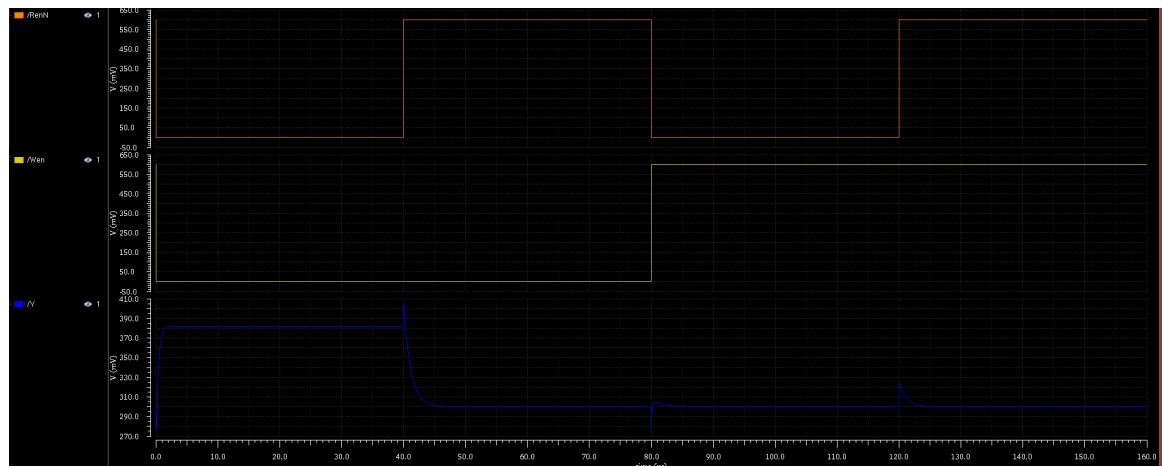
**Layout Area:**  $0.6\mu\text{m} \times 1.71\mu\text{m} = W \times H$

**Symbol with Port Names:**



**Schematic:****Layout:**

**Functional Simulation Waveforms:**



**Comments/Notes:**

## D.6 SAP\_ADDRESS\_ROW\_W

<b>Library Name:</b>	sap1951_FTJ_THESES_45
<b>Cell Name:</b>	SAP_ADDRESS_ROW_W

### Function/Truth Table:

$W_{en}$	$W_{enN}$	$W$	$Ren$	$RenN$	$Y$
0	1	0	1	0	X
0	1	1	1	0	X
0	1	0	0	1	X
0	1	1	0	1	X
1	0	0	1	0	X
1	0	1	1	0	X
1	0	0	0	1	VDD
1	0	1	0	1	VSS

Propagation Delay ( $t_{pdf}$  and  $t_{pdr}$ ) and Output Rise/Fall Time ( $t_f$  and  $t_r$ ):

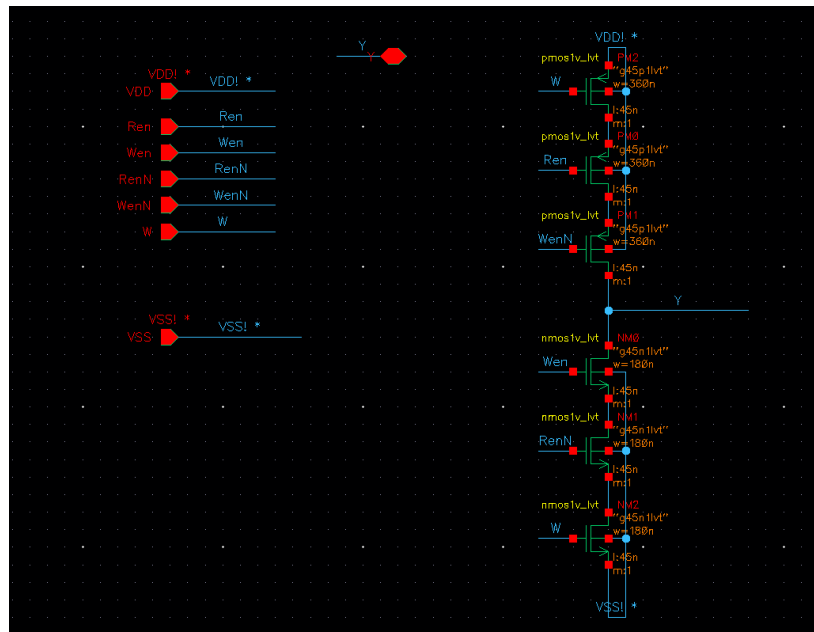
In	Out	$t_{pdf}$	$t_{pdr}$	$t_f$	$t_r$
Wen	Y	$208.7 \times 10^{-12}$	$103.4 \times 10^{-12}$	$124.0 \times 10^{-12}$	$79.94 \times 10^{-12}$
W	Y	$68.36 \times 10^{-12}$	$181.5 \times 10^{-12}$	$116.8 \times 10^{-12}$	$94.81 \times 10^{-12}$
Ren	Y	$102.4 \times 10^{-12}$	$99.75 \times 10^{-12}$	$116.2 \times 10^{-12}$	$90.66 \times 10^{-12}$

Layout Area:  $0.8\mu\text{m} \times 1.71\mu\text{m} = W \times H$

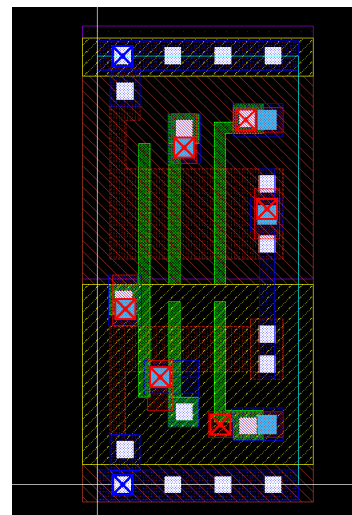
### Symbol with Port Names:



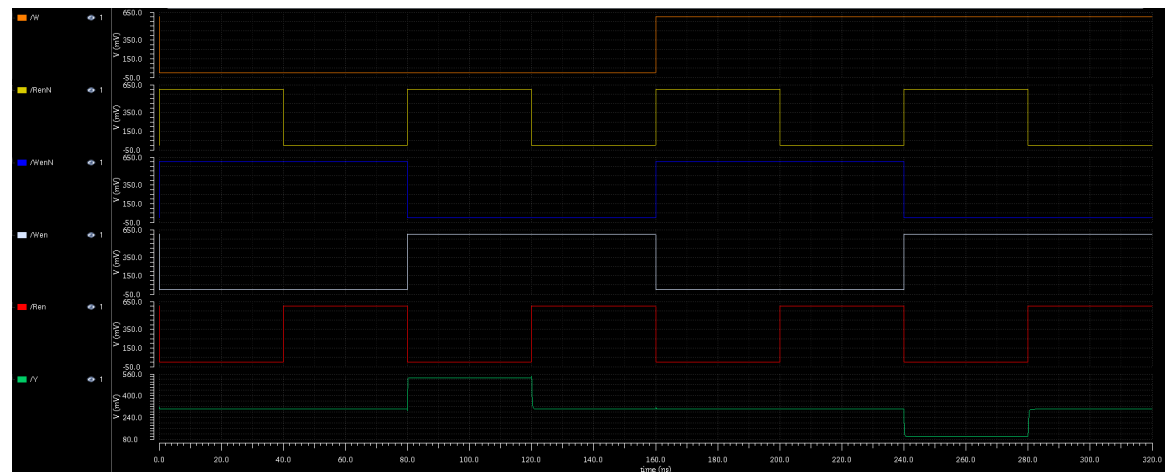
Schematic:



Layout:



Functional Simulation Waveforms:



Comments/Notes:

## D.7 SAP\_ADDRESS\_GND\_vcc

<b>Library Name:</b>	sap1951_FTJ_THESES_45
<b>Cell Name:</b>	SAP_ADDRESS_GND_vcc

**Function/Truth Table:**

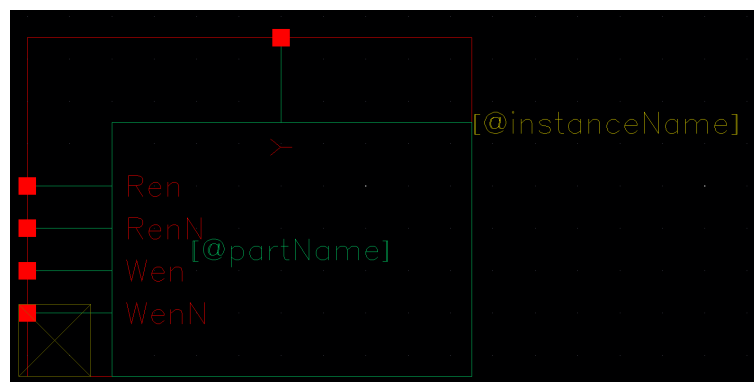
<i>Wen</i>	<i>WenN</i>	<i>Ren</i>	<i>RenN</i>	<i>Y</i>
0	1	1	0	X
0	1	0	1	VCC
1	0	1	0	X
1	0	0	1	X

**Propagation Delay ( $t_{\text{pdf}}$  and  $t_{\text{pdr}}$ ) and Output Rise/Fall Time ( $t_f$  and  $t_r$ ):**

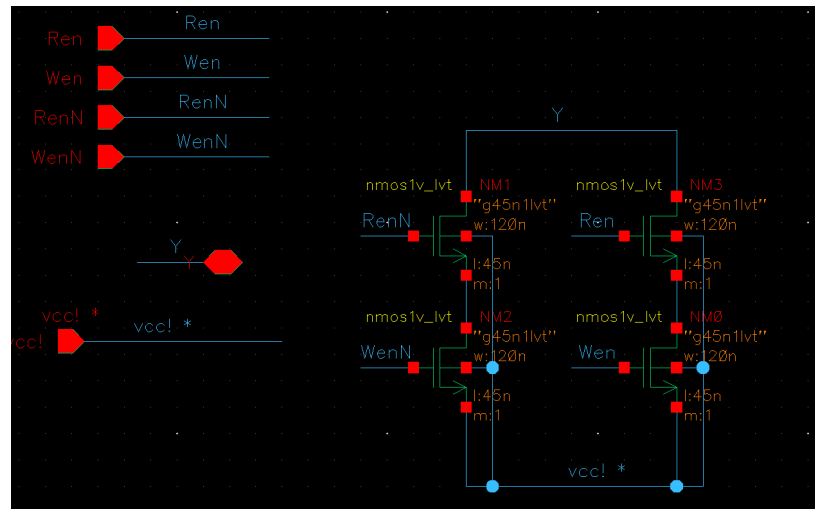
In	Out	$t_{\text{pdf}}$	$t_{\text{pdr}}$	$t_f$	$t_r$
Wen	Y	-	$165.0 \times 10^{-12}$	-	$191.9 \times 10^{-12}$
Ren	Y	-	$158.4 \times 10^{-12}$	-	$188.9 \times 10^{-12}$

**Layout Area:**  $0.8\mu\text{m} \times 1.71\mu\text{m} = W \times H$

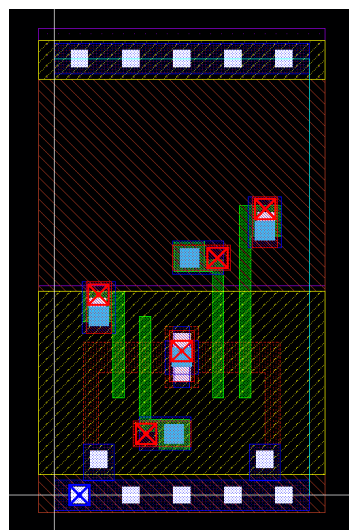
**Symbol with Port Names:**



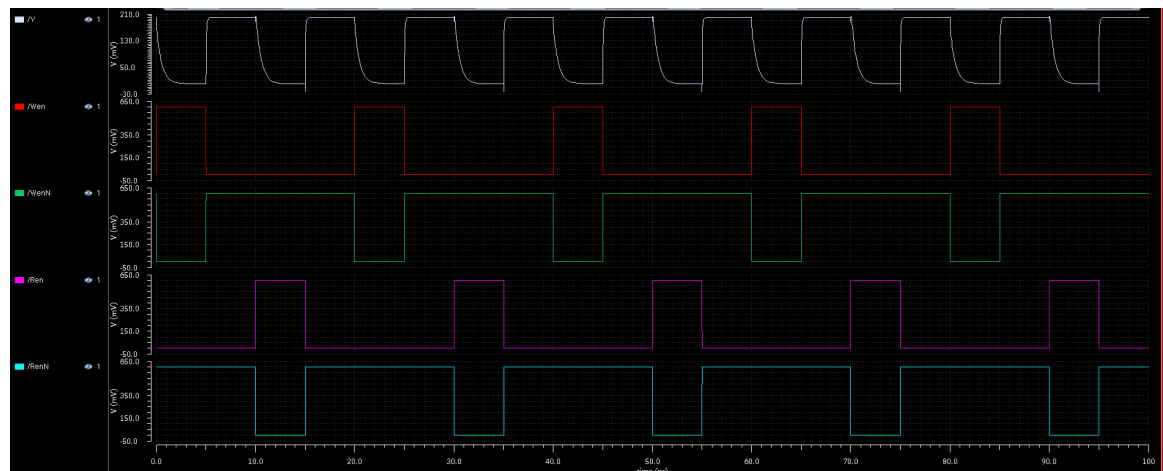
Schematic:



Layout:

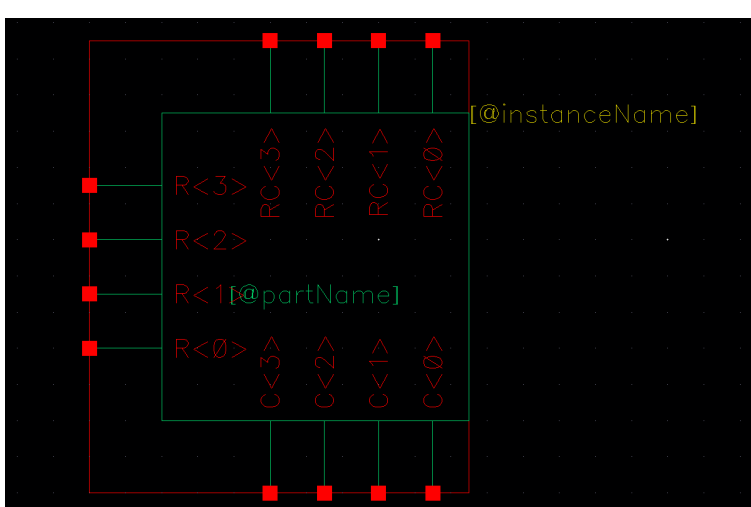


Functional Simulation Waveforms:

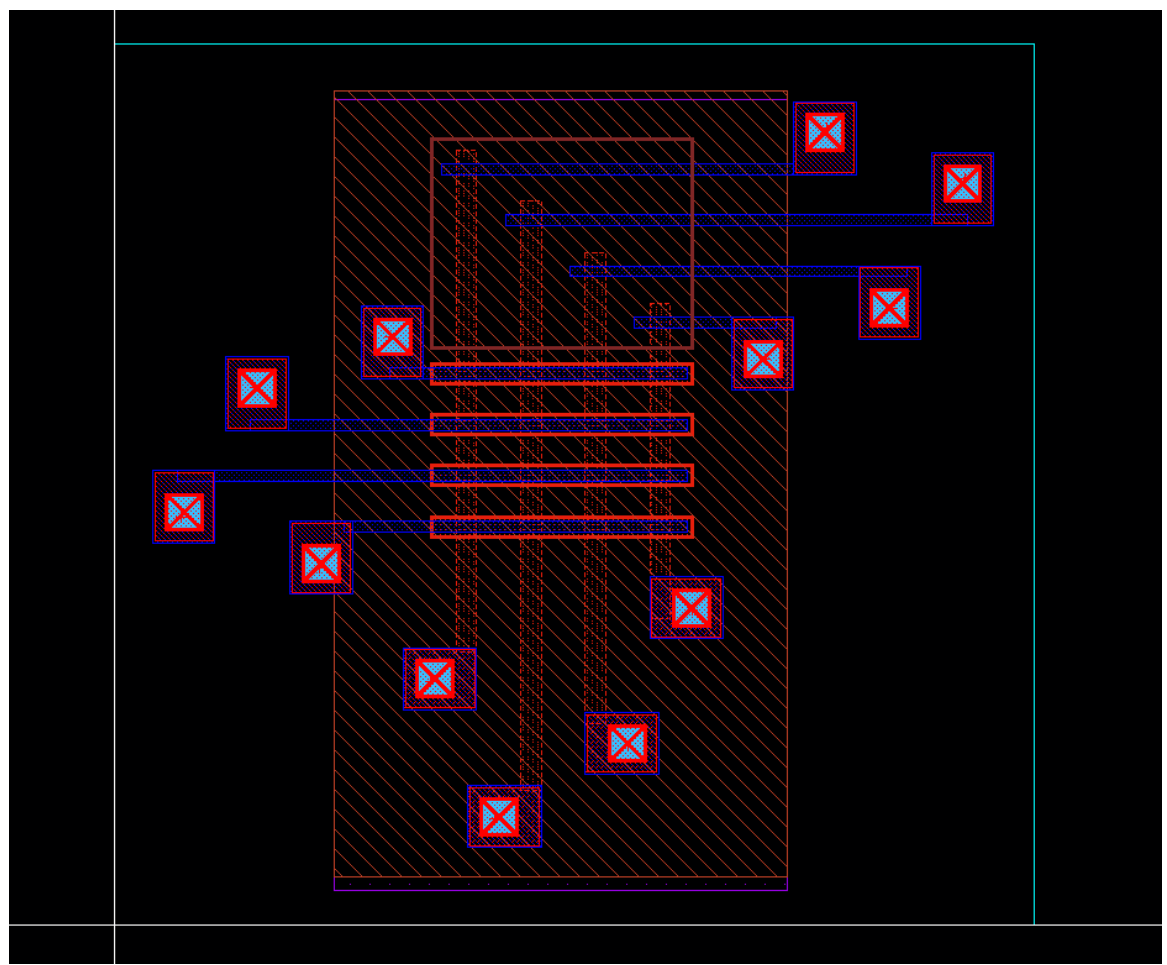


Comments/Notes:

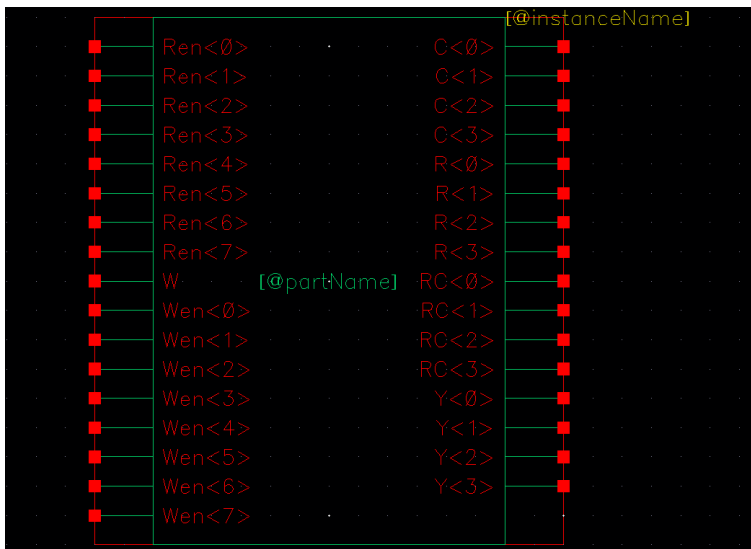
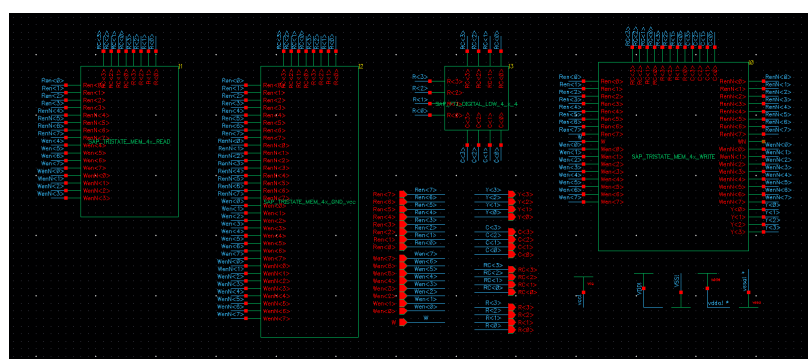
## D.8 SAP\_FTJ\_DIGITAL\_LOW\_4\_x\_4

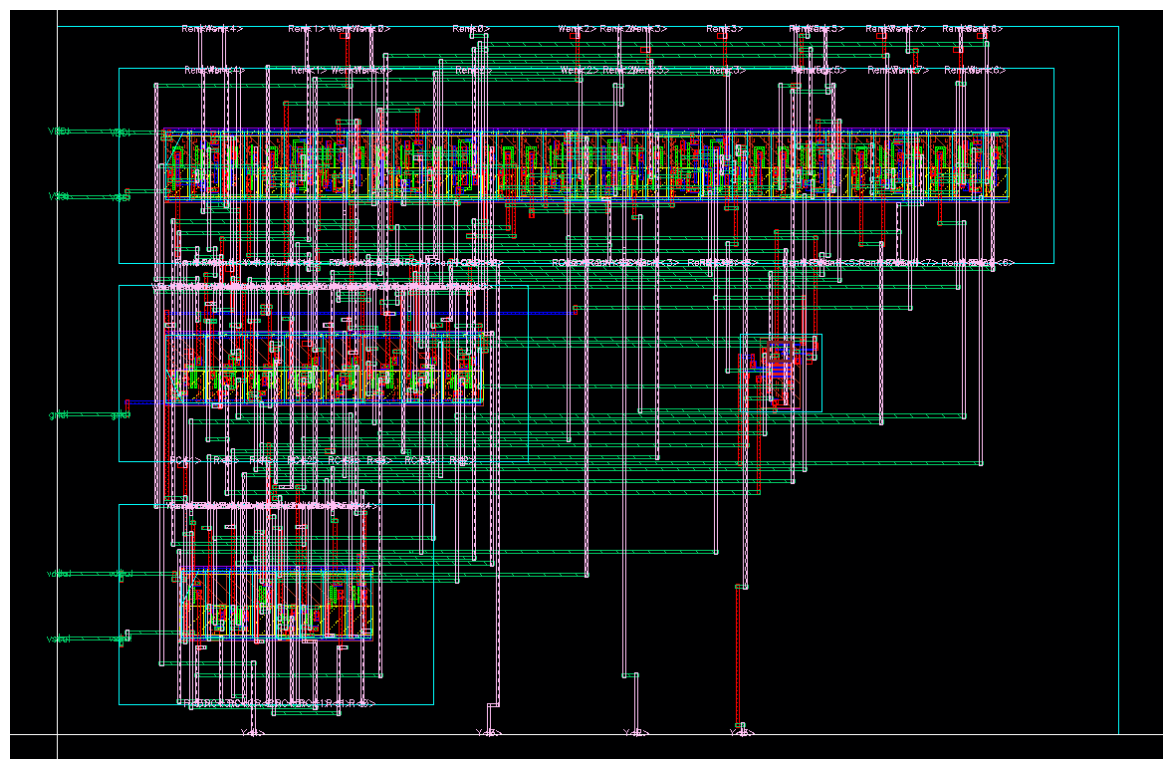
Library Name:	sap1951_FTJ_THESES_45
Cell Name:	SAP_FTJ_DIGITAL_LOW_4_x_4
<b>Layout Area:</b> $2.07\mu\text{m} \times 1.985\mu\text{m} = W \times H$	
<b>Symbol with Port Names:</b> 	
<b>Schematic:</b> 	

Layout:



## D.9 SAP\_TRISTATE\_MEM\_4x\_vcc

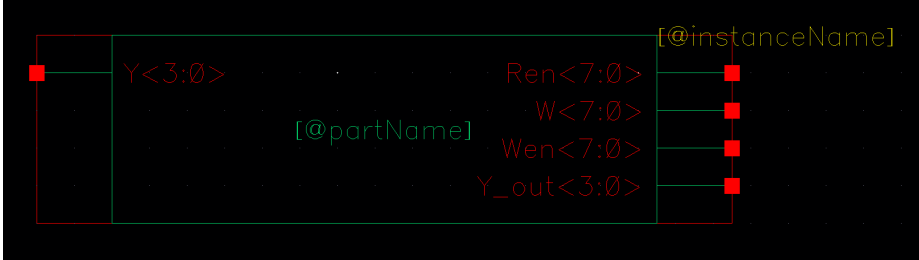
<b>Library Name:</b>	sap1951_FTJ_THESES_45
<b>Cell Name:</b>	SAP_TRISTATE_MEM_4x_vcc
<b>Layout Area:</b> $27 \mu\text{m} \times 18 \mu\text{m} = W \times H$	
<b>Symbol with Port Names:</b>  <p>The symbol shows four vertical columns of ports. The leftmost column contains Ren&lt;0&gt; through Ren&lt;7&gt;. The second column contains Wen&lt;0&gt; through Wen&lt;7&gt;. The third column contains RC&lt;0&gt; through RC&lt;3&gt;. The rightmost column contains C&lt;0&gt; through C&lt;3&gt;, R&lt;0&gt; through R&lt;3&gt;, and Y&lt;0&gt; through Y&lt;3&gt;. A red box highlights the Wen&lt;0&gt; through Wen&lt;7&gt; ports.</p>	
<b>Schematic:</b>  <p>The schematic shows the internal structure of the memory cell. It consists of four main sections, each containing a 4x4 grid of tristate buffers. The sections are labeled Ren0, Ren1, Ren2, and Ren3. Each section has its own set of control and data lines. The entire cell is labeled SAP_TRISTATE_MEM_4x_vcc. External connections include power supply lines VDD and VSS, and ground connections GND.</p>	

**Layout:**

## D.10 SAP\_TRISTATE\_MEM\_4x\_TESTBENCH

Library Name:	sap1951_FTJ_THESES_45
Cell Name:	SAP_TRISTATE_MEM_4x_TESTBENCH

Symbol with Port Names:



The symbol is a rectangle divided into four quadrants by red lines. The top-left quadrant contains a red square. The top-right quadrant contains the text '@instanceName' above five red squares connected by a vertical line. The bottom-left quadrant contains the text '@partName' above five red squares connected by a vertical line. The bottom-right quadrant contains the port names: Y<3:0>, Ren<7:0>, W<7:0>, Wen<7:0>, and Y\_out<3:0>, each preceded by a red square.

### D.10.1 Verilog Model

```
1          //Verilog HDL for "sap1951_FTJ_THESES_45",
2          "SAP_TRISTATE_MEM_4x_TESTBENCH" "
3          functional"
4
5          'timescale 10 ns / 1 fs
6
7          module SAP_TRISTATE_MEM_4x_TESTBENCH(Ren,
8              W, Wen, Y, Y_out);
9
10         input [3:0] Y;
11         output [7:0] Ren, W, Wen;
12         output [3:0] Y_out;
13
14         reg [7:0] Ren, W, Wen;
15
16         reg [3:0] val;
17         integer out;
18         integer outnot;
19         reg [3:0] bg;
20
21         integer errors;
22         integer bgerrors;
23         integer disterrors;
24
25         wire [3:0] Y_out = Y ;
26
27         initial
```

```
23      begin
24          //Write all High (HRS) for 4us
25          errors=0;
26          bgerrors=0;
27          disterrors=0;
28          Ren <= 8'b00000000;
29          W <= 8'b11111111;
30          Wen <= 8'b11111111;
31          bg = 4'b1111;
32      end
33
34      always
35      begin
36          #1;
37          //10us Guard Time
38          Ren <= 8'b00000000;
39          W <= 8'b00000000;
40          Wen <= 8'b00000000;
41          #1;
42          //Read Mem row 7 (1) for 10us
43          Ren <= 8'b10001111;
44          W <= 8'b00000000;
45          Wen <= 8'b00000000;
46          #1;
47          //10us Guard Time
48          Ren <= 8'b00000000;
49          W <= 8'b00000000;
```

```
50          Wen <= 8'b00000000;
51          #1;
52          //Read Mem row 7 (1) for 10us
53          Ren <= 8'b10001111;
54          W    <= 8'b00000000;
55          Wen <= 8'b00000000;
56          #1;
57          //10us Guard Time
58          Ren <= 8'b00000000;
59          W    <= 8'b00000000;
60          Wen <= 8'b00000000;
61          #1;
62          //for loop through all 15 numbers (2^4-1)
63          //and write each one in the first row of
64          //the array
65          for(out=0;out<16;out=out+1)
66          begin
67          outnot=15-out;
68          //write \ac{HRS} for current val
69          W <= 8'b11111111;
70          val=out;
71          Wen <= {4'b1000, val};
72          #1;
73          //guard time 10us
74          Ren <= 8'b00000000;
75          W    <= 8'b00000000;
76          Wen <= 8'b00000000;
```

```
75          #1;
76          //write LRS for current val
77          W    <= 8'b00000000;
78          val=outnot;
79          Wen <= {4'b1000, val};
80          #1;
81          //guard time 10us
82          Ren <= 8'b00000000;
83          W    <= 8'b00000000;
84          Wen <= 8'b00000000;
85          val=out;
86          #1;
87          //read that shit!
88          Ren <= 8'b10001111;
89          W    <= 8'b00000000;
90          Wen <= 8'b00000000;
91          #1;
92          if(Y!=val)
93          begin
94          errors=errors+1;
95          end
96          //guard time 10us
97          Ren <= 8'b00000000;
98          W    <= 8'b00000000;
99          Wen <= 8'b00000000;
100         #1;
101        //read the column directly below!
```

```
102          Ren <= 8'b000101111;
103          W    <= 8'b000000000;
104          Wen <= 8'b000000000;
105          #1;
106          if(Y!=bg)
107          begin
108          bgerrors=bgerrors+1;
109          end
110          //guard time 10us
111          Ren <= 8'b000000000;
112          W    <= 8'b000000000;
113          Wen <= 8'b000000000;
114          #1;
115          //read that shit!
116          Ren <= 8'b100011111;
117          W    <= 8'b000000000;
118          Wen <= 8'b000000000;
119          #1;
120          if(Y!=val)
121          begin
122          disterrors=disterrors+1;
123          end
124          //guard time 10us
125          Ren <= 8'b000000000;
126          W    <= 8'b000000000;
127          Wen <= 8'b000000000;
128          #1;
```

```
129      end
130
130      $display("%d\data\errors , %d\background\
131          disturbances , and %d\data\disturbances\with\an\
132          background\of\b.", errors , bgerrors ,
133          disterrors , bg);
134
134      errors=0;
135
135      bgerrors=0;
136
136      disterrors=0;
137
137      //Write all Low (LRS) for 10us and repeat
138          test!
139
139      Ren <= 8'b00000000;
140
140      W    <= 8'b00000000;
141
141      Wen <= 8'b10001111;
142
142      bg = 4'b0000;
143
143      #1;
144
144      Ren <= 8'b00000000;
145
145      W    <= 8'b00000000;
146
146      Wen <= 8'b01001111;
147
147      bg = 4'b0000;
148
148      #1;
149
149      Ren <= 8'b00000000;
150
150      W    <= 8'b00000000;
```

```
152      Wen <= 8'b00011111;  
153      bg = 4'b0000;  
154      end  
155      endmodule
```